ISSN: 2153-1196 Volume 13, Number 8, August 2022

Scientific Research Publishing

Journal of Modern Physics

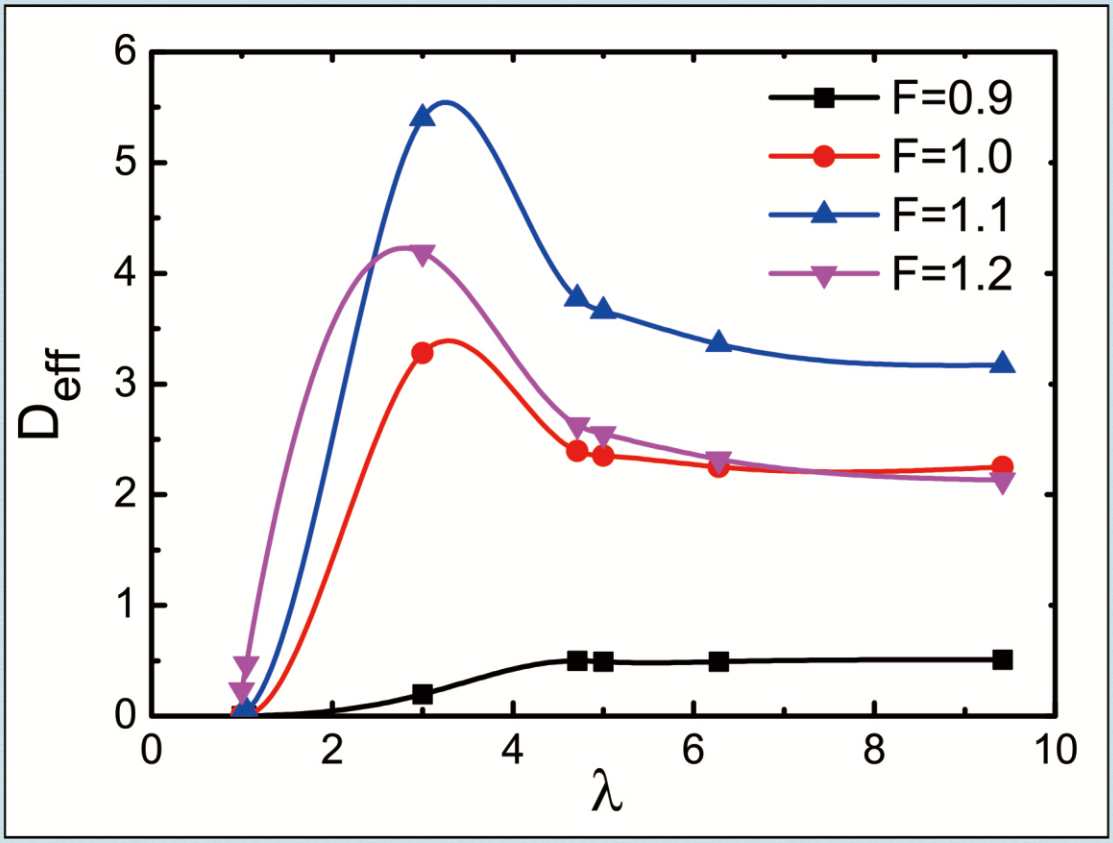

ISSN: 2153-1196

https://www.scirp.org/journal/jmp

Journal Editorial Board

ISSN: 2153-1196 (Print) ISSN: 2153-120X (Online)
https://www.scirp.org/journal/jmp

Editor-in-Chief

Editorial Board

Scientific Research Publishing

Journal of Modern Physics, 2022, 13, 1147-1251
https://www.scirp.org/journal/jmp
ISSN Online: 2153-120X
ISSN Print: 2153-1196

Table of Contents

Volume 13 Number 8 August 2022

The figure on the front cover is from the article published in Journal of Modern Physics, 2022, Vol. 13, No. 8, pp. 1157-1166 by Meng Hu.

Journal of Modern Physics (JMP)
Journal Information

SUBSCRIPTIONS

The *Journal of Modern Physics* (Online at Scientific Research Publishing, https://www.scirp.org/) is published monthly by Scientific Research Publishing, Inc., USA.

Subscription rates:
Print: $89 per issue.
To subscribe, please contact Journals Subscriptions Department, E-mail: sub@scirp.org

SERVICES

Advertisements
Advertisement Sales Department, E-mail: service@scirp.org

Reprints (minimum quantity 100 copies)
Reprints Co-ordinator, Scientific Research Publishing, Inc., USA.
E-mail: sub@scirp.org

COPYRIGHT

PRODUCTION INFORMATION

For manuscripts that have been accepted for publication, please contact:
E-mail: jmp@scirp.org

Scientific Research Publishing

Journal of Modern Physics, 2022, 13, 1147-1156
https://www.scirp.org/journal/jmp
ISSN Online: 2153-120X
ISSN Print: 2153-1196

Including Space-Time in the Extended Group Cl_3^* of Relativistic Form-Invariance

Claude Daviau[1], Jacques Bertrand[2]

[1]Pouillé-les-Coteaux, France
[2]Saint-Gratien, France
Email: daviau.claude@orange.fr, bertrandjacques-m@orange.fr

How to cite this paper: Daviau, C. and Bertrand, J. (2022) Including Space-Time in the Extended Group Cl_3^* of Relativistic Form-Invariance. *Journal of Modern Physics*, **13**, 1147-1156.
https://doi.org/10.4236/jmp.2022.138066

Received: July 16, 2022
Accepted: August 12, 2022
Published: August 15, 2022

Abstract

The inclusion of space-time in the extended group of relativistic form-invariance, Cl_3^*, is specified as the inclusion of the whole space-time manifold in this multiplicative Lie group. First physical results presented here are: the geometric origin of the time arrow, a better understanding of the non-simultaneity in optics and a mainly geometric origin for the universe expansion, and its recent acceleration.

Keywords

Space-Time Manifold, Invariance Group, Standard Model, Acceleration of Expansion

1. Introduction

The inclusion of space-time in the group of form-invariance of the relativistic quantum theory of the electron results from our previous works:

1) We have expressed the Dirac theory of the electron in Cl_3, Clifford algebra of the 3-dimensional space [1] [2] [3].

2) We have extended the form-invariance of the Dirac theory from $SL(2,\mathbb{C})$ to $GL(2,\mathbb{C}) = Cl_3^*$, where Cl_3^* is the multiplicative group of the invertible elements in Cl_3 [4].

3) The value of the quantum wave has been extended to $\mathrm{End}(Cl_3)$, the Lie group of invertible linear applications in Cl_3, with its subgroup Cl_3^* as group of relativistic form-invariance, and the $U(1)\times SU(2)\times SU(3)$ group of the Standard Model as group of gauge invariance [5]-[15].

Nearly a Century Ago

Early quantum physics, as soon as 1927, wrote in the framework of the Pauli's

wave equation:

$$\vec{\mathrm{x}} = \begin{pmatrix} \mathrm{x}^3 & \mathrm{x}^1 - i\mathrm{x}^2 \\ \mathrm{x}^1 + i\mathrm{x}^2 & -\mathrm{x}^3 \end{pmatrix} = \mathrm{x}^1\sigma_1 + \mathrm{x}^2\sigma_2 + \mathrm{x}^3\sigma_3. \tag{1}$$

where the three σ_j matrices are the well-known Pauli matrices. The set $M_2(\mathbb{C})$ of the 2 × 2 complex matrices is isomorphic to the Clifford algebra Cl_3 of the 3-dimensional space (see for instance [14] A.3 for more details). The center of this real algebra is isomorphic to $\mathbb{C}$, this allows quantum physics to identify Cl_3 and $M_2(\mathbb{C})$, the center being identified to the set of scalar matrices.

Starting from the Pauli equation, P.A.M. Dirac wrote a relativistic wave equation [16] [17]. Since this equation uses time at the same level as space coordinates, the relativistic invariance needs an extension of the previous inclusion in $M_2(\mathbb{C})$:

$$\mathrm{x} := \mathrm{x}^\mu\sigma_\mu = \mathrm{x}^0 + \vec{\mathrm{x}} = \begin{pmatrix} \mathrm{x}^0 + \mathrm{x}^3 & \mathrm{x}^1 - i\mathrm{x}^2 \\ \mathrm{x}^1 + i\mathrm{x}^2 & \mathrm{x}^0 - \mathrm{x}^3 \end{pmatrix}; \mathrm{x}^0 := ct. \tag{2}$$

And then space-time is identified with the auto-adjoint subset of the Pauli algebra Cl_3, which is the part of the M elements satisfying $M = M^\dagger$. We note $\overline{\mathrm{x}}$ the co-matrix:

$$\overline{\mathrm{x}} := \mathrm{x}^0 - \vec{\mathrm{x}} = \begin{pmatrix} \mathrm{x}^0 - \mathrm{x}^3 & -\mathrm{x}^1 + i\mathrm{x}^2 \\ -\mathrm{x}^1 - i\mathrm{x}^2 & \mathrm{x}^0 + \mathrm{x}^3 \end{pmatrix}. \tag{3}$$

Thus the space-time metric satisfies:

$$\mathrm{x}\overline{\mathrm{x}} = \overline{\mathrm{x}}\mathrm{x} = \det(\mathrm{x}) = \left(\mathrm{x}^0\right)^2 - \left(\mathrm{x}^1\right)^2 - \left(\mathrm{x}^2\right)^2 - \left(\mathrm{x}^3\right)^2. \tag{4}$$

2. Form-Invariance of the Dirac Equation

Let M be any nonzero element in Cl_3 (that means any fixed nonzero Pauli matrix) and let R be the transformation of space-time into itself such that for any x is associated x' given by

$$\mathrm{x}' = \mathrm{x}'^0 + \vec{\mathrm{x}}' = R(\mathrm{x}) = M\mathrm{x}M^\dagger. \tag{5}$$

We note, if $\det(M) \neq 0$:

$$\det(M) = re^{i\theta},\ r = \left|\det(M)\right|. \tag{6}$$

Then r is the modulus and θ is an argument of the determinant of M. We get:

$$\begin{aligned} &\left(\mathrm{x}'^0\right)^2 - \left(\mathrm{x}'^1\right)^2 - \left(\mathrm{x}'^2\right)^2 - \left(\mathrm{x}'^3\right)^2 = \det(\mathrm{x}') = \det\left(M\mathrm{x}M^\dagger\right) \\ &= re^{i\theta}\det(\mathrm{x})re^{-i\theta} = r^2\left[\left(\mathrm{x}^0\right)^2 - \left(\mathrm{x}^1\right)^2 - \left(\mathrm{x}^2\right)^2 - \left(\mathrm{x}^3\right)^2\right]. \end{aligned} \tag{7}$$

Therefore R multiplies any space-time distance by r and we name this transformation "similitude with ratio r". We name M the "dilator" of the similitude R, and we define the R^μ_ν matrix of this similitude as follows:

$$\mathrm{x}'^{\mu} = R^{\mu}_{\nu}\mathrm{x}^{\nu}. \tag{8}$$

For any dilator $M = \begin{pmatrix} a & b \\ c & d \end{pmatrix} \neq 0$:

$$2R^0_0 = |a|^2 + |b|^2 + |c|^2 + |d|^2 > 0, \tag{9}$$

Thus x'^0 has the same sign as x^0 at the origin: the similitude R conserves the time arrow. Moreover, for any dilator M in Cl_3, we have (proof in [14] A.4.5):

$$\det\left(R^{\mu}_{\nu}\right) = r^4. \tag{10}$$

Hence if r is nonzero $r^4 > 0$: $\det(R) > 0$. Thus R conserves the orientation of space-time and since the transformation conserves the orientation of time, R conserves also the orientation of space. Using only Cl_3 for the Dirac theory (see [14] 1.3) the linear Dirac equation is expressed as:

$$\begin{aligned} &0 = \nabla\hat{\phi}\sigma_{21} + qA\hat{\phi} + m\phi; \hat{\phi} := \overline{\phi}^{\dagger}; \sigma_{21} := \sigma_2\sigma_1 = -i\sigma_3; \nabla := \sigma^{\mu}\partial_{\mu}, \\ &\sigma^0 := \sigma_0 = 1; \sigma^j := -\sigma_j,\ j = 1,2,3. \end{aligned} \tag{11}$$

The form-invariance of the Dirac equation results from:

$$\phi' = M\phi; \mathrm{x}' = M\mathrm{x}M^{\dagger}; \nabla = \overline{M}\nabla'\hat{M}; \nabla' = \sigma^{\mu}\frac{\partial}{\partial \mathrm{x}'^{\mu}} \tag{12}$$

Which gives:

$$0 = \nabla'\hat{\phi}'\sigma_{21} + q'A'\hat{\phi}' + m'\phi', \tag{13}$$

$$qA = \overline{M}q'A'\hat{M}; m = r\mathrm{e}^{i\theta}m'. \tag{14}$$

We then have a double inclusion: space-time of special relativity is included in Cl_3 and the $SU(2)$ group of invariance of non-relativistic quantum theory is a subgroup of $SL(2,\mathbb{C})$, itself a subgroup of $GL(2,\mathbb{C}) = Cl_3^*$, where Cl_3^* is the multiplicative Lie group of the invertible elements in $M_2(\mathbb{C}) = Cl_3$, itself Lie algebra of Cl_3^*. Moreover Cl_3^* is a subgroup of $\mathrm{End}(Cl_3)$, which is a group containing the $U(1)\times SU(2)\times SU(3)$ group of the Standard Model (see [14] Chapter 2 and Chapter 3).

The only difficulty of (14), the $\mathrm{e}^{i\theta}$ factor, is solved with the simplification of the Dirac Lagrangian containing $\overline{\psi}\psi = \rho\cos(\beta) = \Re\left[\det(\phi)\right]$ where we have suppressed the cosine (see [14] 1.5). This gives our improved nonlinear wave equation:

$$0 = \overline{\phi}\left(\nabla\hat{\phi}\right)\sigma_{21} + \overline{\phi}qA\hat{\phi} + m\rho, \tag{15}$$

where the form-invariance of the wave equation results now from:

$$0 = \overline{\phi}'\left(\nabla'\hat{\phi}'\right)\sigma_{21} + \overline{\phi}'q'A'\hat{\phi}' + m'\rho', \tag{16}$$

$$\phi' = M\phi; qA = \overline{M}q'A'\hat{M}; m = rm'. \tag{17}$$

And since each interesting solution of the Dirac equation has values in Cl_3^* (see [14] 1.5.3 and 1.5.7), we may suppose the inclusion of the space-time mani-

fold itself in Cl_3^*. This hypothesis also relies on the experimental building of geometry, by telescopes which are turned before each observation: the invariance under rotation is always assumed [18] and since quantum mechanics replaces the invariance under rotation by the invariance under $SU(2)$, the invariance under a subgroup of Cl_3^* is necessarily at the center of the geometry of the universe. Moreover, space-time is a 4-dimensional manifold, thus Cl_3, which is 8-dimensional, is large enough to host the space-time manifold.

3. Space-Time Manifold in Cl_3^*

3.1. Local and Global Structure of Space-Time

Since any measurement of length is always a measurement of the ratio between two lengths, we let

$$\mathbf{x} := \frac{\mathrm{x}}{l_a}; \mathbf{x} \in Cl_3, \tag{18}$$

where $l_a = \sqrt{\alpha} l_P$ is an absolute length, linked to the fine structure constant α and to the Planck length l_P [15]. The first difference with classical geometry is that the origin of the measure of time and space is at $\mathbf{x} = 1$ (neutral element of the Lie group), not 0 which is the neutral element of the Lie algebra. Second, Cl_3 is the Lie algebra of the Cl_3^* multiplicative group. This means that the vicinity of any point O is isomorphic to Cl_3. This set is a linear space which contains two subsets: Cl_3^*, which is the set of $\mathbf{x}$ satisfying $\det(\mathbf{x}) \neq 0$, and the light cone, which is the set of $\mathbf{x}$ satisfying $\det(\mathbf{x}) = 0$. Third, these conditions exclude themselves, therefore the light cone is included in each (local) Lie algebra, not in the (global) Lie group Cl_3^*. Fourth, the only link between each Lie algebra and the whole Lie group is the exponential function, which we calculate as follows:

$$\mathbf{x} = a + b\mathbf{u}; \mathbf{u} = x^1\sigma_1 + x^2\sigma_2 + x^3\sigma_3; \left(x^1\right)^2 + \left(x^2\right)^2 + \left(x^3\right)^2 = 1,$$

$$\mathbf{x}^n = \frac{1}{2}\left[(a+b)^n(1+\mathbf{u}) + (a-b)^n(1-\mathbf{u})\right] \tag{19}$$

$$\exp(\mathbf{x}) = \sum_{n=0}^{\infty}\frac{\mathbf{x}^n}{n!} = \frac{1}{2}\left[\mathrm{e}^{a+b}(1+\mathbf{u}) + \mathrm{e}^{a-b}(1-\mathbf{u})\right] = \mathrm{e}^a\left[\cosh(b) + \sinh(b)\mathbf{u}\right]. \tag{20}$$

Thus the same unitary vector $\mathbf{u}$ ($\mathbf{u}^2 = 1$) is used for $\mathbf{x}$ and for $\exp(\mathbf{x})$. Moreover, we have:

$$\det\left[\exp(\mathbf{x})\right] = \exp\left[\mathrm{tr}(\mathbf{x})\right] = \mathrm{e}^{2a}. \tag{21}$$

Thus, with $\exp(\mathbf{x}) = A + B\mathbf{u} = A + B\left(x^1\sigma_1 + x^2\sigma_2 + x^3\sigma_3\right)$ we obtain:

$$\mathrm{e}^{2a} = \det\left[\exp(\mathbf{x})\right] = (A + B\mathbf{u})(A - B\mathbf{u}) = A^2 - B^2 \tag{22}$$

This implies that the light cone ($A^2 = B^2$) is the boundary of the space-time manifold and that nothing exists outside this boundary, since $\mathrm{e}^{2a} > 0$. From this sign we may see the purely local character of the classification of events in

five categories.[1] We obtain:

$$\mathrm{e}^{a}=\sqrt{A^2-B^2};\cosh(b)+\sinh(b)\mathbf{u}=\frac{A+B\mathbf{u}}{\sqrt{A^2-B^2}}.$$

$$a=\ln\left(\sqrt{A^2-B^2}\right)=\frac{1}{2}\left[\ln(A+B)+\ln(A-B)\right], \tag{23}$$

$$b=\sinh^{-1}\left[\frac{B}{\sqrt{A^2-B^2}}\right]=\frac{1}{2}\left[\ln(A+B)-\ln(A-B)\right],$$

$$a+b=\ln(A+B);A+B=\mathrm{e}^{a+b}. \tag{24}$$

3.2. The EPR Paradox

Two photons are emitted at the point-event O. We suppose, simplifying the calculation, that they are emitted in two orthogonal directions, σ_1 and σ_2. They are absorbed at the same time $y>0$, also to simplify the calculation. The photon emitted in the direction σ_1 is absorbed at the point-event:

$$\mathbf{x}_1=a_1+b_1\mathbf{u}_1=(a+y)+\left(bx^1+y\right)\sigma_1+b\left(x^2\sigma_2+x^3\sigma_3\right),$$

$$a_1=a+y;\mathbf{u}_1=x_1^1\sigma_1+x_1^2\sigma_2+x_1^3\sigma_3;\left(x_1^1\right)^2+\left(x_1^2\right)^2+\left(x_1^3\right)^2=1,$$

$$\left(x^1+y/b\right)^2+\left(x^2\right)^2+\left(x^3\right)^2=1+2x^1y/b+\left(y/b\right)^2, \tag{25}$$

$$b_1=b\sqrt{1+2x^1y/b+\left(y/b\right)^2};\mathbf{u}_1=\frac{\left(x^1+y/b\right)\sigma_1+x^2\sigma_2+x^3\sigma_3}{\sqrt{1+2x^1y/b+\left(y/b\right)^2}}.$$

The photon emitted in the direction σ_2 is absorbed at the point-event:

$$\mathbf{x}_2=a_2+b_2\mathbf{u}_2=(a+y)+bx^1\sigma_1+\left(bx^2+y\right)\sigma_2+bx^3\sigma_3. \tag{26}$$

And we also have:

$$a_2=a+y;\mathbf{u}_2=x_2^1\sigma_1+x_2^2\sigma_2+x_2^3\sigma_3;\left(x_2^1\right)^2+\left(x_2^2\right)^2+\left(x_2^3\right)^2=1,$$

$$\left(x^1\right)^2+\left(x^2+y/b\right)^2+\left(x^3\right)^2=1+2x^2y/b+\left(y/b\right)^2, \tag{27}$$

$$b_2=b\sqrt{1+2x^2y/b+\left(y/b\right)^2};\mathbf{u}_2=\frac{x^1\sigma_1+\left(x^2+y/b\right)\sigma_2+x^3\sigma_3}{\sqrt{1+2x^2y/b+\left(y/b\right)^2}}.$$

On the space-time manifold, the emission is at $O=\mathbf{x}/l_a=A+B\mathbf{u}$ while the photon emitted in the direction σ_1 is absorbed at the point-event $M=\mathbf{x}_1/l_a=\exp(\mathrm{x}_1)$. The photon emitted in the direction σ_2 is absorbed at the point-event $P=\mathbf{x}_2/l_a=\exp(\mathrm{x}_2)$. The position of the point event P, seen from 1, is:

$$\mathbf{x}_2^0=\left[\exp(\mathbf{x})\right]^{-1/2}\exp(\mathrm{x}_2)\left[\exp(\mathbf{x})\right]^{-1/2}. \tag{28}$$

The position of the point event P, seen from M, is:

[1]E being a given event, the five categories are: events on the future light cone of E; events on the past light cone of E; events inside the future light cone of E; events inside the past light cone of E; elsewhere: all other events.

$$\mathbf{x}_2^1 = \left[\exp(\mathbf{x}_1)\right]^{1/2}\left[\exp(\mathbf{x})\right]^{-1/2}\exp(\mathrm{x}_2)\left[\exp(\mathbf{x})\right]^{-1/2}\left[\exp(\mathrm{x}_1)\right]^{1/2}. \quad (29)$$

The position of the point event *M*, seen from 1, is:

$$\mathbf{x}_1^0 = \left[\exp(\mathbf{x})\right]^{-1/2}\exp(\mathrm{x}_1)\left[\exp(\mathbf{x})\right]^{-1/2}. \quad (30)$$

The position of the point event *M*, seen from *P*, is:

$$\mathbf{x}_1^2 = \left[\exp(\mathbf{x}_2)\right]^{1/2}\left[\exp(\mathbf{x})\right]^{-1/2}\exp(\mathrm{x}_1)\left[\exp(\mathbf{x})\right]^{-1/2}\left[\exp(\mathrm{x}_2)\right]^{1/2}. \quad (31)$$

And we have, since the determinant of a product is the product of the determinants:

$$\det\left(\mathbf{x}_2^1\right) = \mathrm{e}^{a+y}\mathrm{e}^{-a}\mathrm{e}^{2(a+y)}\mathrm{e}^{-a}\mathrm{e}^{a+y} = \mathrm{e}^{2(a+y+y)},$$

$$\det\left(\mathbf{x}_1^2\right) = \mathrm{e}^{a+y}\mathrm{e}^{-a}\mathrm{e}^{2(a+y)}\mathrm{e}^{-a}\mathrm{e}^{a+y} = \mathrm{e}^{2(a+y+y)}. \quad (32)$$

Therefore at each point-event, when a photon is absorbed at the local time $a+y$, each observer sees the absorption of his photon as preceding, with the same length of time *y*, the arrival of the photon for the other observer: the absorption of the other photon is in the future of each observer, not at the moment of arrival. This strange result seems very similar to the fact that each observer sees any length shorter for a moving object: an observer in the moving object also sees the other observer as moving, thus with shorter length. The paradox is that a measurement made on either of the particles apparently collapses the state of the entire entangled system and does so *instantaneously*, before any information about the measurement result could have been communicated to the other particle. Our previous calculation shows the key of the paradox: the instantaneous character of the measurement is simply false, the "collapse" of the quantum wave only results from the supposition (without any mathematical proof) that this situation may be described by a tensor product of Hilbert spaces. Attention! We don't deny quantum entanglement; we say that the paradox is only in the interpretation of this situation by a non-relativistic Hermitian theory, whereas physics must account for this: each "fixed" observer is journeying in time on the space-time manifold, even if he does not travel in space.

The understanding of the true geometry of space-time simply requires the use of the space-time manifold itself, not merely the use of a flat tangent space-time at the particular point-event *O*. The main difference between the flat space-time of restricted relativity and the space-time manifold as part of the Cl_3^* Lie group is the fact that the light cone is not included in the manifold: it is the single boundary of the manifold, included only in the Lie algebra Cl_3. This was difficult to detect, because the only indication to see this inclusion was the two-valued representation of rotations in quantum mechanics.

Einstein, Podolsky and Rosen said [19]: "From this follows that either: 1) the quantum-mechanical description of reality given by the wave function is not complete or 2) when the operators corresponding to two physical quantities do not commute the two quantities cannot have simultaneous reality. For if both of

them had simultaneous reality—and thus definite values—these values would enter into the complete description, according to the condition of completeness."

Experiments with the polarization of two photons simultaneously emitted can neither prove (1) nor (2) because the absorption of these photons cannot be simultaneous at the points where each absorption is effective. The quantum wave used in [14], with value in $\mathrm{End}\left(Cl_3\right)$, not only with value in $\mathbb{C}$, is enough to prove that (1) was true in 1935, independently of what we now think about (2). More generally no contradiction can exist between general relativity and quantum mechanics. Any apparent contradiction results from bad approximations of relativistic laws.

3.3. The Time Arrow and the Expansion of the Universe

Any point of the space-time manifold is at a position:

$$X = l_a \exp\left(a + b\mathbf{u}\right) = l_a\left(A + B\mathbf{u}\right); A = \mathrm{e}^a \cosh\left(b\right); B = \mathrm{e}^a \sinh\left(b\right). \tag{33}$$

Then the time position $l_a \mathrm{e}^a \cosh\left(b\right)$ is the product of positive real numbers: time is an oriented quantity, **the time arrow has a geometric root**. The A variable goes from 0 to $+\infty$.

Now we consider a photon received at this position X, coming from a distant galaxy, for instance with the σ_1 direction. It was emitted at the position:

$$l_a \exp\left[a - y + \left(bx^1 - y\right)\sigma_1 + b\left(x^2\sigma_2 + x^3\sigma_3\right)\right] = l_a \exp\left(a_1 + b_1\mathbf{u}_1\right), \tag{34}$$

with[2]

$$\begin{gathered} a_1 = a - y; \mathbf{u}_1 = x_1^1\sigma_1 + x_1^2\sigma_2 + x_1^3\sigma_3; \left(x_1^1\right)^2 + \left(x_1^2\right)^2 + \left(x_1^3\right)^2 = 1, \\ \left(x^1 - y/b\right)^2 + \left(x^2\right)^2 + \left(x^3\right)^2 = 1 - 2x^1 y/b + \left(y/b\right)^{22}, \\ b_1 = b\sqrt{1 - 2x^1 y/b + \left(y/b\right)^2}; \mathbf{u}_1 = \frac{\left(x^1 - y/b\right)\sigma_1 + x^2\sigma_2 + x^3\sigma_3}{\sqrt{1 - 2x^1 y/b + \left(y/b\right)^2}}. \end{gathered} \tag{35}$$

The photon was emitted at:

$$x_e = l_a \mathrm{e}^{a_1}\left[\cosh\left(b_1\right) + \sinh\left(b_1\right)\mathbf{u}_1\right]. \tag{36}$$

At this point-event the local time was $t_e = l_a \mathrm{e}^{a_1}\cosh\left(b_1\right) \approx l_a \mathrm{e}^{a_1 + b_1}/2$. The same photon is absorbed at the point-event X, then at the local time $t_a = l_a \mathrm{e}^a \cosh\left(b\right) \approx l_a \mathrm{e}^{a+b}/2$. The only constant object of this geometry is the Lie algebra: each local tangent space, in each point of the manifold, is isomorphic to the Lie algebra of the group. We will then suppose that:

$$\mathrm{d}\left(a_1 + b_1\right) = \mathrm{d}\left(a + b\right); \frac{\mathrm{d}t_e}{t_e} = \frac{\mathrm{d}t_a}{t_a} \tag{37}$$

And we have:

[2]Since we now look at past, $a_1 < a$.

$$\frac{\nu_a}{\nu_e}=\frac{\mathrm{d}t_e}{\mathrm{d}t_a}. \tag{38}$$

In first approximation, $b_1\approx b$, we obtain:

$$\frac{1}{1+z}=\frac{\nu_a}{\nu_e}=\frac{\mathrm{d}t_e}{\mathrm{d}t_a}=\frac{\mathrm{d}\left[l_a\mathrm{e}^{a_1}\cosh\left(b_1\right)\right]}{\mathrm{d}\left[l_a\mathrm{e}^{a}\cosh\left(b\right)\right]}\approx\frac{l_a\mathrm{d}a\mathrm{e}^{a-y}\cosh\left(b\right)}{l_a\mathrm{d}a\mathrm{e}^{a}\cosh\left(b\right)}=\frac{1}{\mathrm{e}^{y}}\approx\frac{1}{1+y}. \tag{39}$$

This means that the redshift, previously interpreted as a Doppler effect, due to the expansion of the universe, is a direct effect of the geometry of space-time, and the z parameter, defined as $\left(\nu_e-\nu_a\right)/\nu_a$, is almost equal to y. But this is true only as a crude approximation, or as a false velocity. When y is small this redshift seems proportional to y. The Hubble parameter (73.3 ± 1.4 km/s/Mpc) gives for the distance 1 Mpc the value $z=0.0002443$, thus giving $R=l_a\mathrm{e}^{a+b}/2\approx 6.3\times10^{25}\ \mathrm{m}$.

Using the geometric condition (37), which results from the Lie algebra as the only fixed framework, independent from the space-time position on the manifold, we may calculate more precisely the ratio $\mathrm{d}t_e/\mathrm{d}t_a$ in the case where y is small. We have:

$$\frac{\mathrm{d}\left[l_a\mathrm{e}^{a_1}\cosh\left(b_1\right)\right]}{\mathrm{d}\left[l_a\mathrm{e}^{a}\cosh\left(b\right)\right]}=\frac{\mathrm{d}\left[\mathrm{e}^{a-y}\cosh\left(b_1\right)\right]}{\mathrm{d}\left[\mathrm{e}^{a}\cosh\left(b\right)\right]}=\frac{\mathrm{e}^{-y}\cosh\left(b_1\right)}{\cosh\left(b\right)}=\frac{1}{f\left(y\right)} \tag{40}$$

$$f\left(y\right):=\mathrm{e}^{y}\frac{\cosh\left(b\right)}{\cosh\left(b_1\right)}\approx f\left(0\right)+yf'\left(0\right)+y^2\frac{f''\left(0\right)}{2}+\cdots \tag{41}$$

We use:

$$b_1:=bg\left(y\right)=\sqrt{b^2-2x^1by+y^2};\ g\left(y\right)=\sqrt{1-2\frac{x^1}{b}y+\left(\frac{y}{b}\right)^2},$$

$$g\left(y\right)\approx1-\frac{x^1}{b}y+\frac{1-\left(x^1\right)^2}{2b^2}y^2+\frac{x^1\left[1-\left(x^1\right)^2\right]}{2b^3}y^3+\cdots. \tag{42}$$

And we obtain:

$$f\left(y\right)\approx\mathrm{e}^{y}\frac{\mathrm{e}^{b}}{\mathrm{e}^{b_1}}=\mathrm{e}^{a(y)} \tag{43}$$

$$a\left(y\right)=y+b-b_1\approx\left(1+x^1\right)y-\frac{1-\left(x^1\right)^2}{2b}y^2-\frac{x^1\left[1-\left(x^1\right)^2\right]}{2b^2}y^3+\cdots,$$

$$f'\left(y\right)\approx a'\left(y\right)\mathrm{e}^{a(y)}=\left(1+x^1\right)\left[1-\frac{1-x^1}{b}y-\frac{3x^1\left(1-x^1\right)}{2b^2}y^2+\cdots\right]\mathrm{e}^{a(y)}. \tag{44}$$

From values of the Hubble parameter and of l_a we obtain $a+b\approx142$. We only know that $a>b>0$. The ratio a/b is unknown. If our position in the manifold is anywhere, for instance is $\left(a+b\right)/a\approx a/b$, we could have $a\approx88$ and $b\approx54$. This should give a ratio B/A very close to 1. We now look at the acceleration or deceleration of the expansion.

3.4. Beginning of the Acceleration

Defining h such that $h(y) := f(y)/y$ the redshift seems accelerated if and only if h is increasing, hence if $h'(y) > 0$. We obtain:

$$y^2 h'(y) = y f'(y) - f(y) \approx \left[y a'(y) - 1 \right] \mathrm{e}^{a(y)} = \left[-1 + \left(1 + x^1\right) y - \frac{1 - \left(x^1\right)^2}{b} y^2 - \frac{3x^1 \left[1 - \left(x^1\right)^2 \right]}{2b^2} y^3 + \cdots \right] \mathrm{e}^{a(y)}. \quad (45)$$

For instance if $b = 40$ and $x^1 = 0.6$ we have:

$$y^2 h'(y) \approx \left[-1 + 1.6y - 0.016y^2 - 0.00036y^3 + \cdots \right] \mathrm{e}^{a(y)} \quad (46)$$

Thus, in this case, $h'(y) > 0$ if and only if

$$y > y_0, \; y_0 \approx 0.63. \quad (47)$$

Moreover the sign of the coefficient of y^3 indicates a sign change for large y, but the method of calculation used here does not give the value of this new change of sign.

Hence the acceleration of the expansion seems to begin near y_0, with possible differences depending on the directions of observation. And the expansion seems to decelerate for very large z. Thus there is no need for either black matter (but the movement of stars in galaxies and the movement of galaxies in galaxy clusters is another question) or repulsive gravity to explain all modern observations of cosmological redshifts.

4. Conclusions

The expansion of the Universe, as resulting of the geometry of the whole spacetime, is much more satisfying than cosmological models issued from the hypothesis of a homogeneous and uniform density of matter at a large scale:

1) We obtain, without any other hypothesis than (37), an acceleration of the expansion with a beginning of this acceleration.

2) Since the main part of the expansion is not linked to the density of matter, the cosmic microwave background is necessarily uniform, its non uniformity coming only from the non uniformity of the density of matter. This non-uniformity is automatic since gravitation is highly nonlinear.

3) The hypothesis of uniformity of the matter density at a very large scale is contrary to all observations of modern astronomers [20].

4) We know that there is not enough ordinary matter to satisfy an expansion ruled by gravitation, and no satisfying supplementary matter has been found.

Conflicts of Interest

The authors declare no conflicts of interest regarding the publication of this paper.

References

[1] Daviau, C. (1996) Dirac Equation in the Clifford Algebra of Space. Springer, Boston, 67-88. https://doi.org/10.1007/978-94-011-5036-1_8

[2] Daviau, C. (1997) *Annales de la Fondation Louis de Broglie*, **22**, 87-103. https://doi.org/10.3406/rde.1997.1378

[3] Daviau, C. (1998) *Annales de la Fondation Louis de Broglie*, **23**, 27-37.

[4] Daviau, C. (2005) *Annales de la Fondation Louis de Broglie*, **30**, 409-428. https://fondationlouisdebroglie.org/AFLB-303/aflb303m398.htm

[5] Daviau, C. and Bertrand, J. (2014) New Insights in the Standard Model of Quantum Physics in Clifford Algebra. Je Publie, Pouillé-les-coteaux. https://hal.archives-ouvertes.fr/hal-00907848v1 https://doi.org/10.1142/9780

[6] Daviau, C. and Bertrand, J. (2014) *Journal of Modern Physics*, **5**, 1001-1022. https://doi.org/10.4236/jmp.2014.511102

[7] Daviau, C. and Bertrand, J. (2014) *Journal of Modern Physics*, **5**, 2149-2173. https://doi.org/10.4236/jmp.2014.518210

[8] Daviau, C. and Bertrand, J. (2015) *Annales de la Fondation Louis de Broglie*, **40**, 181-209.

[9] Daviau, C. and Bertrand, J. (2015) *Journal of Modern Physics*, **6**, 2080-2092. https://doi.org/10.4236/jmp.2015.614215

[10] Daviau, C. and Bertrand, J. (2015) *Journal of Applied Mathematics and Physics*, **3**, 46-61. https://doi.org/10.4236/jamp.2015.31007

[11] Daviau, C. and Bertrand, J. (2016) The Standard Model of Quantum Physics in Clifford Algebra. World Scientific, Singapore. https://doi.org/10.1142/9780

[12] Daviau, C. and Bertrand, J. (2016) *Journal of Modern Physics*, **7**, 936-951. https://doi.org/10.4236/jmp.2016.79086

[13] Daviau, C., Bertrand, J., Socroun, T. and Girardot, D. (2019) Modèle Standard et Gravitation. Presses des Mines, Paris.

[14] Daviau, C., Bertrand, J., Socroun, T. and Girardot, D. (2020) Developing a Theory of Everything. Annales de la Fondation Louis de Broglie, Paris. https://fondationlouisdebroglie.org/MEMOS/ToEAFLB.pdf

[15] Daviau, C., Bertrand, J., Socroun, T. and Girardot, D. (2022) Developing the Theory of Everything. Annales de la Fondation Louis de Broglie, Paris. https://www.researchgate.net/publication/362092441_Developing_the_Theory_of_Everything

[16] Dirac, P.A.M. (1928) *Proceedings of the Royal Society of London. Series A*, **117**, 610-624. https://doi.org/10.1098/rspa.1928.0023

[17] Dirac, P.A.M. (1928) *Proceedings of the Royal Society of London. Series A*, **118**, 351-361. https://doi.org/10.1098/rspa.1928.0056

[18] Daviau, C. and Bertrand, J. (2022) Sur la construction de l'espace-temps. Annales de la Fondation Louis de Broglie.

[19] Einstein, A., Podolsky, B. and Rosen, N. (1935) *Physical Review*, **47**, 777-780. https://doi.org/10.1103/PhysRev.47.777

[20] Courtois, H. (2016) Voyage sur les flots de galaxies, Quai des sciences. Dunod, Paris.

Journal of Modern Physics, 2022, 13, 1157-1166
https://www.scirp.org/journal/jmp
ISSN Online: 2153-120X
ISSN Print: 2153-1196

Enhanced Transport of Overdamped Particles in a Disordered Biased Periodic Potential

Meng Hu[1,2]

[1]Department of Mathematics and Physics, North China Electric Power University, Baoding, China
[2]Hebei Key Laboratory of Physics and Energy Technology, North China Electric Power University, Baoding, China
Email: humeng@ncepu.edu.cn

How to cite this paper: Hu, M. (2022) Enhanced Transport of Overdamped Particles in a Disordered Biased Periodic Potential. *Journal of Modern Physics*, **13**, 1157-1166.
https://doi.org/10.4236/jmp.2022.138067

Received: July 14, 2022
Accepted: August 12, 2022
Published: August 15, 2022

Abstract

This paper considers the diffusive properties of Brownian motion driven by an Ornstein-Uhlenbeck (OU) colored noise in a biased periodic potential corrugated by spatial disorders in the form of zero-mean random correlated potential. Through Langevin Monte-Carlo simulation, a giant enhancement diffusion is observed in a range of bias forces. Then, theoretical analysis based on the trajectory of a particle in the random correlated potential (RCP) is performed to investigate the transport phenomenon of particles. The effective diffusion coefficient is measured by the envelope width of the spatial distribution of the particle, and it becomes wider due to the emergence of the RCP. This is because the roughness of the potential causes a large proportion of the test particles to be locked or trapped. Furthermore, the positive-correlation characteristics of the OU noise are considered, and the optimal value of the effective diffusion coefficient is discussed.

Keywords

Diffusion, Enhancement Phenomenon, the Random Correlated Potential, Roughness

1. Introduction

The dynamics of Brownian particles in a biased periodic potential is a basic non-equilibrium model of statistical physics. It describes a surprising range of physical situations, including the Josephson junctions [1], diffusion of atoms and molecules on the crystal surface [2], superionic conductors [3], and cold atoms dwelling in optical lattices [4] [5]. This model is simple but has a rich phenomenology as a nonlinear stochastic system [6]. Diffusion of a particle driven by

white noise in the one-dimensional or two-dimensional biased periodic potential has been investigated in [7] [8] [9] [10], where the effective diffusion coefficient is greatly enhanced and even quantitatively larger than that in the case of free diffusion. The above results can be explained by a simple two-state theory, *i.e.*, test particles exit a locked state or a running state and transfer between each other. However, some disorders should be imposed on such periodic potential to study more realistic reactions such as the protein folding, where the potential surface may have a hierarchical structure [11]-[16].

In recent decades, the random correlated potential (RCP), which is formed of wells and hills and whose location and magnitude are random quantities, attracts much attention [17]. It has been applied to various disordered media [18]-[24], especially the motion of colloidal particles in both experimental observation and numerical simulation [25]. The asymptotical behavior of a force-free particle in the RCP is sub-diffusion at a low temperature. This is caused by a reduction of the kinetic energy related to both friction and the RCP [26]. Meanwhile, it has been pointed out that a nail effect induced by the roughness in a metastable potential leads to an opposite-Arrhenius decrease in the rate with the increase of rough intensity [27]. However, not all occurrences of RCP are harmful. Recent studies [26] [28] on the diffusion have indicated that roughness can help to separate the spatial probability peaks at many disordered barriers when the external tilted force approaches the critical value. So, the diffusion is enhanced, and the value of the effective diffusion coefficient is more pronounced than the peak value of the biased periodic potential. Moreover, this behavior has been observed experimentally when tracking the motion of colloidal spheres through a periodic potential [29].

During the last few years, significant progress has been made in understanding diffusion in nonlinear systems driven by colored noise. This problem is critical not only because of its immediate relevance to numerous particular systems but also because the white-noise approximation is an idealization [30] [31]. The Ornstein-Uhlenbeck (OU) colored noise has been widely investigated and discussed. Especially, the correlation underlying the OU noise is exponential and non-negative [32], which implies that the noise stays in one direction and the direction of the following ones will likely remain consistent with it. In addition, the study [33] has demonstrated an enhancement for the effective diffusion coefficient (D_{eff}) of a particle driven by the OU noise in a one-dimensional and two-dimensional periodic potential.

All these studies present interesting viewpoints and inspire our work. The diffusion of a particle driven by the OU colored noise in the biased and disordered periodic potential might be related to the more complex and realistic processes. This paper aims to explore whether an enhancement phenomenon of a particle driven by the OU noise will appear. Meanwhile, it is important to determine the contributions of the RCP superimposed on the potential to the diffusion process.

The rest of this paper is organized as follows. In Section II, the dynamical equations to describe the over-damped particle driven by the OU noise and detailed characterization of the RCP are presented. Then, a numerical study for the motion of a particle embedded in a biased disordered potential under a biasing external force is presented in Section III. Next, the roles of the parameters of RCP and the noise are studied. Finally, in Section V, some comments and conclusions are given.

2. The Model

This paper considers the motion of overdamped independent Brownian particles evolving in a quenched random potential $U(x)$ and subject to a constant external force *F*. In a one-dimensional scenario, each particle obeys the Langevin equation:

$$\gamma \frac{\mathrm{d}x}{\mathrm{d}t} = -\frac{\mathrm{d}U(x)}{\mathrm{d}x} + F + \varepsilon(t), \tag{1}$$

$$\frac{\mathrm{d}\varepsilon}{\mathrm{d}t} = -\frac{1}{\tau}\varepsilon + \frac{\sqrt{2D}}{\tau}\xi(t), \tag{2}$$

where *x* is the reaction coordinate, *t* is the time, γ is the friction coefficient, *F* is the applied external force, *D* represents the intensity of noise; the Gaussian white noise $\xi(t)$ obeys $\langle \xi(t) \rangle = 0$, and $\langle \xi(t)\xi(t') \rangle = \delta(t-t')$; the angular brackets denote statistical averages.

The OU colored noise $\varepsilon(t)$ has a positive correlation function: $\langle \varepsilon(t)\varepsilon(t') \rangle = D/\tau^{-1} \exp(-|t-t'|/\tau)$, where τ is the correlated time of the OU noise. The OU colored noise will be reduced into the white noise when $\tau \to 0$, and the fluctuation vanishes if $\tau \to \infty$. **Figure 1** presents the stochastic trajectories of the OU colored noise under various correlated time. It can be seen that the OU noise exhibits a positive-correlation characteristic, which means that the particle needs more time to reach the stationary position, especially when the correlated time becomes longer.

The potential $U(x)$ consists of a fixed part and a spatially random part, *i.e.*,

$$U(x) = U_f(x) + U_r(x), \tag{3}$$

where the RCP U_r is characterized by its statistics properties. Its mean $\langle U_r(x) \rangle$ is set to zero, and its correlation function given by

$$\begin{aligned} \langle U_r(x)U_r(x') \rangle &= g_0 \exp\left(\frac{-|x-x'|^2}{2\lambda^2} \right), \\ g_0 &= \frac{\varepsilon}{\sqrt{2\pi}\lambda}, \end{aligned} \tag{4}$$

where the angular brackets indicate a spatial average. The characteristic length λ and the effective intensity ε are two basic parameters characterizing the RCP [26] [34]. The RCP can be generated by the method of discrete Fast Fourier Transform (FFT).

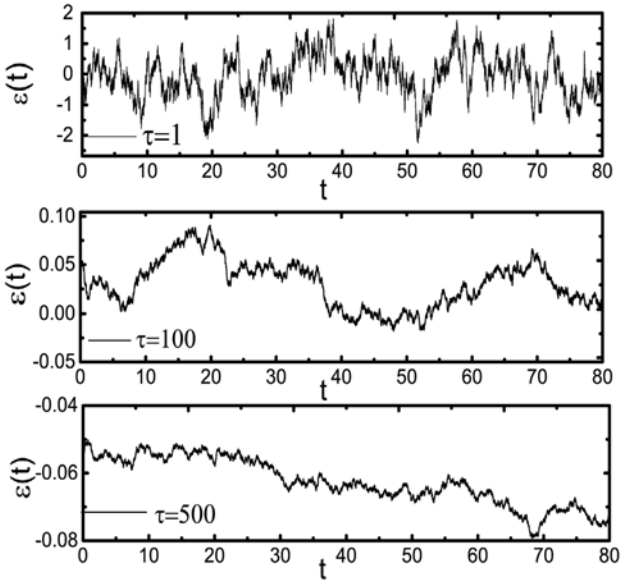

Figure 1. Typical trajectories for the OU noise under various correlated time. The correlated time is $\tau = 1$ (top panel), $\tau = 100$ (middle panel), and $\tau = 500$ (bottom panel), respectively. The parameters used is $D = 0.5$.

The perturbation $U_r(x)$ will be eliminated if $U(x)$ is spatially averaged, and only the smooth background remains. The average of total potential $\langle U(x)\rangle$ over the realization of $U_f(x)$ is set as an periodic potential

$$U_f(x) = -U_0 \cos\left(\frac{2\pi x}{L}\right), \tag{5}$$

where U_0 represents the amplitude strength of the periodic potential, and L represents the spatial period. **Figure 2** shows the realization of the RCP $U_r(x)$ and the background potential $U_f(x)$. It can be seen that there are many barriers in the RCP profile, and the number of barriers increases when the scaled correlation length λ decreases. In contrast, the increase of the intensity g_0 results in deeper wells of the RCP.

3. The Giant Diffusion in Rough Titled Periodic Potential

In our study, the quantity of central interest will be the effective diffusion coefficient. Previous works have shown that it can be expressed as $D_{eff} = \lim_{t\to\infty} \Delta x^2(t)/(2t)$, where $\Delta x^2(t) = \langle x^2(t)\rangle - \langle x(t)\rangle^2$ is the mean square displacement (MSD), and the bracket denotes the average over trajectories [8]. The approach of double-averaging over statistic ensemble and test particles is adopted to calculate the coordinate variance when the RCP is added [27]. The Time-dependent MSD is determined numerically by

$$\langle \Delta x^2(t)\rangle = \frac{1}{K}\sum_{j=1}^{K}\langle \Delta x_i^2(t)\rangle_j, \tag{6}$$

$$\langle \Delta x_i^2(t)\rangle_j = \frac{1}{N}\sum_{i=1}^{N}\left[\langle x_i^2(t)\rangle - \langle x_i(t)\rangle^2\right]_j, \tag{7}$$

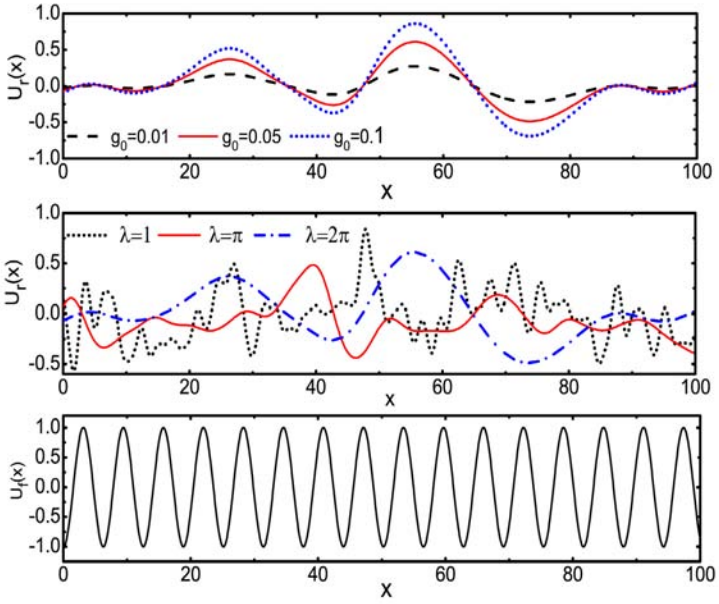

Figure 2. The realization of the RCP $U_r(x)$ and the background potential $U_f(x)$. The parameters used are $g_0 = 0.01$, 0.05, and 0.1 at fixed $\lambda = 2\pi$ (top panel); $\lambda = 1$, π, and 2π at fixed $g_0 = 0.1$ (middle panel); $U_0 = 1$ and $L = 2\pi$ (bottom panel).

where $\left\langle \Delta x_i^2(t) \right\rangle_j$ is the MSD of the *i*-th test particle for the *j*-th rough titled periodic potential at time *t*. The present Monte Carlo simulations involves the time step $\Delta t = 5\times10^{-3}$, total integration time $N_t = 3\times10^4$, and test particles $N = 10^4$. Besides, the particles are initially located at $x(0) = 0$ for all simulations, and the number of the RCP $K = 100$ is considered to perform double statistical averages.

This part first presents the results under the influence of the external biasing force. In **Figure 3**, the D_{eff} as a function of the tilted force F for different g_0 is depicted. Meanwhile, the diffusion behavior of the particle driven by the white noise corresponding to the case of $\tau \to 0$ is shown. The test particles cannot be trapped in well and diffuse freely when the periodic potential is tilted with its local minima disappearing; the motion of the particle is locked only when the tilted force is small. However, a particle experiences diffusion for a medium tilted force *F*, and it exhibits two spatial motion modes: the compact running state and the locked behind state. These two modes coexist and transform, leading to an increase in the effective coefficient of the diffusion. Furthermore, due to the positive correlation characteristic of the OU noise, the diffusion is enhanced, as demonstrated in the subgraph of **Figure 3(a)**. The correlation effect of the noise is beneficial to biased diffusion.

This paper pays more attention to the influence of the roughness of the potential, especially the intensity g_0 that affects the depth of the small potential wells in periodic potential directly. It can be seen from **Figure 3** that D_{eff} increases as the value of g_0 increases. The distinct potential wells will become deeper due to the emergence of the RCP, which results in a large proportion of the test particles

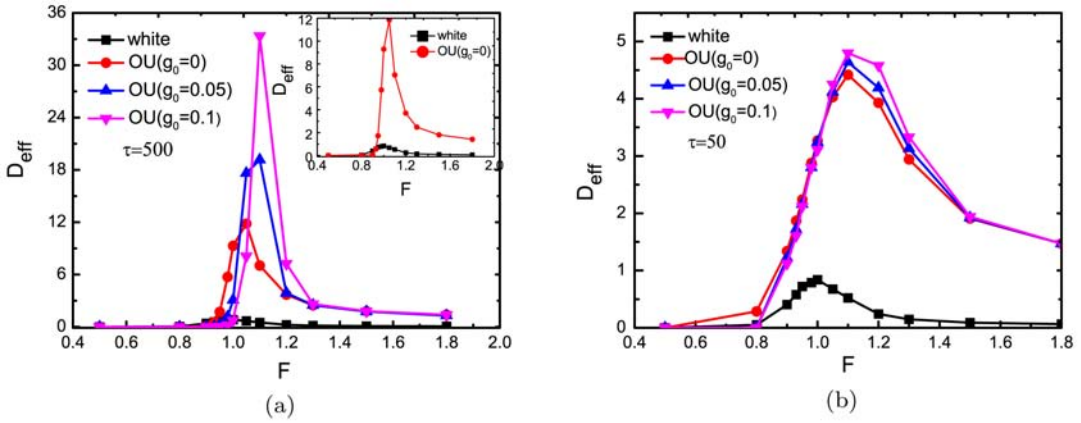

Figure 3. The effective diffusion coefficient D_{eff} as a function of F for different roughness g_0 with the correlated time of the OU noise. The applied parameters are $\lambda = 2\pi$ and $D = 1.0$.

being trapped or locked. This phenomenon is especially pronounced near the critical tilted force F_c, where the value $F_c = 1.0$.

In view of this phenomenon, this paper presents the variation of the diffusion coefficient with the intensity g_0 under different external force values in **Figure 4**. For a small F, the value of D_{eff} decreases as the intensity g_0 increases. Due to the introduction of the RCP, the test particles are almost trapped in a distinct potential well. The locked state does not disappear in the absence of the RCP until the tilted force reaches the critical value. However, due to the existence of RCP, the local minima still exist, and the probability peaks are distributed at the potential barriers even if the external force is greater than the critical value F_c. The number of particles in locked state increases and the particles in the running state also coexist at this time. Thus a giant diffusion appears near the critical force, especially when the value of g_0 increases. The diffusion is also enhanced as the intensity g_0 increase for a larger F comparing with the case when F is small. Similarly, the probability of a particle locked in local minima of the potential increases when g_0 is large. However, due to the large tilting force, the number of the local minima in the potential will decrease, which leads to a reduction of the D_{eff} comparing with the case when F is near the critical value. Moreover, the occurrence of the RCP is not always harmful, which can be a promotion for the movement of particles under the right conditions.

Note that this paper takes two different types of correlated time as examples in **Figure 3** and **Figure 4**. The correlated time τ of the noise also affects the value of the diffusion coefficient. In this regard, this paper conducts a further in-depth study, and the results are illustrated in **Figure 5**. It can be seen that the effective diffusion coefficient D_{eff} does not depend monotonically on the correlated time τ, and there exists an optimal τ that makes the effective diffusion coefficient maximum. In addition, the value of D_{eff} induced by the OU colored noise in the rough potential with a finite τ is larger than that in the tilted periodic potential $g_0 = 0$ under the condition of $F = F_c = 1.0$. When the value of τ is small, the correlation of the noise is weak. As the correlated time increases, the constant

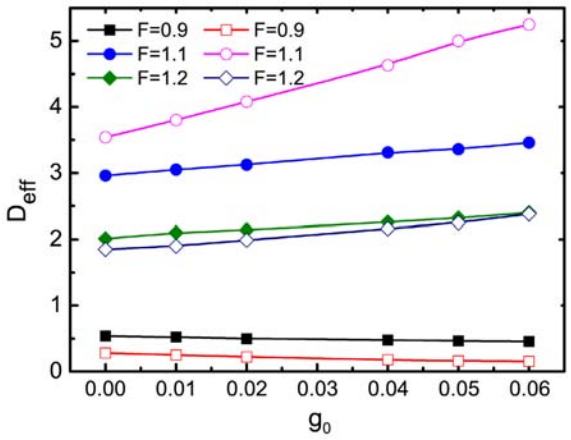

Figure 4. The D_{eff} as a function of g_0 for different correlated time τ, where the solid and open symbols correspond to $\tau = 50$ and $\tau = 100$ respectively. The parameters used are $\lambda = 2\pi$ and $D = 0.5$.

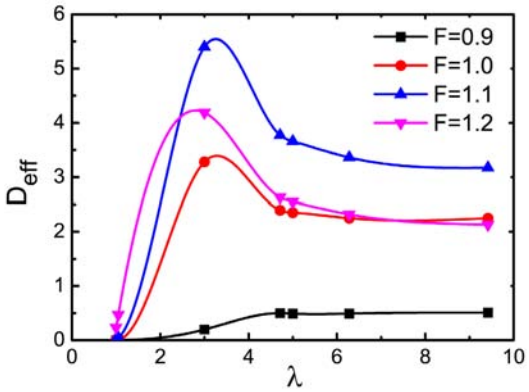

Figure 5. The D_{eff} as a function of τ for different values of roughness g_0 and external force F. The parameters used are $\lambda = 2\pi$ and $D = 1.0$.

driving force increases the kinetic energy of the particle, and thus the particle can move and transfer into the running state. At this time, the envelope width of the spatial distribution of the particle can measures the size of D_{eff}. However, the width of this spatial distribution will shrink when the value of τ is large. For example, $F = 1.0$, $g_0 = 0.05$, and this is because the probability of a particle in the locked state increases. If the value of τ is large enough, all particles will be locked in the located state, and the diffusion coefficient decays to zero.

The correlation length λ, as an important parameter in RCP, also affects the diffusion behavior of the particle. The calculations show that D_{eff} is a non-monotonic function of λ, as shown by Figure 6. From the discussions above, it can be seen that the roughness of the potential helps to separate the peaks of the spatial distribution of the particle around the disordered barrier. Meanwhile, the value of λ directly determines the number of small potential wells. When the value of λ is small, the number increases, causing many particles to be trapped in a small barrier and a locked state. Therefore, the phenomenon of diffusion is not obvious at this time. By contrast, when the value of λ is large, the number of

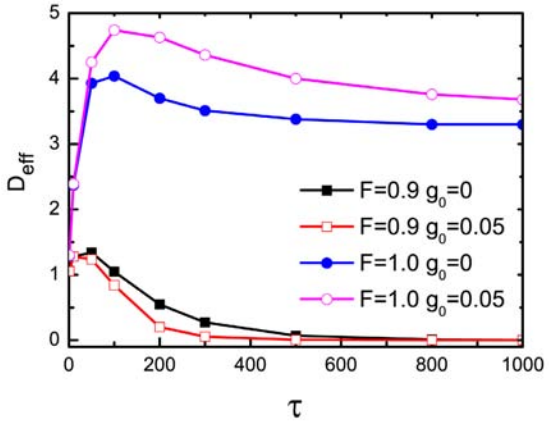

Figure 6. The effective diffusion coefficient D_{eff} as a function of λ for different values of the external force F. The applied parameters are $\lambda = 2\pi$ and $D = 1.0$.

small potential wells will become smaller, as shown by **Figure 5**. In this case, the RCP has little effect on the diffusion of the particles. The coexistence of the locked state and the running state is beneficial to the biased diffusion when λ takes the proper value.

4. Summary

This work explores the diffusive properties of overdamped Brownian motion driven by an Ornstein-Uhlenbeck noise in a biased periodic potential corrugated by the spatial disorder. As for the influence of the roughness of the potential, the rough potential is not conducive to directional transport. However, an enhancement for the effective diffusion coefficient of a particle can be observed when the tilted force is close to the critical value. Particularly, this enhancement is sensitive to the two parameters of the RCP: the correlation length λ and the intensity g_0. The number of the local minima may increase as the roughness decreases. Also, the distinct potential wells become deeper with a larger value of g_0. These all cause a large proportion of the test particles to be trapped or locked, and the whole distribution of the particle forms a wider envelope width. At this time, the effective diffusion coefficient D_{eff} is enhanced. Furthermore, D_{eff} varies non-monotonically with correlated time τ. The probability of a particle in a locked state increases under the effect of the OU noise, which exhibits a positive correlation. Therefore, the diffusion can be enhanced under the co-modulation of these parameters, and even the appearance of non-monotonicity depends on a certain parameter.

Thus, the introduction of roughness can be used to promote the movement of particles under the right conditions. Our results provide a better understanding of the complex transport phenomenon of particles in a rough potential, which may provide useful information for some realistic but complicated problems.

Acknowledgements

This work was supported by the National Natural Science Foundation of China

under Grant No. 11905062 and the Fundamental Research Funds for the Central Universities under Grant No. 2019MS115.

Conflicts of Interest

The author declares no conflicts of interest regarding the publication of this paper.

References

[1] Longobardi, L, Massarotti, D., Rotoli, G., Stornaiuolo, D., Papari, G., Kawakami, A., *et al.* (2011) *Physical Review B*, **84**, Article ID: 184504. https://doi.org/10.1103/PhysRevB.84.184504

[2] Frenken, J.W.M. and Van der Veen, J.F. (1985) *Physical Review Letters*, **54**, 134-137. https://doi.org/10.1103/PhysRevLett.54.134

[3] Fulde, P., Pietronero, L., Schneider, W.R. and Strassler, S. (1975) *Physical Review Letters*, **35**, 1776-1779. https://doi.org/10.1103/PhysRevLett.35.1776

[4] Curtis, J.E. and Grier, D.G. (2003) *Physical Review Letters*, **90**, Article ID: 133901. https://doi.org/10.1103/PhysRevLett.90.133901

[5] Guo, C.-S., liu, X., He, J.L., and Wang, H.T. (2004) *Optics Express*, **12**, 4625-4634. https://doi.org/10.1364/OPEX.12.004625

[6] Regtmeier, J., Duong, T.T., Eichhorn, R., Anselmetti, D. and Ros, A. (2007) *Analytical Chemistry*, **79**, 3925-3932. https://doi.org/10.1021/ac062431r

[7] Reimann, P., Van den Broeck, C., Linke, H., Hänggi, P., Rubi, J.M. and Pérez-Madrid, A. (2001) *Physical Review Letters*, **87**, Article ID: 010602. https://doi.org/10.1103/PhysRevLett.87.010602

[8] Reimann, P., Van den Broeck, C., Linke, H., Hänggi, P., Rubi, J.M. and Pérez-Madrid, A. (2002) *Physical Review E*, **65**, Article ID: 031104. https://doi.org/10.1103/PhysRevE.65.031104

[9] Bao, J.-D. and Lu, K. (2007) *Physical Review E*, **76**, Article ID: 061119. https://doi.org/10.1103/PhysRevE.76.061119

[10] Reimann, P. and Eichhorn, R. (2008) *Physical Review Letters*, **101**, Article ID: 180601. https://doi.org/10.1103/PhysRevLett.101.180601

[11] Khoury, M., Lacasta, A.M., Sancho, J.M. and Linderberg, K. (2011) *Physical Review Letters*, **106**, Article ID: 090602. https://doi.org/10.1103/PhysRevLett.106.090602

[12] Bryngelson, J.D. and Wolynes, P.G. (1989) *The Journal of Physical Chemistry*, **93**, 6902-6915. https://doi.org/10.1021/j100356a007

[13] Pollak, E., Auerbach, A. and Talkner, P. (2008) *Biophysical Journal*, **95**, 4258-4265. https://doi.org/10.1529/biophysj.108.136358

[14] Agudov, N. and Spagnolo, B. (2001) *Physical Review E*, **64**, Article ID: 035102. https://doi.org/10.1103/PhysRevE.64.035102

[15] Dubkov, A.A., Agudov, N.V. and Spagnolo, B. (2004) *Physical Review E*, **69**, Article ID: 061103. https://doi.org/10.1103/PhysRevE.69.061103

[16] Nevo, R., Brumfeld, V., Kapon, R., Hinterdorfer, P. and Reich, Z. (2005) *EMBO Reports*, **6**, 482-486. https://doi.org/10.1038/sj.embor.7400403

[17] Lee, K.L., Grémaud, B. and Miniatura, C. (2014) *Physical Review A*, **90**, Article ID: 043605. https://doi.org/10.1103/PhysRevA.90.043605

[18] Simon, M.S., Sancho, J.M. and Lindenberg, K. (2013) *Physical Review E*, **88**, Article

ID: 062105. https://doi.org/10.1103/PhysRevE.88.062105

[19] Blanter, Y.M. and Vinokur, V.M. (2002) *Physical Review B*, **66**, Article ID: 132101. https://doi.org/10.1103/PhysRevB.66.132101

[20] Chechkin, A.V., Seno, F., Metzler, R. and Sokolov, I.M. (2017) *Physical Review X*, **7**, Article ID: 021002. https://doi.org/10.1103/PhysRevX.7.021002

[21] Sune Simon, M., Sancho, J.M. and Lindenberg, K. (2016) *The European Physical Journal B*, **89**, Article No. 79. https://doi.org/10.1140/epjb/e2016-60963-3

[22] Camboni, F. and Sokolov, I.M. (2012) *Physical Review E*, **85**, Article ID: 050104. https://doi.org/10.1103/PhysRevE.85.050104

[23] Bewerunge, J., Ladadwa, I.,Platten, F., Zunke, C., Heuer, A., and Egelhaaf, S.U. (2016) *Physical Chemistry Chemical Physics*, **18**, 18887-18895. https://doi.org/10.1039/C6CP02559E

[24] Kong, M. and Van Houten, B. (2016) *Progress in Biophysics and Molecular Biology*, **127**, 93-104. https://doi.org/10.1016/j.pbiomolbio.2016.12.004

[25] Lee, S.H. and Grier, D.G. (2006) *Physical Review Letters*, **96**, Article ID: 190601. https://doi.org/10.1103/PhysRevLett.96.190601

[26] Romero, A.H. and Sancho, J.M. (1998) *Physical Review E*, **58**, 2833-2837. https://doi.org/10.1103/PhysRevE.58.2833

[27] Hu, M. and Bao, J.-D. (2018) *Physical Review E*, **97**, Article ID: 062143. https://doi.org/10.1103/PhysRevE.97.062143

[28] Lacasta, A.M., Sancho, J.M., Romero, A.H., Sokolov, I.M. and Lindenberg, K. (2004) *Physical Review E*, **70**, Article ID: 051104. https://doi.org/10.1103/PhysRevE.70.051104

[29] Hanes, R.D. and Egelhaaf, S.U. (2012) *Journal of Physics*: *Condensed Matter*, **24**, Article ID: 464116. https://doi.org/10.1088/0953-8984/24/46/464116

[30] Dykman, M.I., McClintock, P.V.E., Stein, N.D. and Stocks, N.G. (1991) *Physical Review Letters*, **67**, 933-936. https://doi.org/10.1103/PhysRevLett.67.933

[31] Bao, J. -D. and zhuo, Y. -Z. (2003) *Physical Review Letters*, **91**, Article ID: 138104. https://doi.org/10.1103/PhysRevLett.91.138104

[32] Eliazar, I. and Klafter, J. (2009) *Physical Review E*, **79**, Article ID: 021115. https://doi.org/10.1103/PhysRevE.79.021115

[33] Shi, X.-Y. and Bao, J.-D. (2019) *Physica A*: *Statistical Mechanics and Its Applications*, **514**, 203-210. https://doi.org/10.1016/j.physa.2018.09.017

[34] Simon, M.S., Sancho, J.M. and Lacasta, A.M. (2012) *Fluctuation and Noise Letters*, **11**, Article ID: 1250026. https://doi.org/10.1142/S0219477512500265

Journal of Modern Physics, 2022, 13, 1167-1183
https://www.scirp.org/journal/jmp
ISSN Online: 2153-120X
ISSN Print: 2153-1196

Exceedingly Small Quantum of Time Kshana Explains the Structure of an Electron

Shesharao M. Wanjerkhede

Bidar, India
Email: shesharaomwanjerkhede@gmail.com

How to cite this paper: Wanjerkhede, S.M. (2022) Exceedingly Small Quantum of Time Kshana Explains the Structure of an Electron. *Journal of Modern Physics*, **13**, 1167-1183.
https://doi.org/10.4236/jmp.2022.138068

Received: July 3, 2022
Accepted: August 13, 2022
Published: August 16, 2022

Abstract

In this study, an effort is made to find the attributes of an electron based on Maharishi Vyasa's definition of kshana or moment. Kshana or moment is a very small quanta of time defined by Maharishi Vyasa. It is the time taken by an elementary particle to change the direction from east to north. It is found that the value of a kshana in the case of pair production is approximately 2×10^{-21} sec, and the radius of the spinning electron or positron is equal to the reduced Compton wavelength. The mass of the electron is equal to the codata recommended value of electron mass and time required in pair production is about four kshanas equal to spinning period of an electron. During validation, in case of the photoelectric effect, spectral series of hydrogen atoms, Compton scattering, and the statistical concept of motion of electron, the value of the number of kshanas in a second is the same as that found in pair production.

Keywords

Kshana, Pair Production, Photoelectric Effect, Compton Scattering, Fine Structure Constant

1. Introduction

In this paper, my effort is to find some attributes of electrons based on Maharishi Vyasa's definition of kshana or moment, exceedingly small quanta of time [1] [2]. The attributes of electrons include spin, magnetic moment, fine structure constant α, anomalous magnetic moment, and charge quantization. Various physical parameters of the electron such as charge, mass, as well as the spin angular momentum and the magnetic moment have been measured with great precision [3]. Different properties of electrons have revealed some facts about their size and shape [4].

The radius of electron is the key problem in elementary particle physics [5]. Researchers have made various approaches to give the exact value to its radius. Various theoretical and experimental results show that there are eight diverse types of radii of an electron [4].

For example, classical electron radius, Compton radius (electron), electromagnetic radius (electron) etc. [4]. In the paper, Compton radius of electron is discussed. The radius of the electron is found based on Maharishi Vyasa's definition of kshana [1] [2], where kshana is a very small and indivisible unit of time, and Maharishi Kanada's thought on "cause and effect". Maharishi Kanada says that "the attribute of the cause is found to be present in the effect" ("Kaaranagunapurvakaha kaaryaguno drasthaha" 2.1.24) [6]. Therefore, in case of pair production, in the article, it is assumed that (1) the time period (an attribute) of spinning electron or positron (effect) is the same as that of photon (cause), and (2) electron and positron spin with a relativistic velocity of light [7].

2. Definition of a Very Small Unit Time "Kshana" or "Moment"

Maharishi Vyasa, in his commentary on Patanjali Yoga Sutra, defined a very small unit of time called "kshana" or "moment", which is very small and indivisible [1]. According to him, it is the time taken by an elementary particle to change its direction from east to north [2]. Here, in the article, we assumed that the elementary particle is a spinning electron, as shown in **Figure 1**. When a spinning electron changes direction from east to north, the time taken is "t" units. Then, velocity is

$$v' = \frac{\theta R_s}{t} \text{ m/kshana} \tag{1}$$

where "R_s" is the radius of the spinning electron. According to the Maharishi Vyasa's time, "t" is one "kshana," and $\theta = 90^\circ = \pi/2$ radians, as shown in **Figure 1**. Hence

$$v' = \frac{90^\circ \times R_s}{1} = \frac{\pi \times R_s}{2} \text{ m/kshana} \tag{2}$$

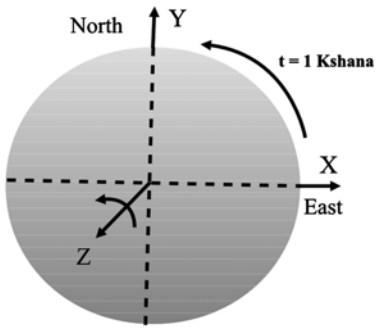

Figure 1. Z is the axis of rotation of a spinning electron, and it changes its direction from east to north. The time taken to change the direction is t = 1 kshana, and for one complete rotation time taken is $T_s = 4$ kshanas.

Similarly, the angular velocity ω' is

$$\omega' = \frac{\theta}{t} = \frac{90^\circ}{1} = \frac{\pi/2}{1} = \frac{\pi}{2}\text{radian/kshana} \tag{3}$$

Substituting the value of π, we obtain ω' = 1.570796326794 radian/kshana. Angular velocity ω' is a constant velocity since π is a constant quantity [2]. Rewriting the Equation (3)

$$1\text{ Moment or kshana} = \frac{\pi/2}{\omega'} = \frac{1.570796326794}{1.570796326794} \tag{4}$$

Thus, 1 moment or 1 kshana is the time taken by a fundamental particle to describe an angle of 90˚ or π/2 radians while changing the direction from "East" to "North" and is just a constant independent of any external forces. Then, from Maharishi Vyasa's definition of kshana [2], we have

$$v' = c' = \frac{2\pi R_s}{T_s} = \frac{2\pi R_s}{4} = \frac{\pi R_s}{2}\text{meter/kshana} \tag{5}$$

where c' meter/kshana is the relativistic velocity of the spinning electron, T_s = 4 kshanas is the time period, and R_s meters is the radius of the spinning electron. The spinning velocity of electrons is equal to the relativistic velocity of light [7] [8]. Therefore, it is assumed that the electron spins with the velocity of light [7].

3. Determination of Number of Kshana in a Second

3.1. Method 1

If there are "n" kshana in a second, then from Equation (5), "n" can be found as shown below:

$$n = \frac{c\text{ m/sec}}{c'\text{ m/kshana}} = \frac{2c}{\pi R_s}\text{kshana/sec} \tag{6}$$

where c is the velocity of light in meters/second and c' is the velocity of light in meters/kshana. Alternatively, we can find the number of kshanas "n" in a second, as shown below:

$$1\text{ kshana} = \frac{T_s}{4} = \frac{2\pi R_s}{4c} = \frac{\pi R_s}{2c}\text{sec} \tag{7}$$

where spinning time period $T_s = 2\pi R_s/c$ sec and 1 kshana = $1/n$ sec. Therefore,

$$n = \frac{2c}{\pi R_s}\text{kshana/sec} \tag{8}$$

Equation (8) is like the Equation (6). Substituting the values for c and π, we have

$$n = \frac{1.9085380\times 10^8}{R_s}\text{kshana/sec} \tag{9}$$

Thus, the number of kshanas "n" in a second is reciprocally related to the radius of the spinning electron R_s.

3.2. Method 2

If T_a is the time period of the electron in the first orbit of the hydrogen atom in sec and T_s is the time period of spinning electrons in sec, then the ratio of time periods is

$$\frac{T_a}{T_s}=\left(\frac{2\pi R_a}{v}\right)\Big/\left(\frac{2\pi R_s}{c}\right)=\frac{R_a c}{R_s v}=\frac{R_a}{\alpha R_s} \tag{10}$$

where R_a, R_s, v, c, and α are the radius of the first orbit of the hydrogen atom in meters, radius of the spinning electron in meters, orbital velocity of the electron in the first orbit of the hydrogen atom in meters per sec, velocity of light in meters per sec, and fine structure constant, respectively. The fine structure constant is $\alpha = v/c$. Rewriting the above equation when time periods $T_a' = nT_a$ and $T_s' = nT_s$ are in kshana, velocities $v' = v/n$ and $c' = c/n$ are in meters/kshana.

$$\frac{T_a'}{T_s'}=\left(\frac{2\pi R_a}{v'}\right)\Big/\left(\frac{2\pi R_s}{c'}\right)=\frac{R_a c'}{R_s v'}=\frac{R_a}{\alpha R_s} \tag{11}$$

where the fine structure constant is also $\alpha = v'/c'$ [2]. If there are "n" kshanas in a second, then 1 sec = n kshanas. Thus, from Equation (11), we have

$$\frac{T_a'}{T_s'}=\frac{nT_a}{T_s'}=\frac{R_a}{\alpha R_s} \tag{12}$$

where orbital time period $T_a' = nT_a$ kshanas and spinning time period $T_s' = nT_s = 4$ kshanas. Rewriting the above equation, we have

$$\frac{nT_a}{4}=\frac{R_a}{\alpha R_s} \tag{13}$$

$$n=\frac{4R_a}{\alpha T_a R_s} \tag{14}$$

But time period for the Bohr first orbit (n = 1), is $T_a = 4\varepsilon_0^2 h^3 / m_0 e^4$ [2] [9]. Substituting this in Equation (14) we have

$$n=\frac{4R_a m_0 e^4}{\alpha 4\varepsilon_0^2 h^3 R_s} \tag{15}$$

But Rydberg constant $R_\infty = m_0 e^4 / 8\varepsilon_0^2 h^3 c$ [2] [9]. Therefore,

$$n=\frac{8R_a c m_0 e^4}{\alpha R_s 8\varepsilon_0^2 h^3 c}=\frac{8R_a R_\infty c}{\alpha R_s}=\frac{k}{R_s} \tag{16}$$

where, $k = 8R_a R_\infty c/\alpha$. Substituting the Bohr radius $R_a = 0.52917721 \times 10^{-10}$ meters, Rydberg constant 10.97373156×10^6/meters, velocity of light $c = 2.99792458 \times 10^8$ meters/sec, and fine structure constant $\alpha = 7.29735256 \times 10^{-3}$ [10], we get $k = 1.90853806 \times 10^8$. Thus, number of kshanas in a second will be

$$n=\frac{1.9085380\times 10^8}{R_s}\text{kshana/sec} \tag{17}$$

Equation (17) is similar to Equation (9) and 1 kshana = $1/n = 0.52396125 \times 10^{-8} R_s$ sec. Thus, the number of kshanas in a second is inversely proportional to the radius of the spinning electron. However, the value of a "kshana" determined

based on the radius of the first orbit of the hydrogen atom is comparatively large [2], and for a large radius, the value of a "kshana" will also be large. Hence divisible, which goes against the definition given by Maharishi Vyasa. Therefore, it becomes necessary to find the value of a "kshana," which is very small, and an indivisible unit of time.

4. Possible Ultimate Indivisible Value of a Kshana

Again, from Equation (16), we can write that

$$n = \frac{8R_a R_\infty c}{\alpha R_s} = \frac{8R_\infty c}{\alpha^2} \text{kshana/sec} \tag{18}$$

where, fine structure constant $\alpha = R_s/R_a$. The ratio of the radius of the sphere (assuming that the electron is a sphere of radius R_s) to the radius of the orbit is equal to the fine structure constant [11]. All the terms on the right-hand side of Equation (18) are constants; hence, the number of kshanas "n" in a second is also constant. Substituting the values of constants R_∞, c, and α, we have $n = 263.1873566 \times 10^{14}/53.2513543849 \times 10^{-6} = 4.94235986370 \times 10^{20}$ kshanas.

Again, from Equation (17) and the value of "n" from Equation (18), which is $4.94235986370 \times 10^{20}$ kshanas, the spinning electron radius R_s will be equal to $3.86159266 \times 10^{-13}$ m, which is also the reduced Compton wavelength [5] [10] [11]. Thus, it is clear that once the exact, ultimate, indivisible value of kshana is known, one can figure out the structure of the electron. From Equation (18), it appears that $1/n = \alpha^2/8R_\infty c$ *i.e.*, 1 kshana $= 2.02332494691 \times 10^{-21}$ sec, may be the ultimate value for a kshana, as defined by Maharishi Vyasa, and this needs further verification by researchers.

5. Validation of Kshana

5.1. Radius, Value of a Kshana in Sec and Mass of a Spinning Electron in Pair Production

In pair production, electromagnetic energy is converted into matter. A gamma ray of sufficient energy creates an electron-positron pair each with a mass equal to the electron mass. If E is the energy of the gamma ray that interacts by pair production, then $E = 2m_0c^2$, where m_0 is the rest mass of the positron or electron and c is the velocity of light. The rest mass energy of the electron or positron is 0.511 MeV so that there is a threshold of 1.022 MeV for this process to take place [12] [13].

The threshold frequency of the gamma ray that undergoes pair production is $\nu = E/h = 1.022$ MeV/h and which is $\nu = 2.4711850260 \times 10^{20}$ Hz.

In the paper, it is assumed that gamma radiation (electromagnetic wave) is present in electrons and positrons [6], as shown in **Figure 2**. As said in the introduction section, the time period (an attribute) of spinning electron or positron (effect) is the same as that of photon (cause), we can calculate the number of wave units (frequency) in an electron by dividing the rest energy of the electron with Planck constant. Therefore, $\nu_1 = 0.511$ MeV/h $= 1.2355925130 \times 10^{20}$

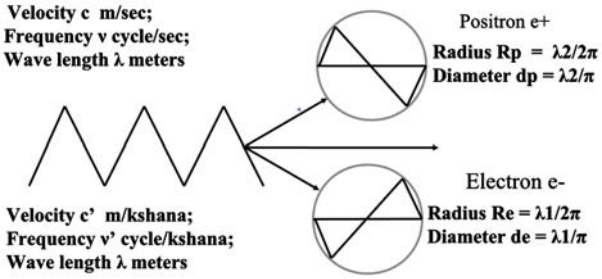

Figure 2. Gamma radiation splits into two equal frequencies with wavelengths equal to $\lambda_1 = \lambda_2$.

wave units [14], which is also equal to $\nu_1 = \nu/2 = 2.4711850260 \times 10^{20}/2 = 1.2355925130 \times 10^{20}$ Hz.

Thus, the frequency associated with electron or positron will be $\nu_1 = 1.235592513 \times 10^{20}$ Hz or cycles/sec, and wavelength will be $\lambda_1 = 2.42631 \times 10^{-12}$ meters.

5.1.1. Radius of a Spinning Electron in a Pair Production

Thus, from Equation (5)

$$c' = \lambda_1 \nu_1' = \frac{\pi R_s}{2} \text{meter/kshana} \tag{19}$$

where ν' cycles/kshana is the frequency of gamma radiation, and R_s meters is the radius of the spinning electron or positron. $T_1' = 1/\nu'$ kshanas is the time period of gamma radiation , which is also equal to the period of the spinning electron. The attributes of gamma rays are assumed to be present in electrons or positrons based on the thoughts of Maharishi Kanada [6].

$$c' = \frac{\lambda_1}{T_1'} = \frac{\pi R_s}{2} \text{meter/kshana} \tag{20}$$

However, from the definition of kshana, the period of spinning electron is $T' = 4$ kshanas. Therefore

$$\frac{\lambda_1}{4} = \frac{\pi R_s}{2} \text{meter/kshana} \tag{21}$$

Thus,

$$R_s = \frac{\lambda_1}{2\pi} \text{meter} \tag{22}$$

Substituting the value of λ_1, we obtain the radius of the spinning electron as $R_s = 3.8615926758 \times 10^{-13}$ meters. The radius R_s can also be found by the law of conservation of energy in the pair production, which is $h\nu_1 = m_0c^2 = 0.51$ MeV [13]. Thus,

$$h\nu_1 = \frac{hc}{\lambda_1} = 0.51 \text{ MeV} \tag{23}$$

$$\frac{hc}{2\pi R_s} = 0.51 \text{ MeV} \tag{24}$$

From Equation (22) substituting the value of λ_1 and the values of other constants in Equation (24), we have

$$R_s = \Lambda_C' = 3.86915646858 \times 10^{-13} \text{ meter} \tag{25}$$

The spinning electron radius (R_s) calculated in Equations (22) and (25) are exactly equal to the reduced Compton wavelength $\Lambda_C' = 3.8615926796\ (12) \times 10^{-13}$ m [10].

5.1.2. Value of a Second in Kshanas

Substituting the value of electron radius from Equation (25) in Equation (9), we have

$$n = \frac{1.90853806367 \times 10^{8}}{3.86915646858 \times 10^{-13}} \text{kshana} \tag{26}$$

Thus, we have $n = 4.942359860 \times 10^{20}$ kshanas and 1 kshana = $2.0233249466 \times 10^{-21}$ sec.

5.1.3. Determination of Planck Constant in Time Unit Kshana

The Planck constant $h = 6.626070040 \times 10^{-34}$ J·sec is converted to a value that has a time unit of kshana instead of sec. Dividing the Planck constant by "n", the new value of h will be

$$h' = \frac{h}{n} = \frac{6.62607004081 \times 10^{-34}}{4.942359860 \times 10^{20}} \text{J} \cdot \text{kshana} \tag{27}$$

Thus, the Planck constant $h' = 1.34066928117 \times 10^{-54}$ J. Kshana.

5.1.4. Determination Velocity of Light and Orbital Velocity of Electron in the First Orbit of Hydrogen Atom in Meters/Kshana

From Equation (5), we have the velocity of light $c' = \pi 3.8615926758 \times 10^{-13}/2 = 6.0657755907 \times 10^{-13}$ meters/kshana. Alternatively, we can find the velocity of light $c' = c/n = 2.99792458 \times 10^{8}/4.942359860 \times 10^{20} = 6.0657755908 \times 10^{-13}$ meters/kshana.

5.1.5. Determination of Absolute Permittivity of the Medium When the Time Unit Is Kshana

In the SI system, the absolute permittivity of the medium is $\epsilon_0 = 8.854187817 \times 10^{-12}$ coul^2/nt·m^2. The unit of ϵ_0 can be written as coul^2·sec^2/kg·m^3. The value of ϵ_0 then when the time unit is kshana is $\varepsilon_0' = 8.854187817 \times 10^{-12} \times (4.942359860 \times 10^{20})^2 = 2.16280546198 \times 10^{30}$ coul^2/kg·m^3·kshana^{-2}.

5.1.6. Mass of a Spinning Electron in Pair Production

By the law of conservation of energy, the mass of the electron can be found as shown below.

$$h'\nu' = m_0 c'^2 \tag{28}$$

where h', ν' and c' are the Planck constant, gamma ray frequency and velocity of light, respectively, in which the time unit is kshana. Substituting $c' = \lambda_1 \nu'$ meters/kshana in the above equation, we have

$$h' = m_0 \lambda_1^2 \nu_1' \tag{29}$$

$$h' = \frac{m_0 \lambda_1^2}{T_s'} \tag{30}$$

where $T_s' = 1/\nu'$ is the spinning period of the electron, which is 4 kshana. Thus

$$h' = \frac{m_0 \lambda_1^2}{4} \tag{31}$$

Rearranging the terms in the Equation (31), we have

$$m_0 = \frac{4h'}{\lambda_1^2} \tag{32}$$

Substituting the values of $h' = 1.340669 \times 10^{-54}$ joule. kshana (Equation (27)) and $\lambda_1 = 2.42631 \times 10^{-12}$ meters, we have a mass of the electron $m_0 = 0.91093834243469 \times 10^{-30}$ kg $= 9.1093834243469 \times 10^{-31}$ kg, which is the same as the reported CODATA value ($m_e = 9.10938356 \times 10^{-31}$ kg) [10]. The rest mass of the electron can also be found by the law of conservation of energy when the time unit is kshana, as shown below.

$$m_0 c'^2 = \frac{0.51}{n^2} \text{MeV} \tag{33}$$

where n is the number of kshanas in a second. Substituting $c' = \pi R_s/2$, and $n = 1.90853806367 \times 10^8/R_s$ in the above equation, we have

$$\frac{m_0 \pi^2 R_s^2}{4} = \frac{0.51 R_s^2}{\left(1.90853806367 \times 10^8\right)^2} \tag{34}$$

$$m_0 = \frac{4 \times 0.51 \times 10^6 \times 1.60217662208 \times 10^{-19}}{\pi^2 \left(1.90853806367 \times 10^8\right)^2} \text{kg} \tag{35}$$

$$m_0 = 9.0915757 \times 10^{-31} \text{kg} \tag{36}$$

The calculated mass of an electron from Equation (32), which originates from wavelength λ_1 of gamma radiation is the same as the electron mass $m_e = 9.10938356 \times 10^{-31}$ kg as reported in CODATA [10] and it shows that the time required in pair production is about four kshanas *i.e.*, equal to the spinning period of an electron. In a kshana electron mass formation is $h'/\lambda_1^2 = 0.22773458 \times 10^{-31}$ kg and in four kshanas it is equal to the reported value of electron mass (Equation (32)) [10]. It shows that the physical change in the matter *i.e.*, electron/positron production is associated with the kshana or moment and its succession. Thus, one can know the end of its succession only at the end of the physical change [1] [2].

The generation of electron and positron is due to the electromagnetic radiation or photon. The electromagnetic wave does not disappear but gets transformed into electron and positron [15]. It relates to mass of the electron and wavelength of the gamma radiation. This is like the concept of electromagnetic origin of mass particle. Erik Haeffner (2000) proposed a concept called Condensed Electromagnetic Radiation (CER) as the electromagnetic origin of mass

particles. Erik Haeffner says, "The new concept CER (Condensed Electromagnetic Radiation), proposed in this article, indicates an electromagnetic origin of mass particles, in fact, an overwhelming amount of experimental evidence confirms that the CER concept is fundamental for the physical explanation of mass particle properties [14]."

5.1.7. Relating the Number of Kshanas in a Second to Absolute Permittivity and Permeability of the Medium

Velocity of light in meter/second is

$$c = \frac{1}{\sqrt{\mu_0 \varepsilon_0}} \tag{37}$$

Rewriting the above equation when the velocity of light and absolute permittivity has the time unit kshana

$$c' = \frac{1}{\sqrt{\mu_0 \varepsilon_0'}} \tag{38}$$

However, by the definition of kshana, the velocity of light $c' = \pi R_s/2$ m/kshana and $\varepsilon_0' = \varepsilon_0 \times n^2$. Therefore, from Equation (38), we have

$$n = \frac{2c}{\pi R_s} \tag{39}$$

The Equation (39) is the same as the Equation (6) or Equation (8).

5.1.8. Photo-Electric Effect and Number of Kshanas in a Second

When the incident photon energy is such that it only liberates an electron from the metal surface without any kinetic energy (*i.e.*, $mv^2/2 = 0$). In such case $h\nu_0 = W_\phi$. where ν_0 is the threshold frequency in cycles per second and W_ϕ is the work function in joule. Now rewriting the equation for the work function having time unit kshana, we have

$$h'\nu_0' = h'\frac{c'}{\lambda_0'} = w_\phi' \tag{40}$$

For $h' = h/n$, $W_\phi' = W_\phi / n^2$, and $\lambda_0 = \lambda_0' = c'/\nu_0'$ meters, we have

$$n = \frac{\lambda_0' w_\phi}{hc'} \tag{41}$$

$$n = \frac{2\lambda_0' w_\phi}{h\pi R_s} \quad \text{since} \quad c' = \frac{\pi R_s}{2} \tag{42}$$

For a tungsten cathode of threshold wavelength $\lambda_0' = \lambda_0 = 2300 \times 10^{-10}$ m, and work function $W_\phi = 5.38$ eV [16], we have

$$n = \frac{1.9085380 \times 10^8}{R_s} \text{kshana/sec} \tag{43}$$

The above equation is same as Equation (9).

Alternatively, from Equation (40), we can find the value of n as shown below:

$$h' = \frac{w_\phi}{n^2 \nu_0'} = \frac{w_\phi}{n^2 \nu_0 / n} = \frac{w_\phi}{n\nu_0} \tag{44}$$

Since $W_\phi' = W_\phi / n^2$, $\nu_0' = \nu_0 / n$, where n is the number of kshanas in one second. From Equation (31), $h' = m_0 \lambda_1^2 / 4$. Therefore,

$$\frac{w_\phi}{n\nu_0} = \frac{m_0 \lambda_1^2}{4} \tag{45}$$

$$n = \frac{4w_\phi}{m_0 \lambda_1^2 \nu_0} = \frac{4w_\phi \lambda_0}{m_0 \lambda_1^2 c} \tag{46}$$

1) For a tungsten cathode with a threshold wavelength $\lambda_0 = 2300 \times 10^{-10}$ m, work function $W_\phi = 5.38$ eV [16], and electron wavelength $\lambda_1 = 2.42631 \times 10^{-12}$ (Section 5.1), From Equation (46), the value of n will be

$$n = 4.932626423359 \times 10^{20} \text{ kshana} \tag{47}$$

2) For Aluminum work function is 4.25 eV [16]. The threshold frequency will be

$$\nu_0 = 1.0276454364795 \times 10^{15} \text{ Hz} \tag{48}$$

and threshold wavelength $\lambda_0 = c/\nu_0 = 2.91727523 \times 10^{-7}$ m. Thus, from Equation (46)

$$n = 4.94236082 \times 10^{20} \text{ kshana} \tag{49}$$

3) For Rb, the work function is 2.16 eV [16]. Then, the threshold frequency will be $\nu_0 = 0.5222856806 \times 10^{15}$ Hz, and the threshold wavelength will be $\lambda_0 = c/\nu = 5.740009 \times 10^{-7}$ m. Thus,

$$n = \frac{4w_\phi}{m_0 \lambda_1^2 \nu_0} \tag{50}$$

$$n = 4.9423608678 \times 10^{20} \text{ kshana} \tag{51}$$

4) For Mg, the work function is 3.66 eV [16], and the threshold frequency will be $\nu = 0.88498407 \times 10^{15}$ Hz.

$$n = \frac{4w_\phi}{m_0 \lambda_1^2 \nu_0} \tag{52}$$

where, $\lambda_1 = 2.42631 \times 10^{-12}$ meters.

$$n = 4.94236089 \times 10^{20} \text{ kshana} \tag{53}$$

5.1.9. Spectral Series of Hydrogen Atom and Kshana

The number of kshanas in a second can also be found by taking the ionization energy of the hydrogen atom, which is 13.6 eV. This is the energy needed to free the electron from the nucleus of the hydrogen atom. In the Lyman series for $n = 1$, the associated wavelength is 1026×10^{-10} meters, and the energy difference is $-3.4 - (-13.6) = 10.2$ eV [9]. Now we can estimate the value of n as shown below. By the law of conservation of energy, we have

$$h'\nu_0 = \frac{10.2 \times 1.6021766208 \times 10^{-19}}{n^2} \tag{54}$$

$$\frac{h'\nu_0}{n} = \frac{10.2 \times 1.6021766208 \times 10^{-19}}{n^2} \tag{55}$$

where $\nu_0 = n\nu_0' = c/\lambda_0$ and λ_0 = 1026 × 10^{-10} meters is the wavelength of the first member of the Lyman series. Thus,

$$h' = \frac{10.2 \times 1.6021766208 \times 10^{-19}}{n\nu_0} \tag{56}$$

$$h' = \frac{10.2 \times 1.6021766208 \times 10^{-19} \lambda_0}{nc} \tag{57}$$

$$h' = \frac{6628.6247 \times 10^{-37}}{n} = \frac{m_0 \lambda_1^2}{4} \tag{58}$$

$$n = \frac{4 \times 6628.6247 \times 10^{-37}}{m_0 \lambda_1^2} \tag{59}$$

Substituting the values of electron rest mass m_0 and λ_1, we get

$$n = 4.944266452 \times 10^{20} \text{ kshana} \tag{60}$$

Equations (26), (47), (48), (49), (51), (53), and (60) show that the number of kshanas in a second is the same, *i.e.*, n = 4.942359860 × 10^{20} kshanas and 1 kshana = 2.0233249466 × 10^{-21} sec.

5.1.10. Validation of Kshana or Moment with Statistical Concept of Movement of Electron

The statistical concept of movement of electron can be considered for validation of kshana. For a free spinning electron with effective Lande'-g factor g^* = 2, the radius R_s of spinning electron is [8]

$$R_s = \frac{5g^*\hbar}{4m_0c} = \frac{5g^*\hbar}{8\pi m_0 c} \tag{61}$$

where Planck constant h = 6.626070040 × 10^{-34}; J·s, rest mass of free electron m_0 = 9.10938356 × 10^{-31} kg, and velocity of light c = 2.99792458 × 10^8 m/s. Substituting these values, we get

$$R_s = 9.6539816887 \times 10^{-13} \text{ meter} \tag{62}$$

Converting Equation (61) for radius with time unit kshana, we get

$$R_s = \frac{5g^*h'}{8\pi m_0 c'} \tag{63}$$

where Planck constant h' = 1.34066928117 × 10^{-54} J. kshana, rest mass of free electron m_0 = 9.10938356 × 10^{-31} kg, and velocity of light c = 6.0657755908 × 10^{-13} meters/kshana. Substituting these values, we get

$$R_s = 9.653981690 \times 10^{-13} \text{ meter} \tag{64}$$

Equations (62) and (64) give the same result even though time units of Planck constant h and velocity light c are different.

Spinning period for free electron is (Ziya Saglam *et al.* [8])

$$T_s = \frac{8\pi R_s^2 m_0}{5g^*\hbar} = 2.023324947 \times 10^{-20} \text{ sec} \tag{65}$$

Rewriting the Equation (65) in which $\hbar$ is replaced with $nh'/2\pi$. Since $\hbar = h/2\pi$ and $h = nh'$ where n is the number of kshanas in a second and h' is in J·kshana or kg·m^2/kshana. Thus, the number of kshanas in a second can be calculated using the rewritten formula for T_s

$$T_s = \frac{8\times 2\pi^2 R_s^2 m_0}{5g^* nh'} \tag{66}$$

$$n = \frac{16\pi^2 R_s^2 m_0}{5g^* h' T_s} \text{ kshanas/sec} \tag{67}$$

For effective g-factor $g^* = 2$,

$$n = 4.9423598634677\times 10^{20} \text{ kshanas/sec} \tag{68}$$

Thus, the value of "n" in Equation (68) is same as in Equations (26), (47), (48), (49), (51), (53), (60) and show that the number of kshanas in a second is the same, *i.e.*, $n = 4.942359860 \times 10^{20}$ kshanas and 1 kshana = $2.0233249466 \times 10^{-21}$ sec.

Alternatively, the ultimate indivisible value of the kshana which is $2.02332494691 \times 10^{-21}$ sec is in good agreement with Ziya Saglam *et al.* [8]. Ziya Saglam *et al.* calculated the spinning period for a free electron which is 1.9×10^{-20} sec (for effective Lande'-g factor, $g^* = 2$). When this value of period is divided by 4 kshanas (since spinning period of free electron is 4 kshanas) give the value of 1 kshana equal to 4.75×10^{-21} sec for free electron. Both the values are of the same order of magnitude *i.e.*, 10^{-21} sec. Ziya Saglam also calculated the period of spin in an atomic state which is $T_{s\,(n=1,\, l=0,\, mj=0,\, ms=1/2)} = 1.48 \times 10^{-21}$ sec (for effective Lande'-g factor, $g^* = 1$). Again, this value of period is divided by 4 kshanas give the value of 1 kshana equal to 0.37×10^{-21} sec for period of spin in an atomic state which also has same order of magnitude *i.e.*, 10^{-21} sec.

The value of a kshana can also be determined using the circular frequency of a spinning electron given by Olszewski [17], which is $2\pi/T_2 = m_e c^2/\hbar = 0.78 \times 10^{21}$ sec^{-1} [17]. Where, period $T_2 = 2\pi/0.78 \times 10^{21}$ sec^{-1} = $8.055365778 \times 10^{-21}$ sec and a kshana is $T_2/4 = 8.055365778 \times 10^{-21}$ sec/4 = $2.0138414446 \times 10^{-21}$ sec. Again, it is same as shown in the above sections of this paper.

5.1.11. Compton Effect and a Kshana

In a Compton scattering, the Compton wavelength $\lambda_C = h(1 - \cos\theta)/m_0 c = h/m_0 c$, whose value is $2.4263102367 \times 10^{-12}$ meters [10] for $\theta = \pi/2$, where h the plank constant, m_0 is the mass of electron, c is the velocity of light and θ is the angle of scattering. Now, the Compton frequency $\nu_C = c/\lambda_C = 2.99792458 \times 10^8/2.4263102367 \times 10^{-12} = 1.2355899 \times 10^{20}$ Hz (or $\nu_C = \omega_0/2\pi = mc^2/2\pi\hbar$ [18]), and period will be $T_C = 1/\nu_C = 0.80932997877 \times 10^{-20}$ sec. Therefore, 1 kshana = $T_C/4 = 0.80932997877 \times 10^{-20}/4 = 0.20233249 \times 10^{-20}$ sec *i.e.*, $2.0233249 \times 10^{-21}$ sec and $n = 4.942359859269 \times 10^{20}$ kshanas, which is same as given in the above sections.

Again, it shows that the value of "n" is same as in Equations (26), (47), (48), (49), (51), (53), (60) and show that the number of kshanas in a second is the

same, *i.e.*, $n = 4.942359860 \times 10^{20}$ kshanas and 1 kshana = $2.0233249466 \times 10^{-21}$ sec.

5.2. Determination of Reduced Compton Wavelength, Fine Structure Constant, Rydberg Constant, Spin Magnetic Moment and Spin Angular Moment

5.2.1. Determination of Compton Wavelength

The Compton wavelength is given by the equation $\lambda_C = h/m_0c$ whose value is $2.4263102367 \times 10^{-12}$ m. The reduced Compton wavelength is $\Lambda_C = \lambda_C/2\pi = h/2\pi m_0 c$ which is equal to $3.8615926764(18) \times 10^{-13}$ m [10]. Writing the reduced Compton wavelength equation where the time unit is kshana is as shown below

$$\Lambda_C = \frac{\lambda_C}{2\pi} = \frac{h'}{2\pi m_0 c'} \text{meter} \tag{69}$$

Substituting the Planck constant $h' = 1.34066928117 \times 10^{-54}$ J. kshana, the velocity of light $c' = 6.0657755908 \times 10^{-13}$ meters/kshana, and mass of the electron $m_0 = 9.10938356 \times 10^{-31}$ kg, we obtain a reduced Compton wavelength equal to $3.8615926760 \times 10^{-13}$ m which is the same as the reported CODATA value.

5.2.2. Determination of Fine Structure Constant

The orbital velocity in the first orbit of the hydrogen atom is $v' = 2.18769126277 \times 10^6/4.942359860 \times 10^{20} = 4.426410307 \times 10^{-15}$ meters/kshana. Fine structure constant is given by the following equation

$$\alpha = \frac{v'}{c'} = \frac{4.426410307 \times 10^{-15}}{6.0657755908 \times 10^{-13}} \tag{70}$$

or

$$\alpha = 0.7297352565620 \times 10^{-2} = \frac{1}{137.0359991528} \tag{71}$$

Thus, the fine structure constant is the same as that reported [10].

5.2.3. Determination of Rydberg Constant

Using the following equation [9], the Rydberg constant R_∞ is found as shown below.

$$R_\infty = \frac{m_0 e^4}{8\varepsilon_0^2 h'^3 c'} \tag{72}$$

$$R_\infty = \frac{60.0247762251 \times 10^{-107}}{546.9856635635 \times 10^{-115}} \Big/ \text{m} \tag{73}$$

The value of the Rydberg constant R_∞ is equal to 10973738.4768/meter. This agrees with the reported value $R_\infty = 10973731.568525(73)/\text{m}$ [10].

5.2.4. Determination of Spin Angular Momentum

The spin angular momentum J is given by the following Equation [7], where the time unit is in seconds.

$$J = \frac{m_0 R_s^2 w}{2} = \frac{m_0 R_s^2 w'}{2} \tag{74}$$

where ω is rad/sec and $\omega' = \pi/2$ rad/kshana are the angular frequencies. From equation $c' = \pi R_s/2$ m/kshana [2], we can write the above equation as

$$J' = \frac{m_0 R_s c'}{2} \tag{75}$$

In semi-classical model of spinning electrons, it is assumed that [7].

$$R_s = \Lambda_c = \frac{\hbar}{m_0 c} = \frac{h}{2\pi m_0 c} = \frac{h'}{2\pi m_0 c'} \text{meter} \tag{76}$$

Substituting the value of R_s from Equation (76) in Equation (75) we have

$$J' = \frac{h'}{4\pi} = \frac{1.3406690 \times 10^{-54}}{4\pi} \tag{77}$$

$$J' = 0.106687049 \times 10^{-54} \tag{78}$$

Converting time unit kshana to time unit sec, we have

$$J = 0.106687049 \times 10^{-54} \times 4.942359860 \times 10^{20} \tag{79}$$

Thus, spin angular momentum is equal to $J = 0.527285789548 \times 10^{-34}$ which is in good agreement with the value provided by CODATA [10].

5.2.5. Determination of Spin Magnetic Moment

The spin magnetic moment of a simple model of spinning electrons [7], is

$$\mu' = IS = \left(\frac{e}{T_s'}\right)\left(\pi R_s^2\right) = \left(\frac{e}{4}\right)\left(\pi R_s^2\right) \tag{80}$$

where current $I = e/T_s'$ and e is the electronic charge. For a simple model of the spin magnetic moment $S = \pi R_s^2$ [7], $T_s' = 4$ kshanas is the spinning period of the electron. From Equation (80)

$$\mu' = \left(\frac{e}{4}\right)\left(\pi R_s \frac{h'}{2\pi m_0 c'}\right) \tag{81}$$

$$\mu' = \left(\frac{R_s}{4c'}\frac{eh'}{2\pi m_0}\right) \tag{82}$$

From Equation (11) keeping the value of c', we have

$$\mu' = \left(\frac{eh'}{4\pi m_0}\right) = 0.018764331838931 \times 10^{-42} \tag{83}$$

where h' has the unit, Joule·kshana. When it is converted to the time unit sec, we have a Bohr magneton value of $0.092740080 \times 10^{-22} = 9.27400 \times 10^{-24}$ J·T^{-1} which is equal to the reported value of Bohr magneton $\mu_B = 927.4009994(57) \times 10^{-26}$ J·T^{-1}.

6. Discussion

The focus of discussion in the paper is definition of kshana or moment and its physical significance. Equation (18) shows that the number of kshanas n in a second is a constant. Since the right-hand side of the Equation (18) has constants

such as Rydberg constant, velocity of light and fine structure constant. The ultimate indivisible value of the kshana is $2.02332494691 \times 10^{-21}$ sec which is in good agreement with Ziya Saglam [8]. Thus, Maharishi Vyasa's time unit "kshana" is very small and indivisible quanta of time which needs further attention.

Equation (17) shows that the number of kshanas in a second are inversely proportional to the radius of spinning electron. Smaller the radius of spinning electron larger the value of number of kshanas in a second. **Table 1** shows the variation in number of kshanas with different values of radius of spinning electron.

This radius of the electron is found based on Maharishi Vyasa's definition of kshana [1] [2]. I obtained a reduced Compton wavelength equal to $3.8615926760 \times 10^{-13}$ m which is the same as the reported CODATA value [10]. Apart from Compton radius, I found the number of kshanas taking classical electron radius ($2.8179403227 \times 10^{-15}$ [10]) into account which is shown in the **Table 1**.

The spinning electron model based on Maharishi Vyasa's definition of kshana is successful in explaining most of the properties of the electron such as radius, spin angular momentum, spin magnetic moment, and rest mass of the electron. The radius of the spinning electron determined based on this definition is the same as the reported value which is equal to the reduced Compton wavelength. However, according to the calculations the value of the electron radius is large compared with the classical electron radius (**Table 1**) [10] and hence needs further attention.

According to Maharishi Vyasa's definition, one "kshana" (exceedingly small quanta of time) is equal to the time taken by the electron to traverse $\pi/2$ radians. Obviously, it appears that it can be subdivided into time intervals needed to traverse smaller angles. However, this goes against the definition of "kshana" as propounded by Maharishi Vyasa and may have some physical significance which needs further investigation. Thus, "kshana" cannot be subdivided by dividing the angle $\pi/2$.

Table 1. Comparison of number of "kshanas" in a sec for various values of radius of the electron.

Radius of an electron in meters	Value of a kshana in sec	Value of a sec in kshanas
Classical electron radius $2.8179403227 \times 10^{-15}$ m [10]	$1.476491549 \times 10^{-23}$ sec	$0.677281221 \times 10^{23}$ kshanas
Electron charge radius 0.0118×10^{-15} m [19]	$6.18274281 \times 10^{-26}$ sec	$1.617405138 \times 10^{25}$ kshanas
Hardon electron radius 10^{-18} m [20]	$5.239612554 \times 10^{-27}$ sec	$1.90853806 \times 10^{26}$ kshanas
Graviton radius 1.369×10^{-76} m [21]	$0.71730295 \times 10^{-84}$ kshanas	$1.394111076 \times 10^{84}$ kshanas

7. Conclusion

The spinning electron model based on Maharishi Vyasa's definition of kshana is successful in explaining most of the properties of the electron such as radius, spin angular momentum, spin magnetic moment, and rest mass. The radius of spinning electron determined based on Maharishi Vyasa's definition is the same as the reported value which is equal to the reduced Compton wavelength.

Acknowledgements

I am very grateful to Prof. V. S. Suryan, retired principal of C. B. College Bhalki, Dist. Bidar, Karnataka, India for incorporating English language emendations in this article. I am also grateful to Prof. Suresh Chandra Mehrotra, Dr. Babasaheb Ambedkar Marathwada University, Maharastra, India, Prof. Balachandra G. Hegade, Prof. and Chairman Rani Channamma University, Karnataka, India, and Prof. B. M. Mehtre, IDRBT, Hyderabad, India, for their feedback.

Conflicts of Interest

The author declares no conflicts of interest regarding the publication of this paper.

References

[1] Patanjali, M. (2003) Patanjal Yoga Darashanm. 2nd Edition, Aarsha Gurukul Mahavidhyalaya, Abu Parvat, Dist. Sirohi (Rajasthan).

[2] Wanjerkhede, S.M. (2021) Kshana—The Smallest Mysterious Unit of Time Exploring the Temporal Variation of Fine Structure Constant.

[3] Das, N.K. (2021) *Journal of High Energy Physics, Gravitation and Cosmology*, **7**, 66-87. https://doi.org/10.4236/jhepgc.2021.71003

[4] Ghosh, S., Choudhury, A. and Sarma, J.K. (2012) *Indian Journal of Physics*, **86**, 481-483. https://doi.org/10.1007/s12648-012-0083-5

[5] Mei, S. and Mei, Z. (2019) *Journal of Physics & Astronomy*, **7**, 1-6.

[6] Kanaada, M. (2014) Vaisesika Darashanm. Arshya Vidhya Prachara Nyasa.

[7] Zhao, H.L. (2017) *Open Physics*, **15**, 652-661. https://doi.org/10.1515/phys-2017-0076

[8] Saglam, Z., Saglam, M., Bayram, B. and Horton, T. (2015) *Journal of Modern Physics*, **6**, 2239-2243. https://doi.org/10.4236/jmp.2015.615229

[9] Gaur, R.K. and Gupta, S.L. (1996) Engineering Physics. Dhanpat Rai & Sons, 1682, Nai Sarak, Delhi.

[10] Mohr, P.J., Newell, D.B. and Taylor, B.N. (2014) *Journal of Physical and Chemical Reference Data*, **45**, Article ID: 043102. https://doi.org/10.1063/1.4954402

[11] Shulman, M.E. (2017) *Journal of High Energy Physics, Gravitation and Cosmology*, **3**, 503-521. https://doi.org/10.4236/jhepgc.2017.33039

[12] Parks, J.E. (2015) The Compton Effect—Compton Scattering and Gamma Ray Spectroscopy.

[13] Hubbell, J. (2006) *Radiation Physics and Chemistry*, **75**, 614-623. https://doi.org/10.1016/j.radphyschem.2005.10.008

[14] Haeffner, E. (2000) A Physical Origin for Mass and Charge.

[15] Bartusch, T. (2020) *Journal of High Energy Physics*, *Gravitation and Cosmology*, **6**, 774-801. https://doi.org/10.4236/jhepgc.2020.64052

[16] Mastwijk, H., Bartels, P. and Lelieveld, P. (2007) The Origin of the Work Function. Condensed Matter: Strongly Correlated Electrons.

[17] Olszewski, S. (2014) *Journal of Modern Physics*, **5**, 2030-2040. https://doi.org/10.4236/jmp.2014.518199

[18] Lan, S.Y., Kuan, P.C., Estey, B., English, D., Brown, J.M., Hohensee, M.A. and Muller, H. (2013) *Science*, **339**, 554-557. https://doi.org/10.1126/science.1230767

[19] Storti, R. and Desiato, T. (2009) *Physics Essays*, **22**, 27-32. https://doi.org/10.4006/1.3062144

[20] Wolfram, S. (1975) *Australian Journal of Physics*, **28**, 479-487. https://doi.org/10.1071/PH750479

[21] Balseanu, M. (2019) Graviton Physics. 1-57.

Scientific Research Publishing

Journal of Modern Physics, 2022, 13, 1184-1196
https://www.scirp.org/journal/jmp
ISSN Online: 2153-120X
ISSN Print: 2153-1196

Is There an Absolute Scale for Speed?

Ricardo B. Ferreira[1], João B. Ferreira[2]

[1]Instituto Superior de Agronomia, University of Lisbon, Lisbon, Portugal
[2]Instituto Português de Oncologia de Lisboa Francisco Gentil, Lisbon, Portugal
Email: rbferreira@isa.ulisboa.pt, ferreiraj@campus.ul.pt

How to cite this paper: Ferreira, R.B. and Ferreira, J.B. (2022) Is There an Absolute Scale for Speed? *Journal of Modern Physics*, **13**, 1184-1196.
https://doi.org/10.4236/jmp.2022.138069

Received: June 28, 2022
Accepted: August 22, 2022
Published: August 25, 2022

Abstract

Except for the speed of photons in vacuum, all speeds are relative. Could we develop an absolute scale for speed in which relative values for speed may be arbitrarily positioned and compared in absolute terms? The currently accepted definition for the meter as the distance covered by photons in vacuum during 1/299,792,458 s, and the view that the greater a material particle is accelerated towards c, the greater time dilation and length contraction will be, suggest that anything disturbing one of the four spacetime dimensions may affect the other three as well. One hypothetical experiment, one real experiment performed in the 1970s, and one experiment from a different field of science are discussed to propose that both time and velocity are only partially relative. In the first experiment, person A is standing still on the Earth's surface, and person B is onboard a train passing by person A at the constant speed of 60 km/h (as measured by person B on the train's speedometer). Persons A and B define two distinct inertial frames of reference, which correspond to two different spacetime conditions and which are therefore characterized by comparatively different lengths of the meter and durations of the second, as predicted by the Lorentz factor. Therefore, if person B onboard the train measures the train's speed relative to person A as 60 km/h, a simple calculation will show that person A will perceive the train passing by at 59.99999999999981455834 km/h. If we consider the speed of photons in vacuum (c = 299,792,458 m/s) as a universal reference, and if we consider that the greater a material particle is accelerated towards c, the greater time dilation and length contraction will be, then person C, occupying an independent, distinct inertial frame of reference, will be unable to determine persons A and B's absolute speeds, but may infer which one is moving at a speed closer to c by comparing, with his own meter and second, the durations of the second and the lengths of the meter experienced by persons A and B. The relativity of time may not be complete due to the bias that derives from the limit imposed on spacetime by c and the Lorentz factor, causing relativity to be

partial. The second and third experiments further help understand this partiality.

Keywords

Spacetime, Relativity, Speed of Light, Space, Time

1. Introduction

Except for the speed of photons in vacuum, all speeds are relative. However, could we develop an absolute scale for speed in which relative values for speed may be arbitrarily positioned and compared?

Suppose we successively accelerate a spacecraft to the constant speeds of $0.1c$, $0.2c$, $0.3c$, …, and $0.9c$ (speeds adjusted at the spacecraft velocimeter) relative to an inertial frame of reference A (or the surface of the Earth, if we discard any effects due to the atmosphere, to gravity and to non-inertial motion). At each constant speed, the spacecraft passes near the Earth, making it possible, from the Earth's surface, to compare the duration of each second and the length of each meter in the moving spacecraft with those measured on the surface of the Earth. It seems reasonable to assume that the faster the speed in relation to the Earth's surface, the comparatively longer the duration of each second will be, and the comparatively shorter the length of the meter will be.

Let us now imagine that two spacecraft, one moving at the constant speed of $0.1c$ and the other at the constant speed of $0.5c$ (speeds adjusted at each spacecraft velocimeters), pass near the Earth. If, from the Earth's surface (or any other place), we succeed in comparing the duration of each second and the length of each meter in the two moving spacecraft, the one with a comparatively longer duration of the second and comparatively shorter length of the meter will be the one moving faster in absolute terms relative to the Earth.

In relation to time alone, this effect has been widely demonstrated. For example, the Global Positioning System (GPS), a United States of America (USA) global satellite-based radio navigation system, may be regarded as a continuous operating experiment since the clocks onboard the satellites are corrected for both gravity-dependent and non-gravity-dependent time dilation to pass time at the same rate as clocks on the surface of the Earth.

The debate about the symmetry or asymmetry of time dilation has been going on for over 100 years. Time dilation symmetry arose as a logical deduction of Einstein's 1905 postulates: if two clocks occupying two distinct inertial frames of reference are in relative motion, each one is expected to run slower than the other [1]. Abramson [2] proposed an alternative view, in which the symmetry would break if the two inertial frames of reference are defined by two widely different masses (e.g., one GPS satellite and the Earth). It is difficult to accept the existence of an absolute reference without breaking the symmetry of time dila-

tion. Nevertheless, as a counterpart of the special theory of relativity, Burde reconciled the existence of a preferred frame with the relativity principle and the universality of the speed of light [3]. However, in the same article [1], Einstein discussed the relative rates of time ticking in one clock located at one Earth pole and in another clock located at the Equator and concluded that "…a balance wheel clock that is located at the Earth's equator must be very slightly slower than an absolutely identical clock, subjected to otherwise identical conditions, that is located at one of the Earth's poles." In the subsequent years, many experiments were performed to test these two theories (including the continuous experiment conducted at the GPS satellites), and the results seem to confirm that time dilation is an asymmetric phenomenon [4].

In 1908, Hermann Minkowski merged the three dimensions of space with time to conceptualize a four-dimensional continuum known as Minkowski space, Minkowski spacetime, or simply spacetime. It seems increasingly evident that space and time do not exist as separate features of our universe and that a change in speed and/or gravitational acceleration of a material object (e.g., a spacecraft) will not only comparatively alter the duration of the second but will also affect the length of the meter in one or in the three dimensions of space. Therefore, as predicted by the Lorentz factor and for a clock at rest on the Earth's surface and another moving at a relativistic speed, the moving clock is expected to dilate time and contract length (or the three dimensions of space) comparatively to the clock at rest. In contrast, the stationary clock will compress time and expand length (or the three dimensions of space) comparatively to the moving clock.

Albert Einstein's special and general theories of relativity have clearly established the basis for understanding the relative nature of spacetime. However, the speed of light in vacuum (c = 299,792,458 m/s) and the Lorentz factor (γ) seem to impose a limit on spacetime. This has implications for observers looking at each other from distinct spacetime conditions, and may ultimately require a third, independent observer. We propose analyzing three experiments to further comprehend this idea.

2. Experiment 1

It is generally accepted that velocities are relative. Imagine two people: person A, standing still on the Earth's surface, and person B, onboard a train passing by person A at the constant speed of 60 km/h (as measured by person B on the speed meter of the train). Both speeds considered (0 and 60 km/h) are relative. Indeed, discarding any effects due to the atmosphere, to gravity and to non-inertial motion, two inertial frames of reference are considered, corresponding to two objects moving at constant velocities relative to one another. Therefore A and B occupy inertial frames of reference, meaning that they are both at rest within each one's frame of reference. The common explanation is as follows: from person B's point of view, person B is inside the train sitting still as he/she

looks through the window at person A passing by at 60 km/h. However, from person A's point of view, person A is standing still outside the train, and it is person B the one who is moving at 60 km/h.

Which one of them (*i.e.*, person A or person B) is truly moving and which one is truly stationary? At first sight, person A seems to be stationary, and person B is moving. However, recall that both person A and the train moving at 60 km/h are standing on Earth, which is rotating and moving around the Solar System's barycenter, which in turn is moving within the Milky Way. In addition, our galaxy is rotating and moving in space. The most obvious explanation would be that there is no absolute rest, *i.e.*, there is no universal stationary reference frame against which all other reference frames may be referenced. Consequently, there is no universal velocity, meaning that only relative velocities exist. Going back to persons A and B, the only relevant conclusion is that the relative velocity between person A and person B is 60 km/h, with neither of them being more or less stationary than the other. This reasoning would be "absolutely" correct if it were not for length contraction, time dilation and the speed limit imposed by the speed of photons in vacuum. Indeed, there seems to exist a universal velocity: *c*. For now, let us ignore rotational and translational movements of the Earth, Solar System and Milky Way, gravitational fields of the Earth and of any other astronomical bodies, and any effects due to the atmosphere. Under these conditions, person A and person B have two points of view which correspond to two different inertial frames of reference, which are characterized by comparatively different lengths of the meter and durations of the second, as predicted by the Lorentz factor, *i.e.*, they are experiencing distinct spacetime conditions. Nevertheless, each one will obviously perceive the meter and the second as normal in their own frame of reference.

If person A and person B experience comparatively different lengths of the meter and durations of the second, and if person B measures the speed of the train as 60 km/h relative to person A, then person A cannot see person B passing by at 60 km/h. If person B onboard the train measures the speed of the train relative to person A as 60 km/h, then person A will look at the moving train and will see each train meter slightly shorter and each train second slightly longer than person A's own meters and seconds (at this non-relativistic speed, such effects are so small that it is not possible to measure them experimentally), as given by the Lorentz factor.[1]

As expected, in what concerns the comparative length of 1 meter and duration of 1 second in the two inertial frames of reference, person A will measure

- m_A in A's own frame of reference, and from A's own frame of reference, 1 m_B = 0.99999999999999845465 m_A in the moving train;

[1]It is important to note that for such low speeds an assumption must be made here, as highlighted below by the results shown in **Table 1**, obtained in the experiments conducted during October 1971 by Hafele and Keating [5] [6]: for the commercial jet flying westwards, time contracted, *i.e.* shorter seconds were recorded, in comparison with the surface of the Earth seconds, and specially in comparison with the duration of the seconds in the commercial jet flying eastwards. Most probably, this derives from all movements and gravitational accelerations persons A and B are subject to.

- s_A in A's own frame of reference, and from A's own frame of reference, 1 s_B = 1.0000000000000154535 s_A in the moving train;

And therefore, from A's own frame of reference, person A will see the train moving at 60 km_B/h_B = 59.99999999999981455834 km_A/h_A.

The main conclusion of this hypothetical experiment is that person B onboard the train will see person A passing by at 60.00000000000000000000 km_B/h_B, whereas person A, standing still on the Earth surface, will see the train moving at 59.99999999999981455834 km_A/h_A.

One other prevailing view is that each one, A and B, will see the other moving at a speed slower than 60 km/h, and therefore each one will perceive a shorter meter and a longer second when observing the other, something which somewhat contradicts the Lorentz factor. This view derives directly from relativity, considering that all speeds are relative. If time dilation were symmetric, we would expect both time dilation values to be identical relative to an external observer (person C).

3. Experiment 2

Of course, several factors other than relative speed will affect length contraction and time dilation. Indeed, if we could consider the movements and gravitational fields of the Earth and beyond, we would obtain different values for the relative speeds between A and B, meaning that the result could be different from that obtained above. The experiment conducted during October 1971 by Hafele and Keating [5] [6] to test Einstein's theory of relativity with macroscopic clocks provides a good example of this situation. Their working hypothesis was to test whether the time recorded (relative to a clock at rest on the Earth surface) by four caesium atomic clocks onboard two regularly scheduled commercial jets flown twice around the world (at typical jet aircraft speeds), one eastward, the other westward, would run faster or slower, depending on the direction and ground speed, after circumnavigation of the Earth. The variables under consideration were the speed (relative to a reference atomic clock maintained at the United States of America Naval Observatory), the altitude, the direction of the circumnavigation and the rotational speed of the Earth.

Special relativity [1] predicts that a moving standard clock will record less time compared with coordinate clocks distributed at rest in an inertial reference space (assuming the Earth surface as an inertial frame of reference). However, since the Earth rotates, coordinate clocks distributed at rest on its surface are not suitable to test Hafele and Keating's working hypothesis [6].

The Earth's rotation is computed by comparison to the "fixed stars", stars that move very slowly relative to the Earth and are therefore considered as a good reference frame. The sidereal period, the time taken by a celestial body within the solar system (the Earth, in the present case) to complete one revolution with respect to the "fixed stars", equals 23 h, 56 min and 4.09053 s. With a circumference of ca. 40,075 km at the equator, an object at the equator on the surface of

the Earth moves, relative to the "fixed stars", with a speed of 460 m/s.[2] As the Earth rotates, everything on the ground, in the water, and in the air (e.g., the atmosphere or airplanes flying inside it) also rotates at the same angular speed because of gravity. Therefore, the rotation of the Earth should have no direct differential influence on how long airplanes take to fly eastward or westward when comparing the airplane clocks with that on the surface of the Earth (considering here the atomic timescale of the USA Naval Observatory as the external, independent observer), but they have a differential influence if the "fixed stars" (in this case considered as the external, independent observer) are taken into account. In addition, there is an indirect influence on the travel time taken by airplanes eastward or westward: as a result of the Earth's rotation, the Coriolis effect is responsible for the high-speed, high-altitude winds of the jet stream, winds prevailing westward at some latitudes and eastward at others. This means that flight times are sometimes shorter eastward and sometimes shorter westward.

The experimental design was based on the predicted assumption that an asymmetry would be found in the time difference between the flying clocks and the ground reference clock, depending on the direction of the circumnavigation [7] [8]. The time elapsed in each case (*i.e.*, eastward, and westward) was compared to that of a reference atomic clock maintained at the USA Naval Observatory (**Table 1**). Consequently, for the flying clocks, and relative to the corotating Earth surface reference clock, circumnavigation in the direction of the Earth's rotation (eastward, comparatively longer seconds, increased speed) should originate a shorter time recording (*i.e.*, time dilation), whereas circumnavigation in the opposite direction (westward, comparatively shorter seconds, decreased speed) should originate a longer time recording (*i.e.*, time contraction). As predicted by general relativity [9], one other factor considered in **Table 1** that also affected time dilation was the difference in gravitational acceleration between the flying and ground reference clocks.

The results recorded, presented in **Table 1**, show direction-dependent time differences which are in good agreement with the predictions of conventional relativity theory. Relative to the atomic timescale of the USA Naval Observatory, the flying clocks measured less 59 ns ± 10 ns during the eastward trip and measured more 273 ns + 7 ns during the westward trip [5]. Obviously, both the atmosphere and the jets are corotating with the Earth surface at the same angular speed (unlike the linear speed relative to the "fixed stars", which increases with the flight altitude). If the speed relativity between both jets and the USA Naval Observatory were 100%, we would expect both time differences (eastward or

[2]Let us assume that an imaginary observer located at one of the "fixed stars" is monitoring the angular velocity of a fixed point on the Earth equator. Ideally, the observer must view the Earth from a position perpendicular to the rotation axis of the Earth. If only the rotation of the Earth is taken into account, the angular velocity, but not the speed, will be zero after successive periods of Earth 23 h, 56 min and 4.09053 s. The only possibility he would have to assess the angular velocity of the equator, albeit impossible to achieve at present, would be to compare the relative duration of each second at the equator with its own.

Table 1. Recorded versus predicted relativistic time differences observed during the experiment performed in October 1971 by Hafele and Keating [5] [6]. Data are presented as the mean ± standard deviation of the results obtained from four different caesium atomic clocks.

Effect	Time difference (ns)	
	Direction: East*	Direction: West
Total (predicted)	−40 ± 23	+275 ± 21
Gravity-dependent (predicted)	+144 ± 14	+179 ± 18
Non-gravity-dependent (predicted)	−184 ± 18	+96 ± 10
Clock 120 (measured)	−57	+277
Clock 361 (measured)	−74	+284
Clock 408 (measured)	−55	+266
Clock 447 (measured)	−51	+266
Total (mean) (measured)	−59 ± 10	+273 ± 7

*Negative signs indicate that upon return the flying clocks showed an earlier time (comparatively longer seconds, increased speed) than the time indicated on the reference atomic clock maintained at the USA Naval Observatory. Positive signs indicate that upon return the flying clocks showed a later time (comparatively shorter seconds, decreased speed) than the time indicated on the reference atomic clock maintained at the USA Naval Observatory.

westward) to be identical relative to an external observer (person C, in the present case the USA Naval Observatory).

If we consider a single airplane in the Hafele-Keating experiment, then we have an experiment similar to that in our Experiment 1. Hafele and Keating could not measure length contraction, but they recorded time dilation/contraction, meaning that time adjustments had to be made.

The results of the Hafele-Keating experiment, presented in Table 1, show the gravity-dependent time dilation predicted values of +144 ns ± 14 ns (eastward flight; shorter seconds) and +179 ns ± 18 ns (westward flight; shorter seconds). This result was expected, as the airplanes were both subjected to a lower gravitational acceleration, resulting in shorter seconds in both flights (implying time dilation asymmetry).

However, different predicted time dilation values were found between the eastward and westward flights for the non-gravity-dependent time dilation: −184 ns ± 18 ns (eastward flight; longer seconds) and +96 ns ± 10 ns (westward flight; shorter seconds). This could be interpreted to mean that, in absolute terms, one plane moved faster (the eastward flight), the other slower (the westward flight) than the clock standing still at the Earth's surface.

A comparison of the relative length of the second in two frames of reference (such as the two airplanes that occupied distinct spacetime conditions) may be

established from any other frame of reference (e.g., the USA Naval Observatory, standing still on the Earth surface).

4. Experiment 3

An interesting analogy may be established with spectrophotometry, used routinely throughout the world in most analytical laboratories (**Experiment 3** in Table 2). If we fill a glass cuvette with an aqueous solution of betanin (betanidin 5-*O*-β-D-glucopyranoside; λ_{max} = 535 nm), the pigment responsible for the red colour of beetroot (*Beta vulgaris*), and measure its absorbance at 535 nm, we get an absorbance value (A''_{535}), a dimensionless number that does not allow us to know the absolute amount or concentration of pigment present in the cuvette. But if we use a blank control, consisting of an identical glass cuvette filled with water, and measure its absorbance also at 535 nm, we get a different absorbance value (A'_{535}), another dimensionless number which is completely unrelated to betanin. However, if we subtract A'_{535} from A''_{535}, we obtain an absolute, dimensionless number which allows us to indirectly determine the absolute concentration of betanin present in the first cuvette.

Table 2. The three experiments selected to obtain absolute values from relative measurements.

	Experiment 1	**Experiment 2**	**Experiment 3**
	Person A standing still on the Earth surface (person B's perspective), and person B onboard a train moving at 60 km/h (person B's perspective)	Caesium clocks onboard two jets, one flying eastward, the other westward	Spectrophotometric measurement of betanin absolute concentration
Relative measurement 1 (person A's perspective)	Person A standing still on the Earth surface	Jet flying eastward	Sample: betanin solution of unknown concentration
Relative measurement 2 (person A's perspective)	Person B onboard a train moving at 60 km/h	Jet flying westward	Blank control
Common reference	Person C occupying any independent spacetime condition, different from those occupied by A and B	Reference atomic clock maintained at the USA Naval Observatory (at rest, on the Earth surface), occupying an independent spacetime condition, different from those occupied by the jets	Anything filling the cuvette holder (e.g., air) against which both A_{535} values are measured
Relative readings to be compared	Comparative time dilation or comparative duration of each second experienced by persons A and B, as measured by person C	Comparative time dilation relative to Earth, or comparative duration of each second in both jets, as measured from a fixed point on the Earth surface	A_{535} readings of sample and blank control
Absolute value obtained	Which person is moving faster in absolute terms	Which jet is moving faster in absolute terms	Betanin absolute concentration

USA: United States of America.

In the 60 km/h-moving train hypothetical experiment, how would it be possible to obtain an absolute value starting from two relative speed measurements? It could be achieved by employing the same reasoning used in the spectrophotometric **Experiment 3** (Table 2). The absolute concentration of betanin may be obtained from two relative absorbance measurements (A'_{535} and A''_{535}), each made against a common reference (which may or may not contain an unknown amount of betanin; this reference is the analogous equivalent to person C in **Experiment 1**, and to the USA Naval Observatory clock in **Experiment 2** (Table 2). In the betanin spectrophotometric experiment, two relative A_{535} readings are made at first. These readings are relative because they are made with reference to a common medium. Most frequently, the spectrophotometric cuvette holder is empty (*i.e.*, filled with air) so that the A'_{535} and A''_{535} values represent the differences in absorbance at λ = 535 nm between each one of the liquid-containing cuvettes and air. However, the common reference may be any, as long as the same is used for both readings. In this experiment, we do not know how much 535 nm radiation is absorbed by the air molecules that fill the cuvette holder. What is really important is that both readings, A'_{535} and A''_{535}, are made against the same reference. Instead of air, we could as well use a cuvette filled with an unknown (or known) amount of betanin, even if this is larger than that present in the blank control or even in the betanin solution, the end result will be the same.

The difference between the two spectrophotometric readings obtained (*i.e.*, A'_{535} and A''_{535}) do not provide directly the amount or concentration of betanin present in each sample. However, they tell us about their relative positions in an imaginable absolute scale, *i.e.*, which sample contains more betanin and which sample contains less. To determine the amounts/concentrations of betanin present in absolute terms, we need to construct the corresponding "imaginable absolute scale", which under laboratory routine conditions is provided by a standard curve, for which a series of pure betanin concentrations are used to relate, under precisely identical conditions, betanin content/concentration with A_{535}. Therefore, within reasonable limits and regardless of the absorbance of the blank control (*i.e.*, A'_{535}), an absolute value for betanin amount/concentration can be obtained from the difference between two relative values, A''_{535} and A'_{535} using a standard curve.

Let us consider that the cuvette holder (most often filled with air) contains a cuvette filled with a residual yet unknown amount of betanin dissolved in water that produces a given A_{535} value (x_{ref}; *i.e.*, analogous to the unknown absolute speed of the Earth in **Experiment 2**, Table 2). As an example, we will consider this betanin concentration as intermediate between that of the blank control and the betanin sample under analysis. If we now measure the absorbance at λ = 535 nm of both blank control (A'_{535}) and betanin solution (A''_{535}), readings will give one value higher ($A''_{535} > x_{\text{ref}}$) and one value lower ($A'_{535} < x_{\text{ref}}$) than that contained in the cuvette holder. By calculating $A''_{535} - A'_{535}$ and using the standard

curve, we will be able to determine the absolute concentration of residual betanin in the cuvette holder.

$$\left(A''_{535} - x_{\text{ref}}\right) - \left(A'_{535} - x_{\text{ref}}\right) = A''_{535} - A'_{535}$$

In addition, we may also conclude that the residual betanin concentration in the cuvette holder is between those of the blank and the betanin sample under analysis.

5. Discussion

A similar reasoning could be applied to the Hafele-Keating experiment [5] [6], which starts with the Earth moving at an unknown absolute speed. The airplanes lift from the Earth's surface, one moving eastward, the other westward. In absolute terms, it is possible to conclude, from the results presented in **Table 1**, that one is moving slower than the Earth's surface reference (*i.e.*, the USA Naval Observatory), the other faster. Which one is moving faster? It takes far more than the rotational movement of the Earth to tackle our planet's absolute speed. It is also necessary to consider its movement in the solar system, that of the solar system within the Milky Way, and so forth. Then, as predicted by the theory of relativity, the complex and constantly changing gravitational field acts differentially on every single particle of our planet. How can we go around it?

By analogy, regardless of the unknown absolute speed of the Earth, a comparison between the relative duration of each second (persons A and B in **Experiment 1**, and jets flying eastward and westward in **Experiment 2**), made from an external, independent spacetime condition (person C in **Experiment 1**, and USA Naval Observatory on the Earth surface in **Experiment 2**), will indicate which one is moving faster in absolute terms. Note that the spacetime condition of the external, independent reference may be unknown, but it must be the one used to compare the two spacetime conditions under analysis. The absolute reference is therefore the speed of light in vacuum, c = 299,792,458 m/s.

Going back to persons A and B and the train moving at 60 km/h (as measured by person B relative to the Earth's surface), if person B were to increase his/her speed gradually towards c, B would obviously experience, at each speed, B's length of the meter and B's duration of the second as unchanging. However, to person A or to any other person occupying a distinct but constant spacetime condition, B's length of the meter and B's duration of the second would comparatively and endlessly decrease and increase, respectively, as predicted by the Lorentz factor. Therefore, the relativity between persons A and B in what speed is concerned is not total, since an external observer, person C, occupying a third, distinct inertial frame of reference, will be able to tell which one, A or B, is moving faster in absolute (*i.e.*, not relative) terms: the one for which person C perceives the length of the meter to be comparatively shorter and the duration of the second comparatively longer. This will be the person moving closer to c.

Let us flip the reasoning followed by Hafele and Keating [5] [6] to analyse the results they obtained in October 1971. The Earth is moving at an absolute speed

which is not known. However, when perceived from a reference point, the greater the speed (towards *c*), the comparatively greater time dilation is.

Although person C cannot look at A and B individually and measure their absolute speeds, C will be able to establish an absolute comparison of their speeds as (with the exception of the intrinsic 60 km/h speed of person B relative to A) each one of them is (almost exactly) identically affected by all possible movements and gravitational fields they may be subjected to. Due to the limit imposed by *c* on spacetime, A and B's measurements are asymmetrical and C is needed to "break the tie".

In summary, from the 1971 Hafele-Keating experiment [5] [6] we may infer that, in absolute terms, the jet flying eastward (time dilation −59 ns ± 10 ns; comparatively longer seconds, shorter meters and increased speed) moved faster than the jet flying westward (time dilation +273 ns ± 7 ns; comparatively shorter seconds, longer meters and decreased speed). The reasoning is as follows: when seen from the Earth's surface, the faster jet is the one in which seconds are perceived to be longer, therefore a lower number of seconds will elapse when compared to the Earth's surface, meaning that less time will pass compared to the Earth, meaning that the jet crew will be slightly younger than the people that remained at the USA Naval Observatory when the jet lands.

One other conclusion may be drawn from the experimental data obtained under the conditions selected for the study performed by Hafele and Keating [5] [6], which used the surface of the Earth as the common reference for both jet flights. In absolute terms, it seems that the jet flying eastward is moving faster than the USA Naval Observatory, whereas the jet flying westward is moving slower.

For any significant degree of accuracy, this analysis should go beyond the speed of the train/jets since, as predicted by general relativity, other factors affect spacetime.

This type of experiment does not depend on the spacetime condition of the common reference (in this case, the Earth's surface). Changing the spacetime condition of the reference would alter the time dilation values of the jet flying eastward (−59 ns ± 10 ns) and of the jet flying westward (+273 ns ± 7 ns). In any case, the relative positions of the westward flying jet, the eastward flying jet and *c* would be unaltered in an absolute speed scale.

Finally, in what spacetime is concerned, a special mention to the absolute universal reference against which all other reference frames may be referenced: the speed of photons in vacuum, *c*.

6. Conclusions

It is assumed that time and the three dimensions of space do not exist as separate features of our universe, but form a four-dimensional continuum known as spacetime. These observations suggest that space is also relative and that anything disturbing one of the four spacetime dimensions will affect the other three

as well. In support of this is the currently accepted definition for the meter as the distance covered by light in vacuum during 1/299,792,458 s, as well as the view that the greater a material particle is accelerated in the direction of *c*, the greater the time dilation and length contraction will be.

In this article, one hypothetical experiment, one real experiment performed in the 1970s, and one experiment from a different field of science are discussed to denote that both time and velocity are relative but subject to an upper limit imposed by the speed of photons in vacuum. In the first experiment, person A is standing still on the Earth surface, and person B is onboard a train passing by person A at the constant speed of 60 km/h (as measured by person B on the train's speedometer). Because we do not know the absolute speed of planet Earth, and since there is no universal, stationary frame of reference against which all other frames of reference may be referenced, we come to conclude that neither person A nor person B is more or less stationary than the other, and both speeds are thusly relative. This reasoning would be "absolutely" correct if it were not for length contraction, time dilation and the speed limit imposed by the speed of photons in vacuum.

Indeed, persons A and B define two distinct inertial frames of reference, which correspond to two different spacetime conditions and which are therefore characterized by comparatively different lengths of the meter and durations of the second, as predicted by the Lorentz factor. Therefore, if person B onboard the train measures the train's speed relative to person A as 60 km/h, then person A cannot see person B passing by at 60 km/h, as person A will look at the moving train and perceive each meter in the train's frame of reference slightly shorter and each second in the train's frame of reference slightly longer than person A's own meters and seconds (at this non-relativistic speed, such effects are so small that it is not possible to measure them experimentally), as given by the Lorentz factor. A simple calculation shows that person A will perceive the train passing by at 59.99999999999981455834 km/h.

If we consider the speed of photons in vacuum (c = 299,792,458 m/s) as a universal reference, and if we consider that the greater a material particle is accelerated in the direction of *c*, the greater time dilation and length contraction will be, then we will have a way to position any two particles' velocity directly and absolutely in relation to *c*, which means we can tell which particle is moving closer to *c*.

If, in addition to persons A and B, there is person C occupying an independent, distinct inertial frame of reference, and considering that such person C is capable of comparatively measuring the duration of 1 second experienced by person A and by person B, person C will be unable to determine persons A and B's absolute speeds, but may infer which one is moving at a speed closer to *c*. How can this inference be reconciled with the understanding that regardless the speed (or more accurately, the spacetime condition) of the observer, he/she will always perceive the speed of photons in vacuum as c = 299,792,458 m/s? The

answer may be provided by the observation that we are not dealing with time or space considered individually, but with spacetime instead.

Acknowledgements

Acknowledgments are due to Instituto Superior de Agronomia from the University of Lisbon (R. B. F.) and to Instituto Português de Oncologia de Lisboa Francisco Gentil (J. B. F.).

Conflicts of Interest

The authors declare no conflicts of interest regarding the publication of this paper.

References

[1] Einstein, A. (1905) *Annalen der Physik*, **322**, 891-921. https://doi.org/10.1002/andp.19053221004

[2] Abramson, N.H. (2018) *Journal of Modern Physics*, **9**, 471-478. https://doi.org/10.4236/jmp.2018.93033

[3] Burde, G.I. (2018) *Journal of Modern Physics*, **9**, 1591-1616. https://doi.org/10.4236/jmp.2018.98100

[4] Buenker, R.J. (2015) *Open Science Journal of Modern Physics*, **2**, 32-41. http://www.openscienceonline.com/journal/osjmp

[5] Hafele, J.C. and Keating, R.E. (1972) *Science*, **177**, 168-170. https://doi.org/10.1126/science.177.4044.168

[6] Hafele, J.C. and Keating, R.E. (1972) *Science*, **177**, 166-168. https://doi.org/10.1126/science.177.4044.166

[7] Hafele, J.C. (1970) *Nature*, **227**, 270-271. https://doi.org/10.1038/227270a0

[8] Hafele, J.C. (1972) *American Journal of Physics*, **40**, 81-85. https://doi.org/10.1119/1.1986450

[9] Einstein, A. (1915) *Sitzungsberichte der Preussischen Akademie der Wissenschaften zu Berlin*, **1915**, 844-847. https://doi.org/10.1007/978-3-662-48039-7_11

Journal of Modern Physics, 2022, 13, 1197-1203
https://www.scirp.org/journal/jmp
ISSN Online: 2153-120X
ISSN Print: 2153-1196

A Plan to Reclaim Deuterons Escaping from the Loss Cone of a Magnetic Mirror

Mitsuaki Nagata

Soft Creator Company, Kyoto, Japan
Email: nagata@heian-kogyo.jpo

How to cite this paper: Nagata, M. (2022) A Plan to Reclaim Deuterons Escaping from the Loss Cone of a Magnetic Mirror. *Journal of Modern Physics*, **13**, 1197-1203.
https://doi.org/10.4236/jmp.2022.138070

Received: June 28, 2022
Accepted: August 22, 2022
Published: August 25, 2022

Abstract

Research on magnetic mirror reactors has had two serious problems since the beginning stage. One is the magnetohydrodynamic instability due to the negative curvature of the magnetic field lines around the center region of a mirror bottle. Another is the loss of charged particles escaping from the loss cone of a magnetic mirror. We have continued to inquire into a means to solve the latter problem. We here propose a new way which will be able to make a magnitude of a loss angle of a magnetic mirror for deuterons virtually zero.

Keywords

Magnetic Mirror, Control of Escaping Deuterons, Plasma Heating by an Extraordinary Wave

1. Introduction

It would seem that researches for a magnetic mirror fusion reactor are far behind in comparison with ones for Tokamak. The cause may be that a magnetic mirror field has configuration being open-ended [1] [2]. However, recently, a new magnetic mirror reactor scheme [3] was proposed. The scheme tries to solve the problem of the negative curvature by making a mirror length very long so that the region with the negative curvature may nearly vanish. Also, it uses helical winding coils at both ends of the mirror bottle. The helical windings resemble those in Stellarator and will be stronger than a magnetic field of a solenoid, with respect to the magnetohydrodynamic instability due to gravity or charge-separation. However, the helical windings do not intend to suppress the number of escaping charged particles as much as possible. We previously reported a plan [4] in which a supplemental magnetic mirror (called SMM) is

connected to the exit of a magnetic mirror bottle. SMM had the spaces for heating charged particles by cyclotron resonance waves within. The main results are as follows: 1) The magnitude of the loss angle decreased from 14.5˚ (in the exit of the bottle) to about 5˚ (in the exit of SMM) by accelerating velocity components perpendicular to the magnetic field. 2) However, nonrelativistic particles (deuterons) had inherent disadvantage that the acceleration invites deuterons from being outside the loss cone into inside the loss cone. Relativistic particles (electrons) were not related to such an effect. 3) Heavy deuterons required a very long flight length and a very powerful electric field in order for those to get a necessary velocity by the acceleration.

Also, we found a mistake (deuterons are not heated, in a high density plasma, by an extraordinary wave with an ion cyclotron frequency). It may be impossible to make a loss angle for deuterons zero by relying only on acceleration with electric waves. In this work, together with re-consideration of the plasma heating by an extraordinary wave [5] [6] [7], we inquire into a new way of reflecting a deuteron having a very fast velocity by a constant electric field which is not extremely large.

2. A New Plan to Reclaim Escaping Deuterons

We assume that the most part of the bottle is filled with such an ideal plasma consisting of electrons and deuterons as shown below:

◎ Electron density n_e = deuteron density $n_i = 10^{21}\ \mathrm{m}^{-3}$.

◎ Plasma temperature $T = 4\times10^{8}\ \mathrm{K}$.

Then, the most probable thermal velocity υ_{im} of deuterons is

$$\upsilon_{im} = \left(2k_B T/m_i\right)^{1/2} = 1.8\times10^{6}\ \mathrm{m/sec}$$

$$k_B = 1.38\times10^{-23}\ \mathrm{J/K},$$

m_i is a deuteron mass $3680m_e$ where m_e is the rest mass of an electron 9.1×10^{-31} kg.

The mean thermal velocity $\overline{\upsilon_i}$ of deuterons is

$$\overline{\upsilon_i} = \left(\frac{8k_B T}{\pi m_i}\right)^{1/2} = 2\times10^{6}\ \mathrm{m/sec}.$$

The mean thermal velocity $\overline{\upsilon}$ of electrons

$$\overline{\upsilon} \simeq \left(\frac{8k_B T}{\pi m_e}\right)^{1/2} = 1.2\times10^{8}\ \mathrm{m/sec}.$$

We show in **Figure 1** a plan to reclaim deuterons escaping from a magnetic mirror bottle. In the exit in the left-hand side of the bottle, Apparatuses (A) and (B) (called App (A), App (B)) are installed. Each of those has a square cross section. App (B) is a rolled one of App (A) by 90 degree. App (A) is divided into an upper space and an under space, and in each space the following electric field is imposed:

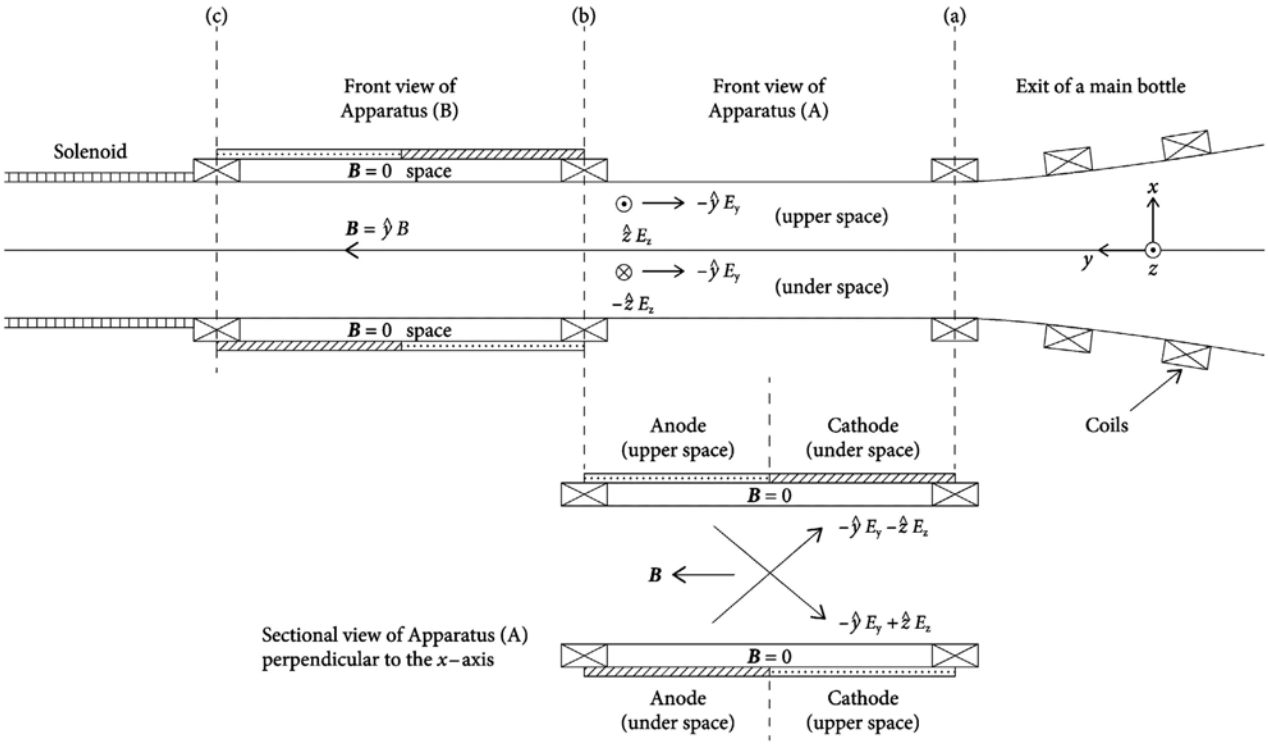

Figure 1. A schematic diagram of an apparatus to reclaim escaping deuterons. Extraordinary waves with ω_{r2} (in Equation (10)) and ω_{r1} (in Equation (9)) are sent to Apparatus (A), Apparatus (B), respectively.

$$\begin{cases} -\hat{y}E_y + \hat{z}E_z \text{ V/m in the upper space,} \\ -\hat{y}E_y - \hat{z}E_z \text{ V/m in the under space.} \end{cases}$$

The left-hand side of App (B) is connected with a system (corresponding to App (B)) in the right-hand side of the bottle by a solenoid. Coils, Solenoid, App (A) and App (B) must be cooled against collisions with high energy particles.

Since heavy deuterons take electrons together through the Coulomb forces, we roughly regard that, in a steady state, gases within App (A) and App (B) are plasmas. A plasma pressure P_p corresponding to $n_i = n_e = 10^{21}\ \mathrm{m}^{-3}$ in the bottle is

$$P_p = (n_i + n_e)k_B T = 1.1\times 10^7\ \mathrm{N/m^2} \simeq 110 \text{ atmospheric pressure.} \quad (1)$$

A necessary magnetic pressure $B^2/2\mu\ \mathrm{N/m^2}$ (where, B is a magnetic field and μ is the permeability of vacuum $4\pi \times 10^{-7}$ mT/A) to stand against P_p is given by

$$P_p = \frac{B^2}{2\mu} = 1.1\times 10^7\ \mathrm{N/m^2} \text{ or } B = 5.26\ \mathrm{T} \quad (2)$$

So, we assume that a magnetic field in the central part of the bottle is 6 T, also that a magnetic field B "in the exit (plane (a)) of the bottle and accordingly within App (A) and App (B)" is 6 × 4 × 4 T. Though a velocity distribution (with respect to the y-components) in plane (a) is unclear, here we consider sending back deuterons with the y-components (denoted by v_y) of velocities between 0

and $2\upsilon_{im}$ to plane (a).

Let us aim a deuteron (called D^+ ion) starting from plane (a) with υ_y given by "$2\upsilon_{im} = 2\left(2k_BT/m_i\right)^{1/2} \equiv \upsilon_{y0}$" at time $t = 0$. D^+ ion is a nonrelativistic particle. The velocity υ_y of D^+ ion decreases according to

$$\upsilon_y = \upsilon_{y0} - \frac{qE_y}{m_i}t \tag{3}$$

In the flight from plane (a) to plane (c), let us an effective length by which the electric field E_y acts on D^+ ion to be ℓ m.

When υ_y of D^+ ion becomes zero in plane (c), a mean velocity of υ_y in the flight is $\upsilon_{y0}/2$. Then, we have

$$\upsilon_{y0} - \frac{qE_y}{m_i}\cdot\frac{\ell}{\upsilon_{y0}/2} = 0$$

or

$$E_y\ell = \frac{1}{2}\frac{m_i\upsilon_{y0}^2}{q} = 1.4\times10^5 \text{ V}. \tag{4}$$

If $\ell = 10$ m, a necessary electric field E_y is 1.4×10^4 V/m. This value will be a producible one. The electric field $\pm\hat{z}E_z$ in App (A) moves D^+ ion in the direction of $(\pm\hat{z}E_z \times \hat{y}B_y)$. The movement-length $\ell_\perp$ is, when $E_z \simeq 10^4$ V/m and an effective length for $\pm E_z$ to act in the flight from plane (a) to plane (b) is $\ell/2 = 5$ m,

$$\ell_\perp = \frac{E_z}{B}\frac{\ell/2}{\upsilon_{y0}/2} = 4.6 \text{ mm} \tag{5}$$

The mean Larmor radius r_L of deuterons is

$$r_L = \frac{m_i\bar{\upsilon}_i}{qB} = 0.78 \text{ mm} \tag{6}$$

Since the ratio $\ell_\perp/r_L$ is 4.6/0.78 ≃ 6, the most part of deuterons escaping from plane (c) to the solenoid ought not to touch the wall of the solenoid. Even if a part of high-energy deuterons collide with the wall, a sincere problem will not arise if only we make the number of colliding deuterons sufficiently small.

3. Plasma Heating by Extraordinary Waves (Called X-Waves)

Since we consider that heating of charged particles should be slowly done outside a main bottle so as not to disturb the stability of a plasma within the bottle, we consider heating deuterons in App (A) with X-wave (the frequency ω_{r2} shown after) and electrons in App (B) with another X-wave (the frequency ω_{r1} shown after).

The refractive index n_x for X-wave with a frequency ω [8] is given by

$$n_x^2 = \frac{\left(1-\beta_i^2\right)\left(1-\beta_e^2\right) - 2\alpha^2\left(1-\beta_i\beta_e\right) + \alpha^4}{\left(1-\beta_i^2\right)\left(1-\beta_e^2\right) - \alpha^2\left(1-\beta_i\beta_e\right)} \tag{7}$$

Here,

$$\beta_e = \frac{\omega_e}{\omega} \qquad \left(\omega_e \simeq \frac{qB}{m_{er}},\ m_{er} = \frac{m_e}{\left(1-\frac{\upsilon^2}{c^2}\right)^{1/2}} \right)$$

where c is the light speed,

$$\beta_i = \frac{\omega_i}{\omega} \qquad \left(\omega_i \simeq \frac{qB}{m_i},\ m_i = 3680 m_e \right)$$

$$\alpha \simeq \frac{\omega_p}{\omega} \qquad \left(\omega_p \simeq \left(\frac{n_e q^2}{m_{er}\varepsilon_0} \right)^{1/2} \right)$$

Two resonance frequencies are found from

$$\left(1-\beta_i^2\right)\left(1-\beta_e^2\right) - \alpha^2\left(1-\beta_i\beta_e\right) = 0 \tag{8}$$

1) When $\beta_e^2 \simeq 1$, Equation (8) is simplified to

$$1-\beta_e^2-\alpha^2 \simeq 0 \ \text{ or } \ \omega^2 \simeq \omega_e^2 + \omega_p^2 \equiv \omega_{r1}^2 \tag{9}$$

2) When $\beta_e^2 \gg 1$, Equation (8) is simplified to

$$-\omega_e^2\left(\omega^2-\omega_i^2\right) - \omega_p^2\left(\omega^2-\omega_i\omega_e\right) = 0$$

Accordingly,

$$\omega^2 = \omega_i^2 + \frac{\left(\omega_i\omega_e-\omega_i^2\right)\omega_p^2}{\omega_e^2+\omega_p^2} \simeq \omega_i^2\left(1+\frac{\omega_p^2}{\omega_i\omega_e\left(1+\frac{\omega_p^2}{\omega_e^2}\right)}\right) \equiv \omega_{r2}^2 \tag{10}$$

From (10), under the condition $\omega_{r2}^2 \ll \omega_e^2$, we have

$$\begin{cases} \text{When } \omega_p^2 \ll \omega_e\omega_i,\ \omega_{r2} \simeq \omega_i, \\ \text{When } \omega_p^2 = \omega_e\omega_i,\ \omega_{r2} \simeq \sqrt{2}\omega_i, \\ \text{When } \omega_p^2 \gg \omega_e^2,\ \omega_{r2} \simeq \left(\omega_i\omega_e\right)^{1/2}. \end{cases} \tag{11}$$

We try concrete numerical calculations on ω_{r1} and ω_{r2}.

We assumed just now that a magnetic field strength B in the exit of the main bottle is $B = 6\times4\times4 = 96\ \mathrm{T}$. A half vertical angle α_h of the magnetic mirror is 14.5 degree, from $\sin\alpha_h = (6/96)^{1/2}$. We roughly regard that a gas within App (A) is a plasma and also that a deuteron density n_A in a steady-state is a quantity of order of

$$n_A = 10^{21}\times\frac{14.5^\circ}{90^\circ} = 0.16\times10^{21}\ \mathrm{m}^{-3}$$

Then, within App (A),

$$\omega_p \simeq \left(\frac{n_A q^2}{m_{er}\varepsilon_0}\right)^{1/2} = 0.68\times10^{12}\ \mathrm{sec}^{-1},\ \left(\varepsilon_0 = 8.855\times10^{-12}\ \frac{\mathrm{Farad}}{\mathrm{m}}\right)$$

$$\omega_e = \frac{qB}{m_{er}} = 1.55\times10^{13}\ \text{sec}^{-1},$$

$$\omega_i = \frac{qB}{m_i} = 4.59\times10^{9}\ \text{sec}^{-1},$$

$$\omega_{r1} = \left(\omega_e^2 + \omega_p^2\right)^{1/2} \simeq 1.551\times10^{13}\ \text{sec}^{-1} \simeq \omega_e \quad \text{(from (9))},$$

$$\omega_{r2} \simeq 2.9\omega_i\ \text{sec}^{-1} \quad \text{(from (10))}.$$

An ordinary wave (O-wave) can pass through a plasma if $1-\left(\omega_p^2/\omega^2\right)>0$. O-wave with ($\omega=\omega_{r1}$) is not cut off because $\omega_p^2/\omega_{r1}^2 \ll 1$. O-wave with ($\omega=\omega_{r2}$) is cut off because $\omega_p^2/\omega_{r2}^2 \gg 1$. However, O-wave passing through a plasma will hardly heat the plasma. Energy of a wave with a resonance frequency ought to be absorbed by a plasma. We presume that the wave with ($\omega=\omega_{r2}$) will heat mainly deuterons because $\omega_{r2} \ll \omega_e$.

4. Discussion and Conclusion

In order to reclaim the most part of deuterons escaping from the loss cone of a magnetic mirror bottle, we have proposed the new means based on the idea of decreasing those velocity components parallel to the magnetic field to zero by the external constant electric fields.

The new plan is under the premise that the external electric fields within Apparatus (A) do not suffer a large variation by escaping charged particles. We consider, in the upper space of the lower figure of Figure 1, movements of charged particles in the $\pm z$-directions. Electrons drift in the -z-direction and some electrons arrive at Anode (upper space) after having passed ($\boldsymbol{B}=0$)-space. Deuterons drift in the z-direction and some deuterons arrive at Cathode (upper space) after having passed another ($\boldsymbol{B}=0$)-space. Let us assume that the number n_a of electrons arriving at Anode per unit time is more than the number n_c of deuterons arriving at Cathode per unit time. Then, the n_c electrons flow as a current in an external circuit, but the $n_a - n_c$ electrons remain in the ($\boldsymbol{B}=0$)-space and create a negative potential space. As a result, a potential on the ($\boldsymbol{B}=0$)-boundary plane becomes lower than the potential of Anode. However, since the charged particles are tightly restrained by very strong magnetic force lines and drift velocities of deuterons and electrons in the $\pm z$-directions ought to be very slow, we consider that such an effect as mentioned above has hardly influence on the magnitudes of E_y and E_z.

"If the constant electric field E_y works well", the apparatus in Figure 1 can make a magnitude of a loss angle for deuterons virtually zero. We consider that a combination of the apparatus in Figure 1 and a long mirror bottle has engineering simplicity.

Conflicts of Interest

The author declares no conflicts of interest regarding the publication of this paper.

References

[1] Mirnov, V. V. and Ryutov, D. D. (1979) *Soviet Technical Physics Letters*, **5**, 279.

[2] Ågren, O., Moiseenko, V.E., Noack, K. and Hagnestål, A. (2011) *Problems of Atomic Science and Technology*, **17**, 3.

[3] Mazzucato, E. (2019) *Fusion Science and Technology*, **75**, 197-207. https://doi.org/10.1080/15361055.2018.1448202

[4] Nagata, M. (2019) *Journal of Modern Physics*, **10**, 145-156. https://doi.org/10.4236/jmp.2019.102011

[5] Moiseenko, V.E. and Ågren, O. (2012) *AIP Conference Proceedings*, **1442**, 199.

[6] Gospodchikov, E.D. and Smolyakova, O.B. (2015) *Radiophys and Quantum Electronics*, **57**, 857. https://doi.org/10.1007/s11141-015-9570-9

[7] Artemyev, A.V., Aqapitov, O.V. and Krasnoselskikh, V.V. (2013) *Physics of Plasmas*, **20**, Article No. 124502. https://doi.org/10.1063/1.4853615

[8] Stix, T.H. (1962) The Theory of Plasma Waves. McGraw-Hill, New York.

Journal of Modern Physics, 2022, 13, 1204-1211
https://www.scirp.org/journal/jmp
ISSN Online: 2153-120X
ISSN Print: 2153-1196

Diffusion of a Brownian Particle in a Periodic Potential with Memory Friction

Meng Hu, Zhanwu Bai*

Department of Mathematics and Physics, North China Electric Power University, Baoding, China
Email: humeng030@163.com, *baizhanwu@126.com

How to cite this paper: Hu, M. and Bai, Z.W. (2022) Diffusion of a Brownian Particle in a Periodic Potential with Memory Friction. *Journal of Modern Physics*, **13**, 1204-1211.
https://doi.org/10.4236/jmp.2022.138071

Received: July 11, 2022
Accepted: August 23, 2022
Published: August 26, 2022

Abstract

This study investigates the diffusive motion of a Brownian particle in a 1D periodic potential. The reactive flux theory for finite barriers and memory friction is developed to calculate the escape rate in the spatial diffusion regime. The diffusion coefficient is obtained in terms of the jump-model. The theoretical results agree well with the Langevin simulation results. The method can be generalized to other colored noises with Gaussian distribution.

Keywords

Escape Rate, Finite Barrier, Memory Friction

1. Introduction

The Kramers rate [1] theory and its successive development for all damping, the original Melnikov and Meshkov (MM) theory for white noise [2], and Pollak, Grabert and Hanggi (PGH) theory for general noise [3], are correct for high potential barriers. Nevertheless, the finite or the lower barrier is universal in practical stochastic processes. Two main approaches are employed for finite barrier correction. One is based on the generalized Langevin equation equivalent to Hamiltonian formulism, and the other is based on the Fokker-Planck equation. The perspective of the former is the finite barrier correction in the framework of PGH theory and improved PGH theory [4]. The improved PGH theory with finite barrier correction for Ohmic friction is quite accurate over the whole friction range up to the reduced barrier height 4. However, high accuracy agreement between theoretical and numerical exact results in the spatial diffusion regime cannot be expected, especially when the reduced barriers are low, because the perturbation parameter in the theory is no longer small. Within the framework of the Fokker-Planck processes in the spatial diffusion regime, a perturbation

theory was developed to calculate the finite barrier escape rate by means of the flux over population expression, the Rayleigh quotient, and the mean first passage time to the stochastic separatrix [5]. Although a simple analytical perturbation solution can be obtained for a polynomial potential, obtaining a simple analytical solution for a nonpolynomial potential is difficult. The two approaches mentioned above have some limitations. The equivalent Hamiltonian approach is a perturbation theory for weak damping and extrapolation to spatial diffusion regime is questionable. In addition, obtaining a simple analytical expression from the finite barrier correction to the PGH theory is difficult. The Fokker-Planck equation approach relies on the existence of a Fokker-Planck equation. However, this situation is not always the case for a generalized Langevin equation with general noise and an arbitrary potential. This approach is also based on perturbation expansion, which is not suitable for low barriers.

To develop a simple, accurate and widely applicable approach to incorporate the finite barrier correction in analytical calculation of the escape rate, the reactive flux theory for finite barriers is proposed in [6]. The theoretical results match well with the simulation results until lower barriers for a Brownian particle moving in a cubic metastable potential and subjected to a Gaussian white noise.

The Brownian motion in a periodic potential can model many physical and chemical situations, such as the motion of ions in superionic conductors [7], the Josephson supercurrent in tunneling junctions [8] [9], the mass transport in solids [10] [11], and the diffusion on surfaces [12]. Several analytical results with finite barrier correction were given in the spatial diffusion regime for the diffusion of a Brownian particle in a periodic potential. The escape rate for an internal Ornstein-Uhlenbeck noise has been investigated within the frameworks of Grote-Hynes [13] theory with high potential barriers and PGH theory [14] [15] for not too large damping and correlation time. In the present work, we extend our finite barrier correction scheme [6] to an internal Ornstein-Uhlenbeck noise to calculate analytically the diffusion coefficient in the spatial diffusion regime with finite barrier correction.

2. Reactive Flux Theory for Finite Barriers and Memory Friction

We consider a Brownian particle with unit mass diffusing in a 1D periodic potential under the influence of an internal Ornstein-Uhlenbeck noise. The particle is in contact with a heat bath at temperature T, which provides fluctuation and dissipation. The dynamics of the process is governed by the following generalized Langevin equation:

$$\ddot{x}+\int_0^t \mathrm{d}t'\gamma\left(t-t'\right)\dot{x}\left(t'\right)=-V'\left(x\right)+\varepsilon\left(t\right). \tag{1}$$

where $\varepsilon\left(t\right)$ is the Ornstein-Uhlenbeck noise, which is associated with the memory kernel function $\gamma\left(t\right)$ by the fluctuation-dissipation theorem:

$$\left\langle \varepsilon(t)\varepsilon(t')\right\rangle = k_B T\gamma(t-t'), \tag{2}$$

where k_B is the Boltzmann constant, $\gamma(t)$ is the memory kernel function, given by

$$\gamma(t) = \frac{\gamma}{\tau}\exp(-t/\tau), \tag{3}$$

where τ is the correlation time of the noise, and γ is regarded as the effective friction coefficient due to $\gamma = \int_0^\infty \mathrm{d}t\gamma(t)$. In Equation (1), $V(x)$ is the 1D periodic potential, given by

$$V(x) = V_0 \cos x. \tag{4}$$

What we want to investigate is the diffusion coefficient in the spatial diffusion regime, which can be attributed to the calculation of escape rate, because single jump is dominate in the spatial diffusion regime.

In the traditional reactive flux formulation, an initial equilibrium distribution is assumed for the trajectories of particles starting at the top of the barrier. The equilibrium state assumption at the top of the barrier is reasonable for higher potential barriers because the current is small. It is no longer a good approximation for lower potential barriers where the current is not small enough. For finite barriers, we remove the starting point of the trajectories to somewhere $x = x_0$ in the potential well where the probability distribution can be regarded as an equilibrium one, and replace the potential barrier from x_0 to x_b (top of the barrier) with an equivalent parabolic barrier in the spatial diffusion regime. x_0 is given by $V(x_0) = V_b - k_B T$, where $V_b = 2V_0$ is the potential barrier height, and $k_B T$ is the average energy fluctuation of a quasi-equilibrium distribution. The equivalent potential $V_e(x)$ is given by

$$V_e(x) = V_b - \frac{1}{2}m\omega_b^2 x^2. \tag{5}$$

The equivalent potential barrier frequency ω_b can be determined by the potential approach scheme in the barrier region, that is by minimization of the following average

$$I = \int_{x_0}^{x_1} \mathrm{d}x\left[V(x) - V_e(x)\right]^2 P_e(x), \tag{6}$$

where $P_e(x)$ is the Boltzmann distribution normalized in barrier region, in which the potential $V_e(x)$ is used. x_0, x_1 are two intersection points of the straight line $V = V_b - k_B T$ with the original potential. Similar to the derivation of the escape rate in original reactive flux theory, the expression of the escape rate for Gaussian white noise can be worked out [6]:

$$k = \frac{k_B T}{nQ\omega_b}\left[\sqrt{\omega_b^2 + \gamma^2/4} - \gamma/2\right]\exp\left(-\frac{V_b}{k_B T}\right). \tag{7}$$

The population n in the expression can be approximated by

$$n = \frac{1}{Q}\int_{-\infty}^{x_0}\mathrm{d}x\int_{-\infty}^{\infty}\mathrm{d}v_0 \exp\left(-\frac{V(x)}{k_B T}\right)\exp\left(-\frac{v_0^2}{2mk_B T}\right), \tag{8}$$

where Q is the partition function for the particles in the potential well.

When the theory is extended to an internal Ornstein-Uhlenbeck noise, a difficulty is encountered: the second order moments appearing in the probability density in barrier region is a oscillation function and the limits as time t tend to infinite do not exist, that is, the steady-state probability density does not exist. The steady-state probability density only exists for a small parameter region below the dashed line in Figure 1.

By using the method of characteristic function, the Fokker-Planck equation for transition probability density $P(x,v,t)$ in the barrier region is given as follows [16]:

$$\frac{\partial P}{\partial t} = -v\frac{\partial P}{\partial x} - \tilde{\omega}_b^2(t)x\frac{\partial P}{\partial v} + \tilde{\gamma}_b(t)\frac{\partial (vP)}{\partial v} + \psi_b(t)\frac{\partial^2 P}{\partial x \partial v} + \phi_b(t)\frac{\partial^2 P}{\partial^2 v}, \tag{9}$$

where the subscript b signifies the dynamical quantities defined at the barrier top. The expressions of these quantities can be found in [16]. $\tilde{\omega}_b(t)$ and $\tilde{\gamma}_b(t)$ in the above equation can be called the renormalized (by the noise) potential barrier frequency and friction coefficient, and the original potential barrier frequency can be called bare frequency. For an internal Ornstein-Uhlenbeck noise, the steady-state transition probability density only exists in the region below the dashed curve in Figure 1. We use $s_i\,(i=1,2,3)$ to denote the three poles of the Laplace transformation of the coordinate Green function, *i.e.*, the roots of the following characteristic equation:

$$s^3 + as^2 + bs + c = 0, \tag{10}$$

with $a = 1/\tau, b = \gamma/\tau - \omega_b^2, c = -\omega_b^2/\tau$. For large time, *i.e.*, $-(s_1 + Res_2)t \gg 1$, $\psi_b(t), \phi_b(t)$ in Equation (9) can be approximated as

$$\psi_b(t) = k_B T\left(\tilde{\omega}_b^2(t)/\omega_b^2 - 1\right), \phi_b(t) = k_B T\tilde{\gamma}_b(t), \tag{11}$$

and $\tilde{\omega}_b^2(t), \tilde{\gamma}_b(t)$ are given by

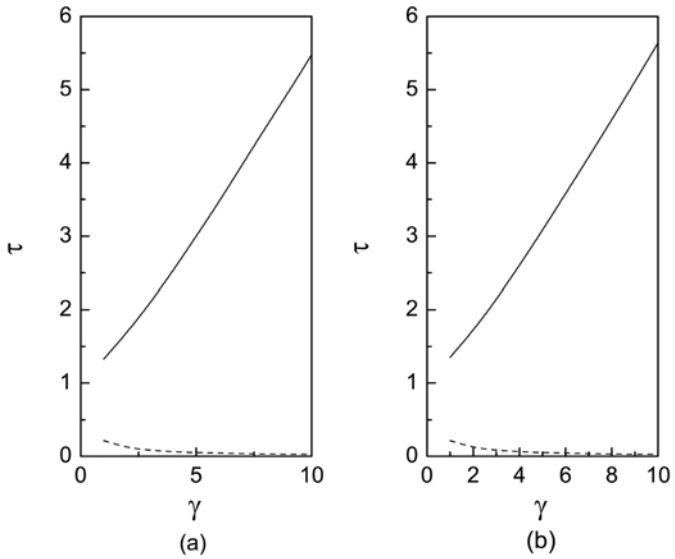

Figure 1. The applicable parameter region of the theory is below the solid line. (a) for $T = 0.4$, (b) for $T = 0.6$.

$$\tilde{\omega}_b^2(t) = \frac{\omega_b^2 \mathrm{Re}s_2}{\tau|s_2|^2} + \frac{\omega_b^2 \mathrm{Im}s_2}{\tau|s_2|^2}\tan(\mathrm{Im}s_2 t), \tag{12}$$

$$\tilde{\gamma}_b(t) = -(s_1 + Res_2) + Ims_2 \tan(Ims_2 t),$$

where s_1 and s_2 denote the roots of Equation (10) with the maximal and the secondary maximal real parts, respectively, and "Re" and "Im" denote the real and imaginary parts of the complex, respectively. If the root s_2 satisfies $|\mathrm{Im}s_2|t \gg 1$, we integrate two sides of the Fokker-Planck equation for large number periods, which results in an effective steady-state Fokker-Planck equation satisfied by an effective probability density, which is the long term average of the usual probability density and is just the quantity we need for the calculation of the mean escape rate for the time. If $|\mathrm{Im}s_2|t \gg 1$ is not satisfied, the imaginary part of $\tilde{\omega}_b^2(t)$, $\tilde{\gamma}_b(t)$ can be neglected because of the large barrier passing time t and the effective steady-state Fokker-Planck equation remains in the same form. Some details can be found in our previous work [17]. The barrier frequency ω_b in the above expressions is the renormalized one, which incorporates the finite barrier correction. The expression of the escape rate has the same form as (7), but ω_b^2, γ are replaced with the renormalized long term average frequency and damping, given by

$$\left\langle \tilde{\omega}_b^2(t) \right\rangle = -\frac{\omega_b^2 \mathrm{Re}s_2}{\tau|s_2|^2}, \tag{13}$$

$$\left\langle \tilde{\gamma}_b(t) \right\rangle = -(s_1 + Res_2),$$

and the expression of the escape rate is

$$k = \frac{k_B T}{nQ\sqrt{\left\langle \tilde{\omega}_b^2(t) \right\rangle}} \left[\sqrt{\left\langle \tilde{\omega}_b^2(t) \right\rangle + \left\langle \tilde{\gamma}_b(t) \right\rangle^2 / 4} - \left\langle \tilde{\gamma}_b(t) \right\rangle / 2 \right] \exp\left(-\frac{V_b}{k_B T} \right), \tag{14}$$

n is given by Equation (8). Because single-jump is dominant in the spatial diffusion regime, the diffusion coefficient is given by

$$D = \frac{1}{2}\Gamma d^2 = kd^2, \tag{15}$$

where $\Gamma = 2k$ is the total jump rate, and d is the spatial period of the potential, here $d = 2\pi$. For some parameters, $\left\langle \tilde{\gamma}_b(t) \right\rangle \le 0$, which is physically unreasonable. The theory is applicable below the solid line (plotted with $\left\langle \tilde{\gamma}_b(t) \right\rangle = 0$) in **Figure 1**. In contrast to the PGH theory [14], the proposed method can also be applied to large damping and correlation time case provided that the parameter is below the solid line in **Figure 1**.

3. Diffusion Coefficient: Theory versus Simulation

To avoid a direct simulation of the generalized Langevin Equation (1), we introduce an auxiliary variable

$$z = -\int_0^t \mathrm{d}t' \gamma(t - t') \dot{x}(t') + \varepsilon(t), \tag{16}$$

which satisfies the following differential equation

$$\dot{z}+\frac{\gamma}{\tau}v+\frac{1}{\tau}z=0, \tag{17}$$

in which the fluctuation-dissipation theorem (2) has been used, and v is the velocity. Hence, the generalized Langvin Equation (1) is equivalent to the following Markovian-type Langvin equations

$$\begin{aligned}\dot{x}&=v\\ \dot{v}&=-V'(x)+z\\ \dot{z}&=-\frac{\gamma}{\tau}v-\frac{1}{\tau}z\end{aligned} \tag{18}$$

We simulate the Langevin Equations (18) by the second-order Runge-Kutta algorithm. In the calculation, the natural unit ($m=1$, $k_B=1$), the dimensionless parameter $V_0=1$, and the time steps are $\Delta t=10^{-4}$ for $\tau=0.1$ and $\Delta t=5\times10^{-4}$ for $\tau=0.4$. The test particles start from the a potential well and have zero velocity. The number of test particles $N=5\times10^5$ is used to describe the diffusion motion of a Brownian particle. The mean square displacement $\left\langle\left(\Delta x(t)\right)^2\right\rangle$ reveals a good linear relation at long times. The diffusion coefficient D is obtained by the long time behavior of the mean square displacement

$$\left\langle\left(\Delta x(t)\right)^2\right\rangle=2Dt. \tag{19}$$

Figure 2 shows that the theoretical results of the diffusion coefficient (Equation (14) and Equation (15)) match well with the Langevin simulation results. In

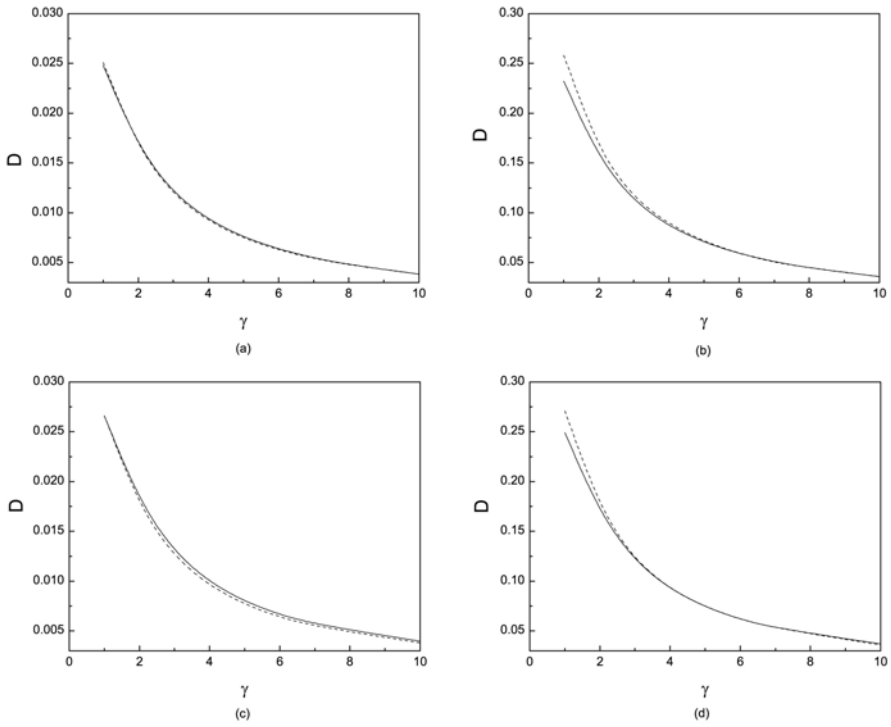

Figure 2. Diffusion coefficient: theory versus simulation. The solid lines are theoretical results, and the dashed lines are simulation results. Where $V_b=2$, other parameters are: (a) $T=0.4,\tau=0.1$; (b) $T=0.4,\tau=0.4$; (c) $T=0.6,\tau=0.1$; (d) $T=0.6,\tau=0.4$.

the spatial diffusion regime, specified by $\gamma \geq 2\omega_b$, the maximal errors are about 4% for $T = 0.4, \tau = 0.4$ and 2% for other cases.

For higher temperatures or lower reduced potential barrier heights, the error increases, which can be interpreted as the jump-model being no longer a good approximation.

4. Summary

In the spatial diffusion regime, the calculation of diffusion coefficient is attributed to the calculation of the escape rate. The reactive flux theory for finite barriers is developed to incorporate finite barrier effect. The starting point of the Brownian particle is removed into the potential well where the probability density can be viewed as an equilibrium one, and the potential barrier is equivalent to a parabolic one. An equivalent steady-state Fokker-Planck equation is established to overcome the difficulty of the absence of the steady-state probability density. The theoretical results for diffusion coefficient indicate a good agreement with the Langevin simulation results in a certain range of parameters.

Conflicts of Interest

The authors declare no conflicts of interest regarding the publication of this paper.

References

[1] Kramers, H. (1940) *Physica*, **7**, 284-304. https://doi.org/10.1016/S0031-8914(40)90098-2

[2] Melnikov, V.I. and Meshkov, S.V. (1986) *The Journal of Chemical Physics*, **85**, 1018. https://doi.org/10.1063/1.451844

[3] Pollak, E., Grabert, H. and Hanggi, P. (1989) *The Journal of Chemical Physics*, **91**, 4073. https://doi.org/10.1063/1.456837

[4] Pollak, E. and Ianconescu, R. (2016) *The Journal of Physical Chemistry A*, **120**, 3155-3164. https://doi.org/10.1021/acs.jpca.5b11502

[5] Talkner, P. (1994) *Chemical Physics*, **180**, 199-213. https://doi.org/10.1016/0301-0104(93)E0426-V

[6] Bai, Z.W. (2021) *Physical Review E*, **103**, Article ID: 042144.

[7] Dieterich, W., Fulde, P. and Peschel, I. (1980) *Advances in Physics*, **29**, 527-605. https://doi.org/10.1080/00018738000101406

[8] Bttiker, M., Harris, E.P. and Landauer, R. (1983) *Physical Review B*, **28**, 1268. https://doi.org/10.1103/PhysRevB.28.1268

[9] Ben-Jacob, E., Bergman, D.J., Matkowsky, B.J. and Schuss, Z. (1982) *Physical Review A*, **26**, 2805. https://doi.org/10.1103/PhysRevA.26.2805

[10] Munakata, T. and Kawakatsu, T. (1985) *Progress of Theoretical Physics*, **74**, 262-271. https://doi.org/10.1143/PTP.74.262

[11] Kawakatsu, T. (1986) *Progress of Theoretical Physics*, **75**, 747. https://doi.org/10.1143/PTP.75.747

[12] Agassi, D. and Eberly, J.H. (1985) *Physical Review Letters*, **54**, 34. https://doi.org/10.1103/PhysRevLett.54.34

[13] Grote, R.F. and Hynes, J.T. (1980) *The Journal of Chemical Physics*, **73**, 2715. https://doi.org/10.1063/1.440485

[14] Ianconescu, R. and Pollak, E. (2014) *The Journal of Chemical Physics*, **143**, Article ID: 104104. https://doi.org/10.1063/1.4929709

[15] Ianconescu, R. and Pollak, E. (2016) *Faraday Discussions*, **195**, 111-138. https://doi.org/10.1039/C6FD00105J

[16] RayChaudhuri, J., Chattopadhyay, S. and Banik, S.K. (2007) *Physical Review E*, **76**, Article ID: 021125. https://doi.org/10.1103/PhysRevE.76.021125

[17] Fan, W.Y., Bai, Z.W., Zhang, W. and Ding, L.P. (2020) *Physica A*, **547**, Article ID: 123836. https://doi.org/10.1016/j.physa.2019.123836

Journal of Modern Physics, 2022, 13, 1212-1215
https://www.scirp.org/journal/jmp
ISSN Online: 2153-120X
ISSN Print: 2153-1196

Lorentz Transformation Leads to Invariance of the Difference between the Electric and Magnetic Field Intensity

Stanislaw Olszewski

Institute of Physical Chemistry, Polish Academy of Sciences, Warsaw, Poland
Email: solszewski@ichf.edu.pl

How to cite this paper: Olszewski, S. (2022) Lorentz Transformation Leads to Invariance of the Difference between the Electric and Magnetic Field Intensity. *Journal of Modern Physics*, **13**, 1212-1215.
https://doi.org/10.4236/jmp.2022.138072

Received: August 1, 2022
Accepted: August 27, 2022
Published: August 30, 2022

Abstract

In course of a direct calculation we demonstrate the activity of parameters of the Lorentz transformation entering the original electric and magnetic field vectors $\boldsymbol{E}$ and $\boldsymbol{H}$. The validity of the transformation is shown with the aid of the relation $\boldsymbol{E}^2 - \boldsymbol{H}^2 = \boldsymbol{E}'^2 - \boldsymbol{H}'^2$ which holds for any suitable pair of the vectors $\boldsymbol{E}$, $\boldsymbol{H}$ and $\boldsymbol{E}'$, $\boldsymbol{H}'$. No special geometry of the vector pairs entering $(\boldsymbol{E}, \boldsymbol{H})$ and $(\boldsymbol{E}', \boldsymbol{H}')$ is assumed. The only limit applied in the paper concerns the velocity ratio betweeen v and c which should be smaller than unity.

Keywords

Electric and Magnetic Intensity Pairs, v Denotes the Velocity Ratio between Two Vector Systems

1. Introduction

The aim of the paper is to examine the effect of the Lorentz transformation of the electromagnetic field when the field formulae are general. The Lorentz transformation of the electromagnetic field is a well-known tool applied in numerous motion occasions [1] [2]. But, in spite of its importance, a general kind of the Lorentz transformation concerning three dimensions of the electromagnetic field, seems to be rather seldom discussed. Usually the transformation is limited to a special geometry assumed for a moving particle, or specific values of the applied mechanical parameters.

The main aim of applying the Lorentz transformation seems to be a search for the application of some invariant expressions which remain exactly unchanged.

A well-known example is a tensor built up of the electric and magnetic components [1] [2]:

$$\left(F_{ik}\right)=\begin{pmatrix} 0 & H_z & -H_y & -iE_x \\ -H_z & 0 & H_x & -iE_y \\ H_y & -H_x & 0 & -iE_z \\ iE_x & iE_y & iE_z & 0 \end{pmatrix} \tag{1}$$

which represent field intensities belonging to one four-dimensional electromagnetic tensor [2].

2. Requirements Concerning the Lorentz Transformation

In general the Lorentz transformation replaces the original components of the electromagnetic field, viz.

$$\begin{aligned} &E_x, E_y, E_z, \\ &H_x, H_y, H_z, \end{aligned} \tag{2}$$

by the new components

$$\begin{aligned} &E_{x'}, E_{y'}, E_{z'}, \\ &H_{x'}, H_{y'}, H_{z'}. \end{aligned} \tag{3}$$

Both kinds of components are coupled according to the fomulae [2]:

$$E_x = E_{x'}, \tag{4}$$

$$E_y = \frac{E_{y'} + \frac{v}{c}H_{z'}}{\sqrt{1-\frac{v^2}{c^2}}} = \frac{E_{y'}}{p(v/c)} + \frac{\frac{v}{c}H_{z'}}{p(v/c)}, \tag{5}$$

$$E_z = \frac{E_{z'} - \frac{v}{c}H_{y'}}{\sqrt{1-\frac{v^2}{c^2}}} = \frac{E_{z'}}{p(v/c)} - \frac{\frac{v}{c}H_{y'}}{p(v/c)}, \tag{6}$$

$$H_x = H_{x'}, \tag{7}$$

$$H_y = \frac{H_{y'} - \frac{v}{c}E_{z'}}{\sqrt{1-\frac{v^2}{c^2}}} = \frac{H_{y'}}{p(v/c)} - \frac{\frac{v}{c}E_{z'}}{p(v/c)}, \tag{8}$$

$$H_z = \frac{H_{z'} + \frac{v}{c}E_{y'}}{\sqrt{1-\frac{v^2}{c^2}}} = \frac{H_{z'}}{p(v/c)} + \frac{\frac{v}{c}E_{y'}}{p(v/c)}. \tag{9}$$

Here

$$p(v/c) = \sqrt{1-\frac{v^2}{c^2}} \tag{10}$$

where v represents the velocity of the system.

It should be noted that sometimes a simplification is done in which instead of (10) the number

$$p \approx 1 \tag{11}$$

is assumed. Our aim is however, to perform the Lorentz calculation on an accurate basis of (4) - (9), and not with the aid of the Formula (11).

3. Lorentz Transformation and a Search for the Difference $E^2 - H^2$

We find that our application of the Lorentz transformation gives as a result that the invariance property of the difference

$$\boldsymbol{E}^2 - \boldsymbol{H}^2 = \text{const} \tag{12}$$

does hold.

The first term on the left of (12) becomes:

$$\begin{aligned} \boldsymbol{E}^2 &= E_x^2 + E_y^2 + E_z^2 \\ &= E_{x'}^2 + \frac{E_{y'}^2}{p^2(v/c)} + \frac{2H_{z'}\frac{v}{c}E_{y'}}{p^2(v/c)} + \frac{H_{z'}^2\frac{v^2}{c^2}}{p^2(v/c)} \\ &\quad + \frac{E_{z'}^2}{p^2(v/c)} - \frac{2H_{y'}\frac{v}{c}E_{z'}}{p^2(v/c)} + \frac{H_{y'}^2\left(\frac{v}{c}\right)^2}{p^2(v/c)}. \end{aligned} \tag{13}$$

In the next step, the second term on the left of (12) taken without a minus sign gives:

$$\begin{aligned} \boldsymbol{H}^2 &= H_x^2 + H_y^2 + H_z^2 \\ &= H_{x'}^2 + \frac{H_{y'}^2}{p^2(v/c)} - \frac{2\frac{v}{c}H_{y'}E_{z'}}{p^2(v/c)} + \frac{\left(\frac{v}{c}\right)^2 E_{z'}^2}{p^2(v/c)} \\ &\quad + \frac{H_{z'}^2}{p^2(v/c)} + \frac{2\frac{v}{c}H_{z'}E_{y'}}{p^2(v/c)} + \frac{\left(\frac{v}{c}\right)^2 E_{y'}^2}{p^2(v/c)}. \end{aligned} \tag{14}$$

Because of the minus sign which has the expression for $\boldsymbol{H}^2$ in (12) we obtain the following result for the difference in (12):

$$\begin{aligned} \boldsymbol{E}^2 - \boldsymbol{H}^2 &= E_{x'}^2 - H_{x'}^2 + \left(E_{y'}^2 + E_{z'}^2 - H_{y'}^2 - H_{z'}^2\right)\frac{1}{p^2}\left(1 - \frac{v^2}{c^2}\right) \\ &= E_{x'}^2 - H_{x'}^2 + \left(E_{y'}^2 + E_{z'}^2 - H_{y'}^2 - H_{z'}^2\right) \\ &= \boldsymbol{E}^2 - \boldsymbol{H}^2. \end{aligned} \tag{15}$$

Here the full Formula (10) concerning expression $p(v/c)$ is taken into account.

4. Summary

The paper examines the Lorentz transformation extended to the case when the

electromagnetic field represented by a general vector formula acting on a system is applied.

We show that also in this situation the difference of the square values of the electric and magnetic field remains equal to a constant term which is uninfluenced by the transformation.

Conflicts of Interest

The author declares no conflicts of interest regarding the publication of this paper.

References

[1] Landau, L.D. and Lifshitz, E.M. (1969) Mechanics. Electrodynamics. Izd. Nauka, Moscow. (in Russian)

[2] Landau, L.D. and Lifshitz, E.M. (1948) Field Theory. 2nd Edition, OGIZ, Moscow. (in Russian)

Journal of Modern Physics, 2022, 13, 1216-1251
https://www.scirp.org/journal/jmp
ISSN Online: 2153-120X
ISSN Print: 2153-1196

Prediction of Radioactive Half-Lives and Atomic Nucleus Dimensions in a Concentric Shell Model or Flocon Model

Marc Mignonat

Société d'Astronomie des Pyrénées Occidentales, Pau, France
Email: mmignonat@libertysurf.fr

How to cite this paper: Mignonat, M. (2022) Prediction of Radioactive Half-Lives and Atomic Nucleus Dimensions in a Concentric Shell Model or Flocon Model. *Journal of Modern Physics*, **13**, 1216-1251.
https://doi.org/10.4236/jmp.2022.138073

Received: June 10, 2022
Accepted: August 28, 2022
Published: August 31, 2022

Abstract

Considering only the wave aspect, we determine the energy of a bond between 2 nucleons; this quantified energy is associated with a standing wave. Then, starting from the mass loss corresponding to this energy, we determine the number of bonds in this nucleus. The mass defect value for a link is used to determine a specific length at that link. Fixing a precise distance between nucleons makes it possible to determine a geometry of the nucleus and its dimensions. It makes it possible to understand when this bond is stronger than the electrostatic force and allows deducing a shell model built in a precise order. The calculation on the mass defect will also make it possible to determine that one or more nucleons concerned by the radioactivity will be bound by a single bond to the rest of the nucleus or, on the contrary, bound by several bonds which induce short ½ lives or, on the contrary, very long. The analysis of the bonds on H, He and C make it possible to write formulae which are then applied to the nuclei to find the radioactive ½ lives. To find by equations the radioactive ½ lives does not call into question the standard model since it concerns only the defect of mass of the nuclei with energies that are not used to find the main particles of the standard model. This model, which favours a geometric approach to the detriment of a mathematical approach based on differential equations, can lead to theoretical questions about the possibility of interpreting the structure of the nucleus in a more undulatory way. It is possible to explain radioactivity in a more deterministic way.

Keywords

½ Radioactive Lives, Atomic Nucleus Dimensions, Shell Model

1. Introduction and Theoretical Postulate

For each particle, we will consider only the wave aspect, which will allow studying the binding as interferences or combinations of waves. The calculation is made from the number of proton-neutron bonds δ that will be isolated and counted from the mass defect Δm. (Δm is the difference between the masses of the neutron and the proton and it is considered that this corresponds to the energy of a bond).

1) The nucleons are thus considered as a combination of waves of which we can determine a main or resulting wave whose frequency f is calculated simply by posing $E_p = m_p c^2$ and $E_p = hf_p \Rightarrow f_p = m_p c^2 h^{-1}$ (with E_p proton energy, m_p proton mass, c = light velocity, h = Planck constant, f_p proton associated frequency); Similarly the frequency associated with the neutron will be $f_n = m_n c^2 h^{-1}$

2) The frequency Δf of the resulting interference wave of 2 others waves will be $\Delta f = |f_n - f_p|$

The bonds inside stable nuclei, such as helions, are not taken into account in the calculation of the ½ lives. Nor is there any attempt to find the bond energies of particles such as mesons, bosons or gluons. These particles from the standard model have energies far superior to the mass defect of the binding energies.

This p-n interference wave takes an energy of $\Delta m = 0.001389$u to the neutron, the neutron and the proton vibrate at the same frequency. It is postulated that this induces a standing wave which will favour and thus determine a very precise distance d between the nucleons corresponding to a ½ wavelength λ of the period P_p of proton vibration ($P_p = 0.433 \times 10^{-23}$ s), so $d = 0.65 \times 10^{-15}$ m. The anti-node of this standing wave explains an "attractive force" between 0.65 and 0.97 fm and a "repulsive force" when the distance is less than 0.65 fm. It provides an explanation to a repulsive strong interaction when the distance tends to 0 and attractive at medium distance. In fact, theoretically and thus verifiable, depending on the distance with other anti-nodes, the force would be alternately repulsive or attractive. (Attractive when $n \times 0.65$ fm $< d < n \times 0.97$ fm, $n \in N$). The size of a proton can thus be defined as the distance between 2 anti-nodes or 0.65 fm on average with a maximum size of 0.97 fm. This size assumption is consistent with the estimated radius of the proton (proton radius = 0.831 fm [1]) (see Figure 1).

In fact, it is assumed that the binding between two nucleons consists of standing waves and an interference wave. This postulate with a standing wave therefore induces a precise and necessary distance d for the bond to be established between a proton and a neutron. This precise distance forces the nucleus to have a precise geometry. Thus, if the distance between a proton and a neutron can remain fixed, the bond will be stable. If geometry prevents the nucleon from staying at this ideal distance, the bond will be unstable.

The energy E of a wave is of the form $E = \int \psi^2 \mathrm{d}x$ (ψ = amplitude of the wave), therefore for a wavelength λ, E is of the form $E = \psi^2 \lambda$ or for the standing wave since $d = \lambda/2$, $E = \psi^2 d$. When d increases, the energy or the mass defect

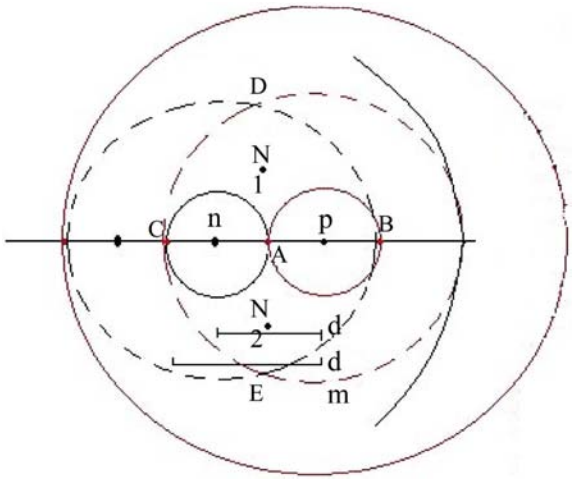

Figure 1. Proton-neutron liaison. The proton p has a period of 4.3×10^{24} s or a wavelength of 1.29×10^{-15} m. When the neutron n loses 0.00139 u in the p-n bond, standing waves can be established between the 2 nucleons. We take the shortest possible distance d or a ½ wavelength, which means that the nucleons are "in contact". The anti-nodes of the standing wave are at points A, B, C. The centres p and n of the 2 nucleons will tend to remain at the nodes where the vibrations are of lower amplitudes. The maximum distance dm without break will be when the point n reaches C with the point p remaining in place or when the point p reaches B with the point n remaining in place. $d_m = d/2 = 0.9675 \times 10^{-15}$ m. B and C are points where the amplitudes of the waves from n and p cancel each other out. It is the same beyond B and C. However on the right perpendicular to BC passing by A, there will be maxima of amplitude in D and E and beyond. There will be nodes in N1 and N2 located exactly at the distance d from n and p that will allow 2 other nucleons to be positionned there.

increases. If d corresponds to an energy Δm, then we can write that the total length of the bonds d_t corresponds to a total mass defect Δm_t.

$$d_t = \left(d/\Delta m\right) \times \Delta m_t \tag{1}$$

3) It is the P_{pn} periods of the interference bond and the nucleon period that are useful in determining the ½ lifes.

If a bond assumes 2 identical frequencies so that a standing wave can be established, it is necessary that the neutron loses $\Delta m = 0.001389$ u to have a vibration frequency identical to the proton; thus, there may be a interference pn in the bond between a proton and a neutron; 2 isolated neutrons will tend to group in pairs with no additional loss of mass. With this rule, nothing prevents a nucleon from interfering with several nucleons or groups of nucleons as long as their vibration frequencies are identical and it is located at a vibration node. When the nucleon is located at one or more distances d, the bond and thus the nucleus is stable.

We do know, however, that for a theory, stationary wave superimposition is a questionable element. Sazdjian [2] writes in his thesis that the superimposition will see "the position of the zero point move over time with a certain pulsation" and will no longer correspond to a fixed point. When the distance d cannot be identical for 2 bonds, there will be superposition of several standing waves of

slightly different periods, which will cause instability in the binding with a computable period.

2. Method of Calculation

2.1. Reminder of the Equivalence between Frequencies, Periods and Mass Defect

The interference wave p-n will have a frequency $\Delta f_{pn} = f_n - f_p$ (f_n frequency of neutron vibrations, f_p frequency of proton vibrations). Its period P_{pn} will therefore be $P_{pn} = 1/|f_n - f_p| = 3.19 \times 10^{-21}$ s (This period can be calculated directly by posing $P_{pn} = h/E$ with h = Planck constant, E = energy in J corresponding to 0.00139u which is the mass difference between a neutron and a proton. For the neutron, the period would be 0.44×10^{-23} s and for the proton 0.433×10^{-23} s)

The period P_{pn} of the interference pn will have a larger period than the standing wave of period P_p in a ratio $P = P_{pn}/P_p$. the standing wave and the interference wave will therefore be in phase with this periodicity P.

This periodicity P in the bond L, depending on whether we consider the period of the proton P_p or that of the neutron P_{ne}, will be equal to

$$P = P_{pn}/P_p \tag{2}$$

or

$$P = P_{pn}/P_{ne}\ . \tag{3}$$

Considering the frequencies, (2) and (3) become:

$$P = f_p/\Delta f_{pn} \tag{4}$$

or

$$P = f_n/\Delta f_{pn} \tag{5}$$

(The frequencies f_n, f_p and Δf_{pn} are all of the form $f_x = m_x c^2 h^{-1}$. There is therefore a simplification that allows to directly calculate the period P from the masses in u)

$$P = m_p/\Delta m \tag{6}$$

or

$$P = m_n/\Delta m \tag{7}$$

(with $\Delta m = m_n - m_p$; $m_n = 1.008665$ u and $m_p = 1.007276$ u)

(The order of magnitude is $P = m_p/\Delta m = 725.18$ s (if the nucleon has lost more mass, e.g. $5\Delta m$, then the bond will have a P period equal to 720.18 s ($P = (m_n - 5\Delta m)/\Delta m$))

2.2. Calculation Methods That Can Be Used to Determine the Number of Isolated Bonds

1) The mass defect Δm_t found for each nucleus, will make it possible to determine how many bonds δ with an energy of 0.000139u ($\delta = \Delta m_t/0.001389$ (8)). We can reasonably assume that when the number of bonds within a group is

very large, the group will be particularly stable: for helium4, we find a mass defect corresponding to 21 bonds p-n ($\delta = 21.07$), which confirms the special role of this grouping. The mass defect for a helium nucleon can so reach $5\Delta m$ (the maximum of isolated bonds does not exceed 9 for the heaviest elements) (See Table A1 in Appendix 2).

2) The number of bonds corresponding to the number of N helions present in the nucleus (21 bonds per helion) is subtracted and so the number of bonds of the triplets 3H (6 bonds) or 3He (5 bonds), or doublet 2H (1 bond) when they are present. These groupings are formed primarily as shown by the results on how the mass defect increases, the analysis of the elements from H to C, and the consequence that the elements with odd Z are monoisotopic. We thus determine the number of isolated bonds δ' between the helions or with the groups 3H, 3He, 2H starting with the stable elements.

$$\delta' = \delta - 21.07N - 6.41N_1 - 5.17N_2 - N_3 \tag{9}$$

(N_1, N_2, N_3 are respectively the number of ^{3}H, ^{3}He, ^{2}H; N_1, N_2, N_3 are 0 or 1, when one is 1, the other 2 are 0)

3) Finally, for a given isotope Y of greater and generally radioactive mass, the number of additional bonds δ'' in relation to the precedent lower isotope X is determined, taking into account that these additional bonds may be double on shell 2, triple on the 3, etc. (on multiple bonds and shells, see paragraph 3-3-2).

$$\delta'' = \left(\delta_y - \delta_x\right)/n \tag{10}$$

(δ_y = total number of bonds of Y, δ_x = total number of bonds of X, $n = 1$ for a single bond, $n = 2$ from shell 2)

2.3. Half-Life Calculation

Figure 2 shows the ½ radioactive lives of 3337 radioactive isotopes from H to Pb elements from Nubase [3] [4] [5] [6]. Most of the ½ radioactive lives are between 10^{-4} and 10^{7} s, a small part around 10^{-7} s; the ½ long lives above 10^{10} s are divided into 4 undulations; a peak of ultrashort lives is around 10^{-22} s. These 3 distribution zones correspond to different mass defects:

Since there are 3 zones and a correlation between the times of ½ lives and the number of bonds δ'' (see Table A1), we considered 3 ways of interfering for waves:

- Interferences of several bonds for one nucleon ($\delta'' > 3$) for 1/2 long lives.
- Interference of a bond of one nucleon with another ($0 < \delta'' \leq 3$) for short 1/2 lives.
- Pass time ($\delta'' \leq 0$) for the ultra short 1/2 lives.

2.3.1. ½ Life When There Is a Nucleon for Several Bonds ($\delta'' > 3$)

The nucleon concerned by radioactivity will have several bonds with different nucleons located at distances d_1, d_2, d_n. Each link will have an average period of 725 s when d is the average distance. The relationship between the period and the distance is given by

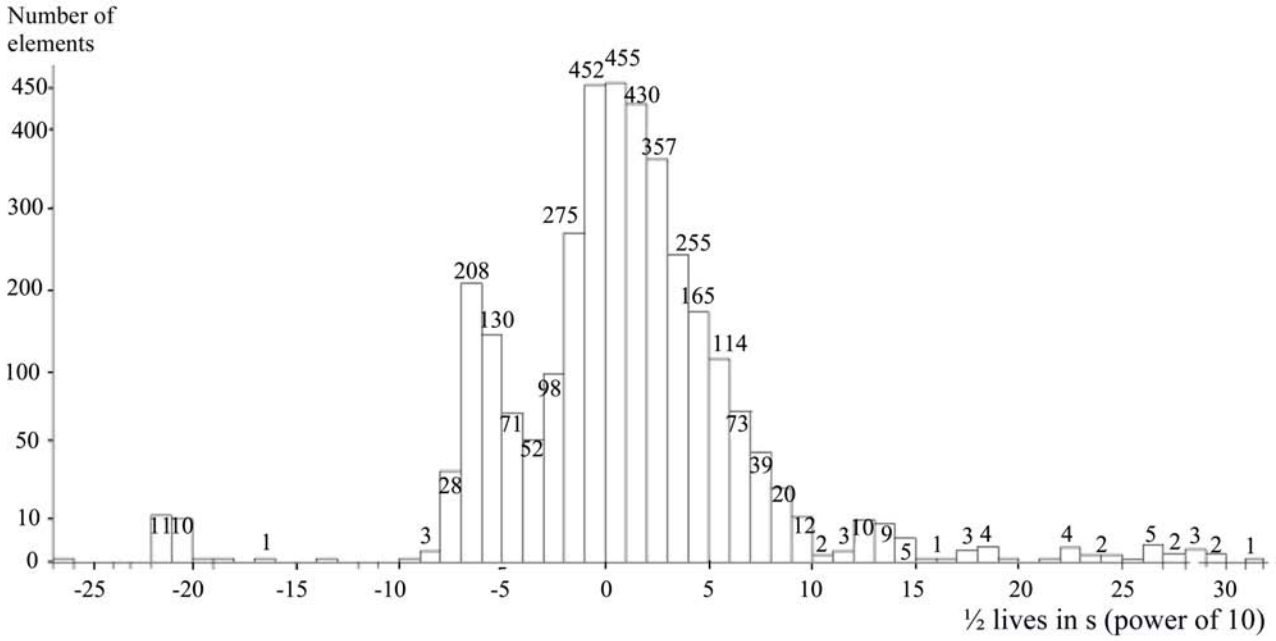

Figure 2. Distribution of radioactive ½ lives of 3337 isotopes: There is: 1) a central zone with a main peak between 10^{-4} and 10^{7} s where most ½ lives are located (median between 10 and 10^{2}). 2) A peak between 10^{-22} and 10^{-20} s. 3) Another peak around 10^{-7} s. 4) Above the central zone, 4 increases in the number of ½ lives are observed from 10^{10} to 10^{15}, from 10^{15} to 10^{20}, from10^{20} to 10^{25}, from 10^{25} to 10^{30} s. These 4 increases could correspond to wave combinations, but the number is statistically small.

$$P = P_{pn} \times c/2d \tag{12}$$

(see calculation Appendix 2). (The distance d varying between a minimum and a maximum, the period P will vary between 363 s and 1088 s) It is assumed that radioactivity will occur when the nucleon or helion has several such bonds in phase. This is a long half-life.

Thus a neutron with k bonds of period P will have a 1/2 life

$$T = P^{k} \tag{17}$$

2.3.2. ½ Life When There Is One or More Nucleons for a Bond ($\delta'' = 1$ or 2)

The nucleon concerned by the radioactivity will have a 1/2 life T due to the difference of periods P_1 and P_2 of 2 waves.

$$T = P_1 - P_2 \tag{15}$$

or

$$T = \left(P_{pn} \times c/2\right) \times \left|d_1 - d_2\right| / d_1 d_2 \tag{16}$$

This formula (calculation in Appendix 2) allows us to find, according to the constraints on distances d1 and d2, the durations of the 1/2 lives for isotopes with ½ lives between 10^{-4} and 10^{7} s.

2.3.3. Ultra Short 1/2 Lives Less Than 10^{-20} s ($\delta'' = 0$ or -1)

For the 1/2 lives of the order of 10^{-20} s, there is no additional bond since there is no additional mass defect and we propose to interpret this time as that of the

passage time of a wavelength or a vibration. The additional nucleons, cannot interfere long enough to create bonds with the vibrations of the neighboring nucleons. When the ½ life is of the order of 10^{-21} s (e.g., for 5He) this could correspond to the vibration period of the interference pn of 3.2×10^{-21} s.

When the period is of the order of 10^{-24} s, it could correspond either to the period of vibration of the nucleon (4.33×10^{-24} s), or to the time of passage of an interference in a part of the nucleus since a fm is traversed in 0.33×10^{-24} s.

3. Results in Applying This Method to the Different Isotopes

The results of the number of bonds from the mass defect, and the correlation with the 1/2 lives are reported in Appendix 2 Table A1. This table shows that:

1) There is a substantial increase of δ to $21\Delta m$ from ^{3}He to ^{4}He.

2) Whenever, when Z is even, the number N of neutron reaches Z, then there is an increase of δ allowing the formation of a new helion.

3) When, in addition to helions, there are 1 proton and 2 neutrons, they will form a ^{3}H. Similarly, when 2p and 1n are available, δ' increases by 5 to form a ^{3}He.

4) Stable elements can be spotted; δ'' is highest for stable or very long 1/2 life elements ($\delta'' > 3$). For short 1/2 lives: $0 < \delta'' \leq 3$ and for 1/2 ultra short lives: $\delta'' \leq 0$.

3.1. H and He (Nucleon-Nucleon Interaction)

- ^{2}H-total mass defect $\Delta m_t = 0.001848$, (8) $\Rightarrow$ $\delta = 1$ (1.3) There is only one bond that cannot interfere with others; the distance d between the centres of neutron n and proton p can remain constant around an average value; the nucleus is therefore stable.

  (The total length of the deuterium will therefore be $2d$ or 1.3 fm)
- ^{2}He cannot exist since there is no pn interference to put the 2 protons at the distance d [and] the repulsive electrostatic force dominates at this distance d. The energy of the bond corresponding to 0.00139u is $E_{pn} = 2.0711 \times 10^{-13}$ J. Since there is a distance $d = 0.645$ fm between the centres of 2 nucleons, the energy E_e of the electrostatic force of Coulomb between 2 protons can be calculated and is 3.567×10^{-13} J ($E_e = K_c \times q^2/d$ with K_c constant of Coulomb $= 8.987 \times 10^{-9}$, q charge of a proton). Between 2 protons, energy E_e decreases to $E_{pn} = 2.0711 \times 10^{-13}$ J at a distance $d_p = 1.111 \times 10^{-15}$ m which is greater than the maximum distance dm of 0.9675×10^{-15} m (see Figure 1). So the bond cannot be made.
- ^{3}H have a mass defect. $\Delta m_t = 0.00891$ u or $\delta = 6.41$. The total mass defect corresponds to 6 bonds. (The additional mass defect δ'' compared to ^{2}H corresponds to 5 proton-neutron bonds). Each neutron being equivalent, we can say that there are 3 bonds per neutron ($k = 3$). As shown in Figure 1, the positioning of a 2nd nucleon seems possible in N3 or N4, which requires the proton and the 1st neutron to be positioned at a wavelength that is a distance

$2d$ (see Figure 3). N3 is located exactly $2.24d$ from the centre of the 2 other nucleons. The total of the bonds is of $6.48d$ allowing to predict an energy corresponding to $6.48\Delta m$ according to Equation (1). The observed mass defect is $6.41\Delta m$. The value of the radioactive 1/2 life (3.88×10^8 s) will be perfectly recovered by the calculation ((17) $\Rightarrow$ $T = 3.83 \times 10^8$ s) since, spatially without interference, the 3 nucleons can be placed at an ideal distance multiple of d.

- ^{3}He The mass defect Δm_t corresponds to the energy of 5.17 bonds (or $5.17\Delta m$). As for ^{3}H, we can imagine a geometric configuration allowing to find the defect of mass: the 2nd proton binds with the neutron. The electrostatic force brings proton and neutrons to the maximum distance of $1.5d$. The protons will be on a node of the bond between the neutron and the other proton. The total distance between the 3 nucleons is then $5.12d$ (see Figure 4).

Using figure 1, a second neutron can be positioned in N3, the distance np is then increased to 2d, which brings the point N3 to exactly 2.24d of n and p.
The total of the 3 bends is 6.48d corresponding to an mass defect of 6.48Δm (observed mass defect : 6.41Δm)

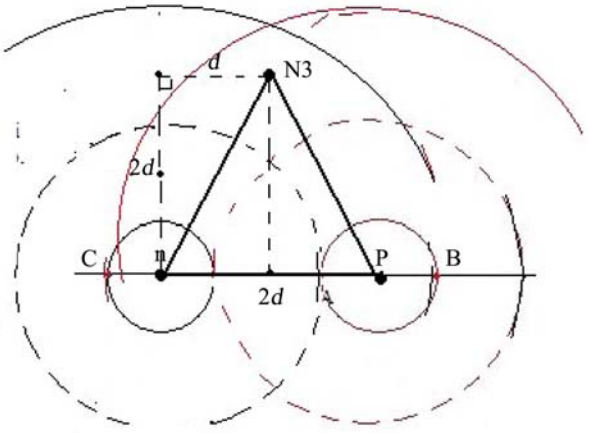

Figure 3. Possible geometry of the nucleus ^{3}H.

Another simple geometric configuration can be imagined to find the mass defect of 5.17Δm of the helium3.
Due to electrostatic repulsion, the bond pn is increased to its maximum of 1.5d. The position of a proton is located in the zone of the node vibration N3, on the perpendicular in n of the bond between the neutron and the other proton.
The total length of the 3 bonds is 5.12 d

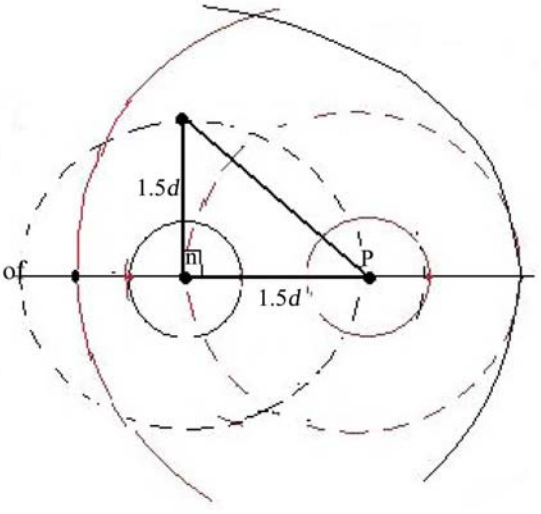

Figure 4. Possible geometry of ^{3}He. This configuration of ^{3}He where the nucleons have only one antinode of vibration instead of two with a distance between them does not vary is a hypothesis that would explain why ^{3}He which contains yet 2 protons is more stable than ^{3}H.

- ^{4}He has a significant mass defect $\Delta m_t = \Delta f_a = 0.02930$ corresponding to $\delta =$ 21.07 bonds L. This significant mass defect Δf_a with many bonds involves a very stable nucleus and makes it possible to say that nucleons first form helions or particles alpha; these mass defects are found whenever 2 protons and 2 neutrons can be grouped by 4. We can imagine many geometric solutions to explain this mass defect of $21.07\Delta m$ and it would be very risky, because of the lack of precise dimensions of the nucleus, to say which one is the right one. We give an example (see Figure 5) simply to say that the hypothesis of a precise geometry with standing waves makes it possible to find the defect of mass. The total d_t of the bonds ($d_t = 21.07d$) makes it possible to find a maximum diameter of the nucleus at 3.379 fm in accordance with the measured diameter of the ^{4}He nucleus at 3.35648 fm [7].
- ^{5}He with an atomic mass M_a of 5.0123 u will have: $\Delta m = 2p + 3n - \Delta f_a - M_a =$ –0.00085u, $\delta' = 0$ therefore no additional bond ($\delta'' = 0$) for the 3rd neutron. It is a neutron emission decay with a 1/2 life of 0.7×10^{-21} s, which could correspond to the period of one vibration or to the passage time of a part of the path of the interference pn which has a period of 3.2×10^{-21} s. (1/4 of the wavelength beats in 0.8×10^{-21} s and is 0.25×10^{-14} m, length of the order of magnitude of the nucleus). So, it could be interpreted as a nucleon that passes at the level of the nucleus and that interferes only the time of its passage.
- ^{6}He has a 1/2 life of 806 ms and with $\Delta m = 0.00136$ u has a single additional bond compared to ^{4}He ($\delta' = 1$) for 2 neutrons that form a halo.

Since $\delta'' = 1$ (a single additional bond compared to ^{5}He, the precedent lower isotope), the 1/2-life T will be calculated from the difference between 2 adjacent periods P_1 and P_2 according to Equation (16). A 1/2 life of $T = 0.806$ s corresponds to a variation of length Δd of only 0.007 fm.

- ^{7}He ($\Delta m = 0.00057$ u so $\delta'' = 0$ additional bond compared to ^{6}He. It is a disintegration by neutron emission as for ^{5}He. The 1/2 life will also correspond to the passage time of a wavelength (we can try the ad hoc explanation that this 1/2 life of 2.9×10^{-21} s corresponds to the time that passes 3/4 of the wave pn, that is 2.4×10^{-21} s).

3He has a mass defect of 5.17 Δm; it is assumed that the additional neutron recreates an identical figure, thus we have a total of 10.34 Δm, after it is multiplied by 2 considering that the nucleons are at one wavelength from each other, so the total is 20.68 Δm. The argument in favor of this geometric conjecture is that the dimension is that of a square of side 4d or 2.58fm with a diagonal of 5.24d or 3.379fm; the measured diameter of the nucleus 4He is 3.35648 fm (7)

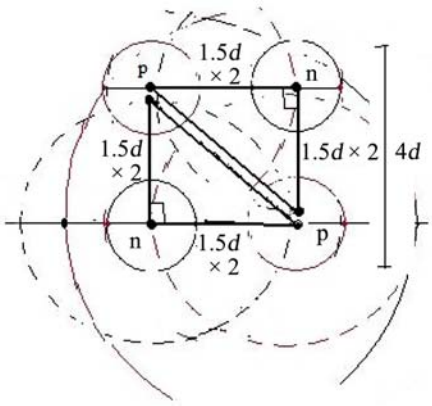

Figure 5. Hypothetical example on the geometry of ^{4}He. If we consider the atomic mass of ^{4}He, the vibration period is 1.1×10^{-24} s.

- ^{8}He (½ vie = 119 ms) will have two bonds ($\delta' = 2.40$) for the four neutrons in halo. The spatial configuration is a hypothesis that would make it possible to better explain the different daughter isotopes (see Figure 6).

3.2. From Li to C

- ^{4}Li $^{\text{and}}$ ^{5}Li release a p and have ½ lives of 0.09×10^{-21} s and 0.37×10^{-21} s.
- ^{6}Li, $\delta = 23.5$, there are $21\Delta m$ to form a helion, $1\Delta m$ for a bond p-n and $1.5\Delta m$ for 2 bonds between the group pn and the helion.
- ^{7}Li, $\delta'' = 6$, the group pn is replaced by a group ^{3}H with its 6 internal bonds.

^{8}Li, $\delta'' = 1.5$, which suggests a bond of $1.5d$ for the last neutron and that the group ^{3}H of the ^{7}Li is not modified. Therefore, the halo should be non-symmetrical since it consists of a neutron and of a group ^{3}H and not 1p + 3n.

^{9}Li, $\delta'' = 3.1$ there are 3 bonds more than the ^{8}Li; a bond will unite the new neutron to the previous; the group will be bound to the central nucleus by a double bond $2d$. So, ^{9}Li will have an elongated shape. When this neutron becomes a proton, there will be formation of 2 ^{4}He and depending on whether the remaining neutron will have its 2 bonds straddling the 2 He or on a single one, we will have the 2 modes of decay at 50% (see Figure 7).

^{10}Li releases a neutron and has a 1/2 life of 1.35 to 3.7×10^{-21} s that can be conjectured to correspond to a passage time proportional to the diameter of the nucleus variable according to the isomer.

^{11}Li has an additional bond to ^{10}Li or ^{9}Li. The pair of neutron attaches to a distance $1d$. The long length of ^{11}Li would thus reach about $9d$.

^{12}Li emits a neutron and we find an ultrashort 1/2life.

- ^{8}Be ($M_a = 8.0053$ u) 4p + 4n − $2\Delta f_\alpha - M_a = -0.00006$. $\delta' = 0$, there is no bond, so this element exists only the time of a wave passage.
- ^{9}Be (9.01218u): $\delta'' = 1.34$. This element is interesting: it is stable despite a small δ'' allowing for the neutron a bond with each of the helions at a short distance ($0.67d$). The stability, with the idea of standing waves, would be due

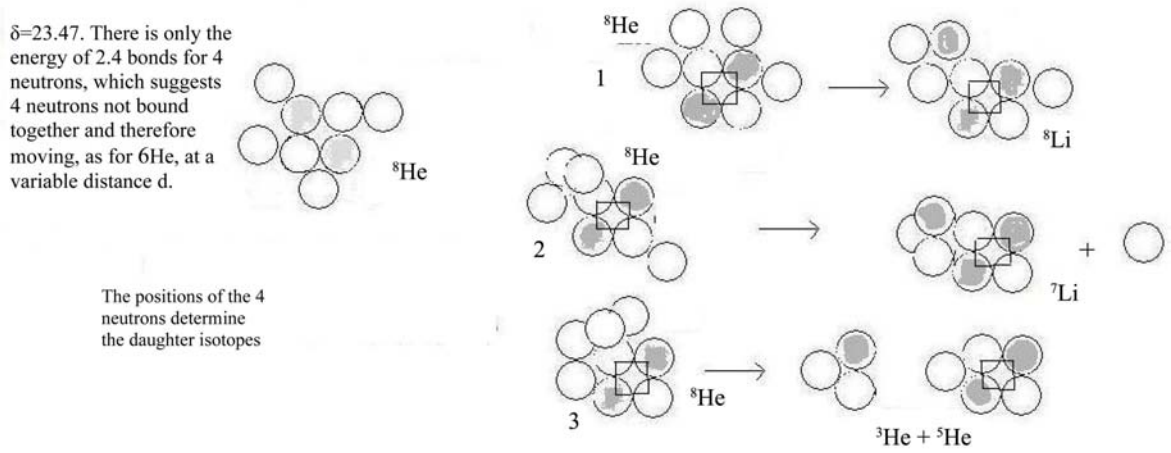

Figure 6. Spatial configuration and ^{8}He daughter isotopes. The configuration 1 where neutrons are dispersed is the most common (83.1%); 1) in 2, 3 nucleons are grouped together (16%); 2) in 3, the 4 nucleons are grouped together (0.09%).

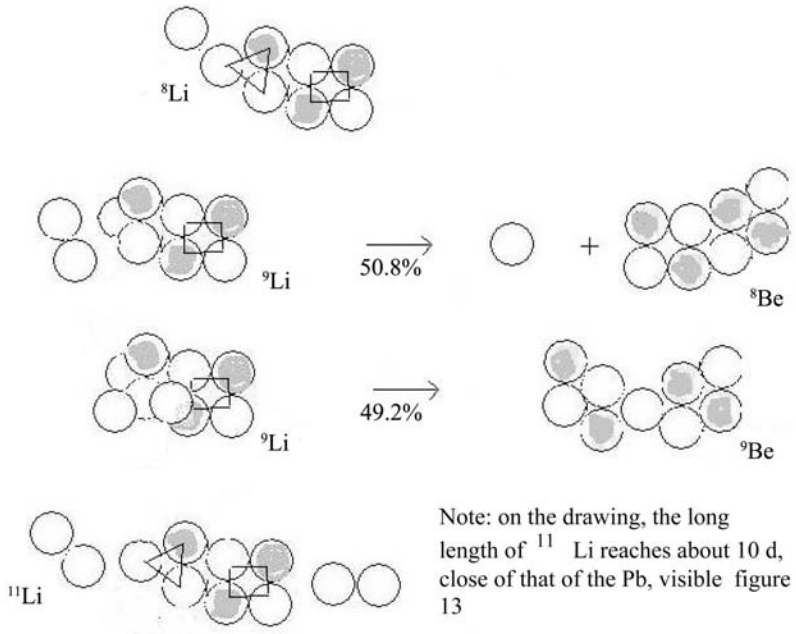

Figure 7. Possible configurations of lithium and berylium. 8Li has 10 bonds in addition to the helion, that is 6 bonds to make a group ^{3}H and 4 bonds to unite at a distance $2d$ the group ^{3}H and the nucleon to the helion. ^{9}Li has 3 additional bonds. The 2 n can grouped together in pair. The position of the 2 n relative to the group ^{3}H at the time of decay could explain the daughter isotopes. ^{11}Li: The peripheral neutrons could be grouped by two because the isolated neutron of the ^{10}Li remains only 2×10^{-21} s.

to the fact that the geometry allows the 2 bonds to have identical distances and therefore frequencies of vibrations without phase shift (Figure 7). The shape of the ^{9}Be that can be deduced is consistent with that described by Ebran, *et al.* [8].

- The carbon atom ^{12}C: it will be composed of 3 helions; subtraction of 3 times the mass defect of one helion makes it possible to find 6 bonds L (we can suppose that each proton of one helion interferes with one of the six neutrons of another helion):

$6p + 6n - 3\Delta f_{\alpha} - 6\Delta f_{pn} = 12.09714 - 3 \times 0.0297 - 6 \times 0.00138 = 11.99971$. We find the exact mass of the ^{12}C, which makes it possible to assume that all 6 bonds have the ideal distance d and that this nucleus is particularly stable.

For ^{13}C, the mass defect ($\delta'' = 3.82$) makes it possible to find 4 additional bonds p-n, which makes it possible to imagine that the additional neutron is fixed by 2 double bonds (bonds of length $2d$ as for ^{3}H) (see Figure 8).

For ^{14}C, there are 6 additional bonds compared to ^{13}C, the last neutron can be linked by 4 bonds (2 doubles and 2 singles).

3.3. Above C, It Is Possible to Construct the Hypothesis of a Model in Shells or Corona

3.3.1. Starting from C, We Start from the Findings from Table A1

1) Helions are primarily constituted. Systematically, for all isotopes, when the number of neutrons reaches the even number of protons Z, there is a loss of

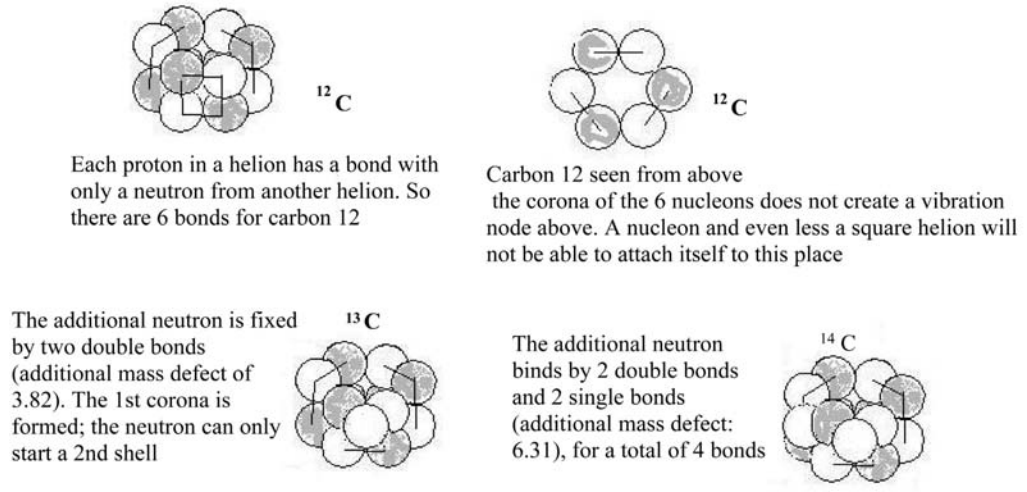

Figure 8. The atom of carbon.

additional mass of at least $21\Delta m$ allowing to constitute a new helion. If a helion cannot be formed, it can be seen that then, first of all, the triplets ^{3}H or ^{3}He are formed (there is a defect of additional mass of 6 or $5\Delta m$).

2) Table A2 (Appendix 2) recalls that, above C, the number of stable nuclei is greater when Z is even. For elements where Z odd, an additional neutron added to the stable isotope will be converted by radioactivity β^- into a proton to form a new helion (When Z odd, the lower-mass stable element above nitrogen is always made up of helions with or without neutron pairs and a group ^{3}H (see paragraph 3-3-3)).

3.3.2. A Model of the Nucleus Will Be Able to Be Drawn from Stable Nuclei Which, Like C, Have a Number of Helions Multiple of 3 (see Figure 9)

We note that for the ^{12}C, there are 6 bonds ($6\Delta m$) between the 3 helions, or 2 bonds by helion.

To interpret the large number ($12\Delta m$) of additional bonds of $^{24}_{12}$Mg for the 3 new helions compared to the ^{12}C:

1) Or we imagine a very large number of connections between the 3 new helions and then, the bigger the nucleus would be the more stable it would be. The nucleus being less stable when it grows, this hypothesis must be rejected.

2) The other hypothesis to explain the large number of additional bonds (the important mass defect) is to say that the distance between the new helions is $2d$ (2 nodes on the standing wave forming the bond) and not d (distance between 2 nodes). (This is the hypothesis we made for ^{3}H and resumed for ^{4}He, ^{13}C and ^{14}C). Each link at a $2d$ distance that we will now call double bond corresponds to an average mass defect of $2\Delta m$.

This hypothesis also has the advantage of being able to describe an excited nucleus. An excited nucleus could be a nucleus where the nucleons are placed at distances of 2, 3 or $4d$. This is consistent with the representations of excited nuclei [8].

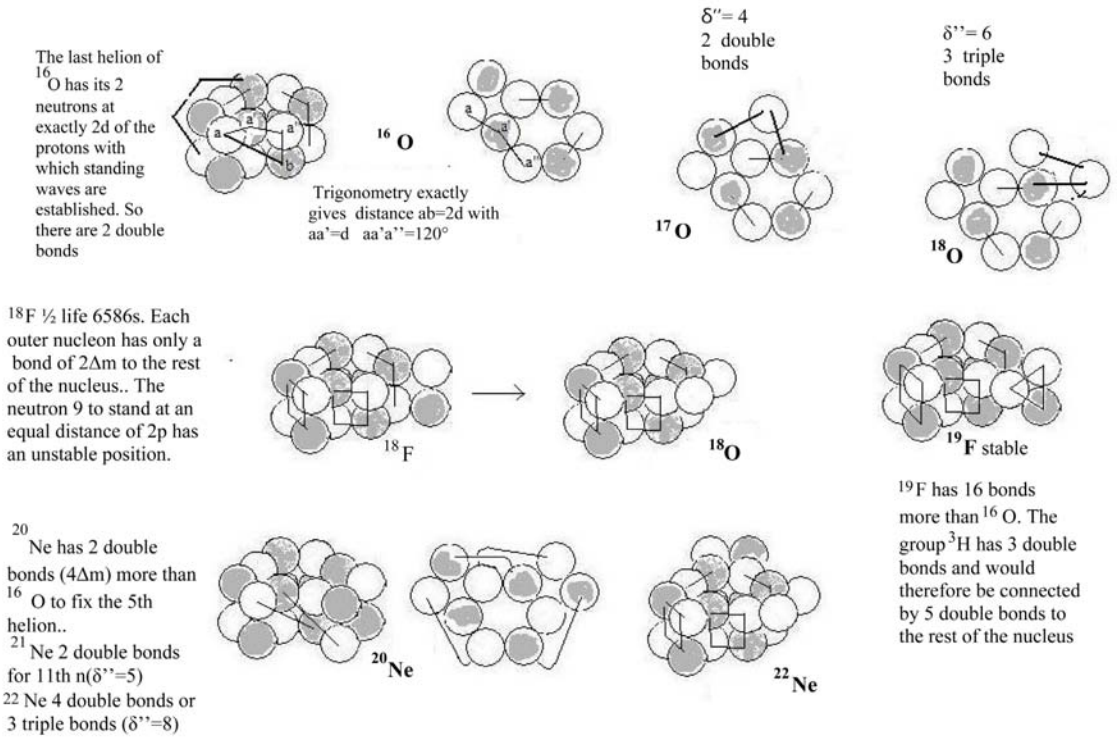

Figure 9. Formation of a 2nd shell.

- So for ^{16}O, if there are still 2 bonds by helion, with a loss of mass of 5.53 Δm, the additional helion will attach itself to the outer part of the ^{12}C corona starting a second shell. Trigonometry makes it possible to verify that the distance between a neutron of this helion and a proton of the 1st shell is exactly 2*d*. The geometry does not allow it to attach itself to the top of the corona because the square shape of the new helion does not correspond to the hexagonal shape of the ^{12}C. Placing the new helion above would not keep the nucleons at a distance d and protons would be in contact (see **Figure 9**).
- It is the same for ^{20}Ne where 4 additional Δm allow to link a new helion on the second shell by 2 double bonds.

For $^{24}_{12}$Mg, there is a mass defect allowing two double bonds to connect the 3rd helion on shell 2. This hypothesis where the distance increases with the size of the nucleus could explain an increasing instability and goes in the direction of the model of the nucleus in shells. Thus, most of the mass defect of $^{36}_{18}$Ar is explained if the 3 additional helions are connected on a 3rd shell by 6 triple bonds. Similarly, 6 quadruple bonds are obtained for ^{50}Cr and 6 quintuple bonds for ^{64}Zn (**Figure 10**).

- This principle of connecting as soon as possible the last 3 helions per n times 6 bonds allows, from the mass defect (and more precisely the additional mass defect δ_s compared to the previous element multiple of 3 helions), to determine on which shell n are the last 3 helions and to define a fill order. $n = \delta_s/6$ with $\delta_s < 25$ (18). This empirical formula is valid until neutrons are needed to stabilize the nucleus. Neutrons use a variable number of bonds depending on

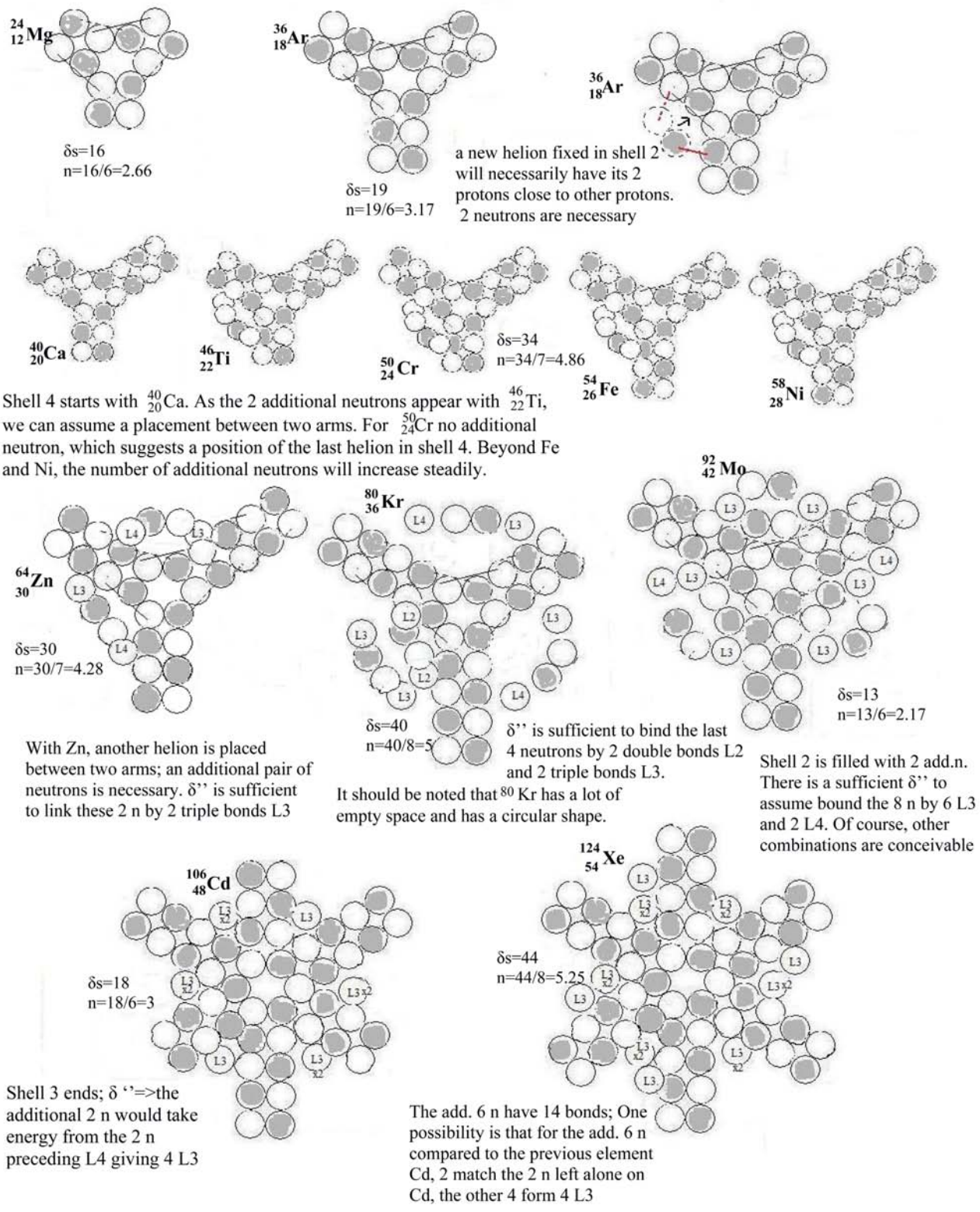

Figure 10. Formation of shells 3 to 5. The shell number n is given by $n = \delta_s/6$ when there is no neutron in addition to the helions. δ_s is the additional mass defect for an element with helions multiple of 3 compared to the previous element, multiple of 3 helions. n will become $\delta_s/7$ then $\delta_s/8$ depending on the number of additional neutrons. δ'' (number of new bonds in relation to the next lower isotope) is indicative of the number of bonds between the new neutrons and the new helion. (nuclei are seen from above, so only half of each helion is seen).

the shell in which they are fixed and this must be taken into account. So, when $35 > \delta_s > 25$, (18) becomes $n = \delta_s/7$ (19), when $\delta_s > 35$, (18) becomes $n = \delta_s/8$ (20). For the other multiple elements of 3 helions, $^{50}_{24}\mathrm{Cr}$ will have 4 shells ($n = 4.85$), $^{64}_{30}\mathrm{Zn}$ will fill the rest of the shell 4 ($n = 4.28$), $^{80}_{36}\mathrm{Kr}$ will have 5 shells ($n = 5.00$). $^{92}_{42}\mathrm{Mb}$ will fill the rest of shell 2 ($n = 2.17$), $^{106}_{48}\mathrm{Cd}$ will fill the rest of shell 3 ($n = 3.00$), $^{124}_{54}\mathrm{Xe}$ part of shell 5 ($n = 5.5$) as $^{142}_{60}\mathrm{Nd}$ ($n = 5.25$) (see **Figure 10** and **Table A4**).

- This filling helps to understand the role of additional neutrons and how they stabilize the nucleus. The filling brings, after the $^{40}_{20}\mathrm{Ca}$, helions to have their protons in contact with other protons. Two pairs of protons will be in contact (at a distance of 0.645 fm where the electrostatic repulsive force is stronger), which will bring each helion in this position to need two neutrons to be stable. For the construction of the nucleus, this leads to say that a helion that does not need 2 neutrons is fixed on one of the three branches; a helion that needs 2 neutrons is fixed between two branches. Thus, above the $^{40}_{20}\mathrm{Ca}$, it can be assumed that the last helion of $^{46}_{22}\mathrm{Ti}$ is fixed between 2 branches, that the last helions of $^{54}_{26}\mathrm{Fe}$ and $^{56}_{28}\mathrm{Ni}$ are fixed on the branches. From $^{64}_{30}\mathrm{Zn}$, there is a steady increase in the number of neutrons. It is tempting to interpret the decrease in mean energy per nucleon from the Fe and Ni by this neutron augmentation mechanism; this is in agreement with the Aston curve. It can be verified on **Table A4** and **Table A5** in the Appendix 2 that the increase of neutrons for the stable elements is 2 in 2. We can see that, when Z is even, the number of neutrons in addition to those of the helions is even and that, for each element, the stable isotopes of lower mass between Ca and Pb, 32 elements, all have stability for $2n$ neutrons then $2n + 2$ neutrons (e.g. ^{54}Fe and ^{56}Fe, ^{64}Zn and ^{66}Zn) (exception of $^{46}_{22}\mathrm{Ti}$ and $^{47}_{22}\mathrm{Ti}$ which are stable, ^{90}Zr with ^{91}Zr and ^{142}Nd with ^{143}Nd) It can however be noted that this does not explain why, almost systematically, there is a stable isotope with an odd number of neutrons $2n + 3$ (e.g.; ^{57}Fe, ^{67}Zn, …).

From $^{124}_{54}\mathrm{Xe}$, the order in which the shells are filled and how the additional neutrons are placed is easier to understand by taking the excess of mass loss for each additional helion (see **Table A5**). The increase in the loss of mass from one nucleus to another to uranium is variable but remains in a narrow range correlated with the number of neutrons required for the stability of the nucleus.

This filling can be followed on the geometry of the nucleus and is more understandable on a graphical representation. The geometric form in trifide corona by growing creates spaces that are then occupied (see **Figure 11**).

The existence of empty spaces within the nucleus is one hypothesis that has already been made by several studies speaking of a "bubble structure" [9] [10]

The nucleus gradually takes the form of a 6-pointed star with 5 levels or shells. (at no time is there a mass defect sufficient to form a 6th shell and bind the new neutrons) Between the branches, spaces are available and we note that the filling of shell 5 which can contain 14 He ends with the Pb (**Figure 12**) (NB: On the figure, at shell 5, there are 2 times between 2 branches of the star, 2 He instead of

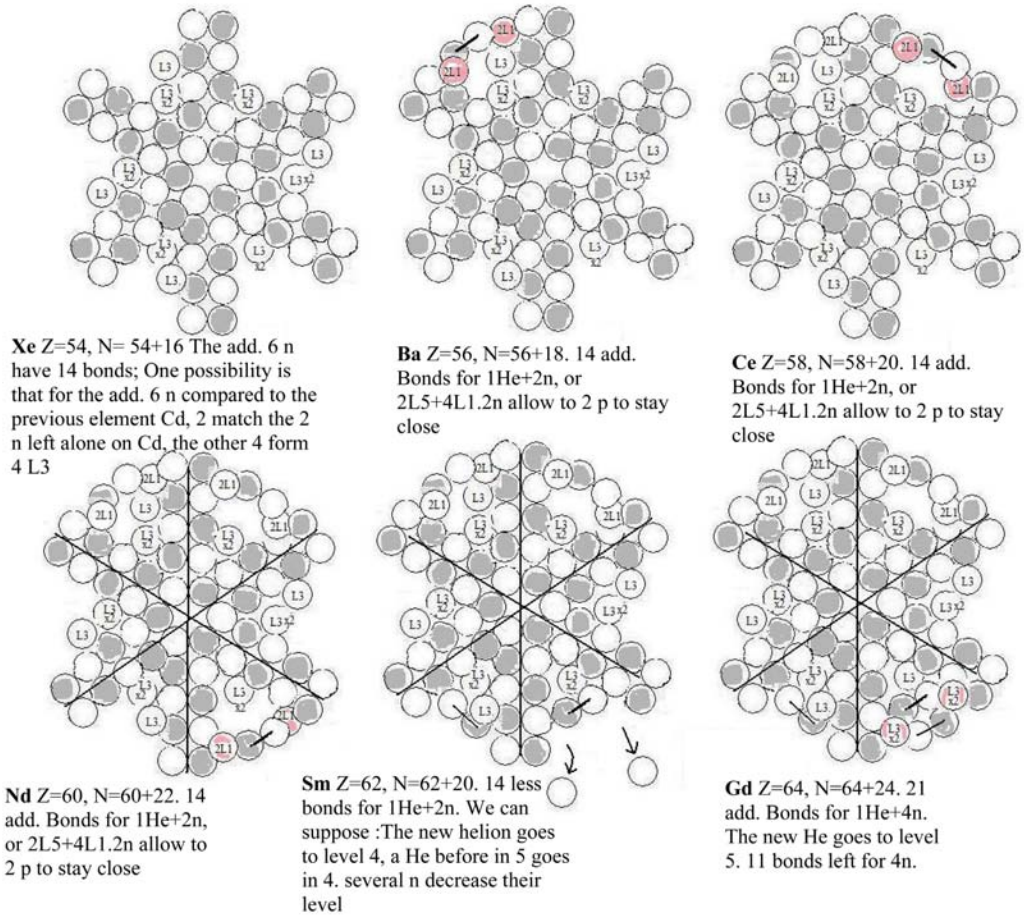

Figure 11. Filling of the spaces of the nucleus and hexagon shape.

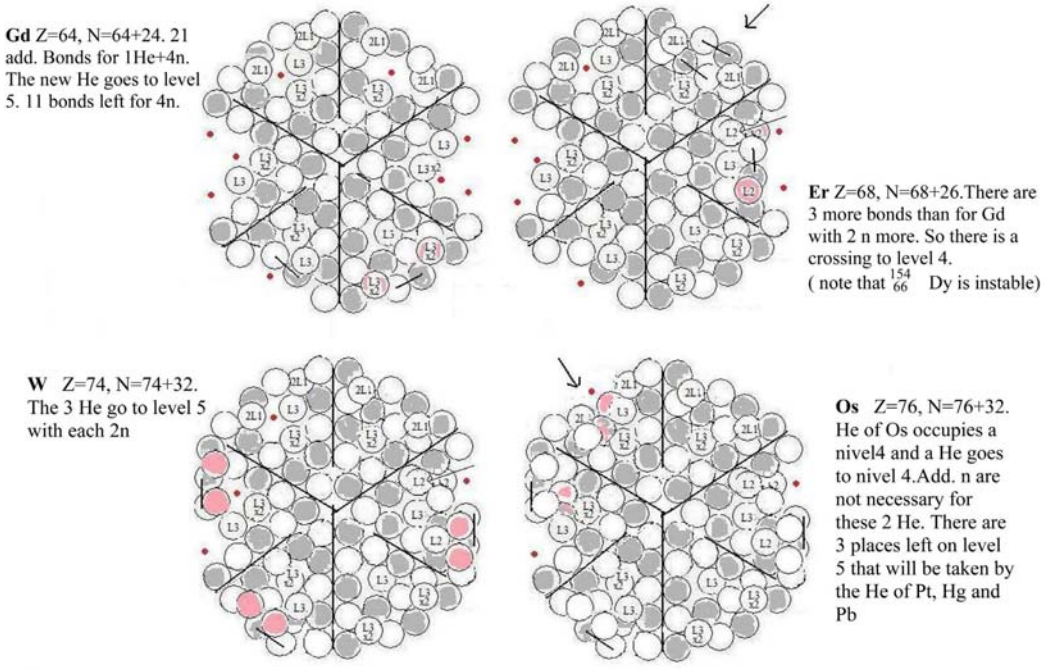

Figure 12. End of filling of shell 5 with Pb.

one, which is logical since with a diameter of 9*d*, the outer limit of the 4th shell can contain exactly 14.01 He of dimension 2*d*). As part of a corona model, it is happy to see that this filling based on geometry could give us an explanation: and the principle of quantum numbers associated with shells and sub-shells, and to an exclusion principle since each helion having a specific place, there cannot be 2 helions in the same place. It should be noted, however, that our 5 shells do not correspond to quantum shells and that we do not systematically find a correlation with magic numbers.

- Between Pb and U, there is always an average increase of 2 neutrons for each additional helion with only an average of 3.2 bonds for a helion with 2 neutrons. This excess mass defect of 3.2 is small and comparable to that of lighter elements below C. Also, instead of considering a sixth shell, this small increase in the number of bonds makes us think that helions, as for the C, will group by 3 with one or two helions of the shell 5 and that these latter helions will have weaker links with the rest of the nucleus. This is a hypothesis that could explain the fissions of heavy elements where Ra gives Pb + C, Th becomes O + Pb or Yb + Ne + Ne or Hg + Ne, U becomes Pb + Ne or Hg + Mg or Hf + Ne + Ne. This suggests for our model that the magnification of the nucleus above the Pb is done by fixing an extension having the shape of a C, a O, a Ne or a Mg (see Figure 13).

Our model suggests that there is no super-heavy stable element. The magnification of the nucleus above Pb is done by fixing an extension in the form of a C, O, Ne or Mg. It then seems logical to think that the larger this extension, the more unstable the nucleus.

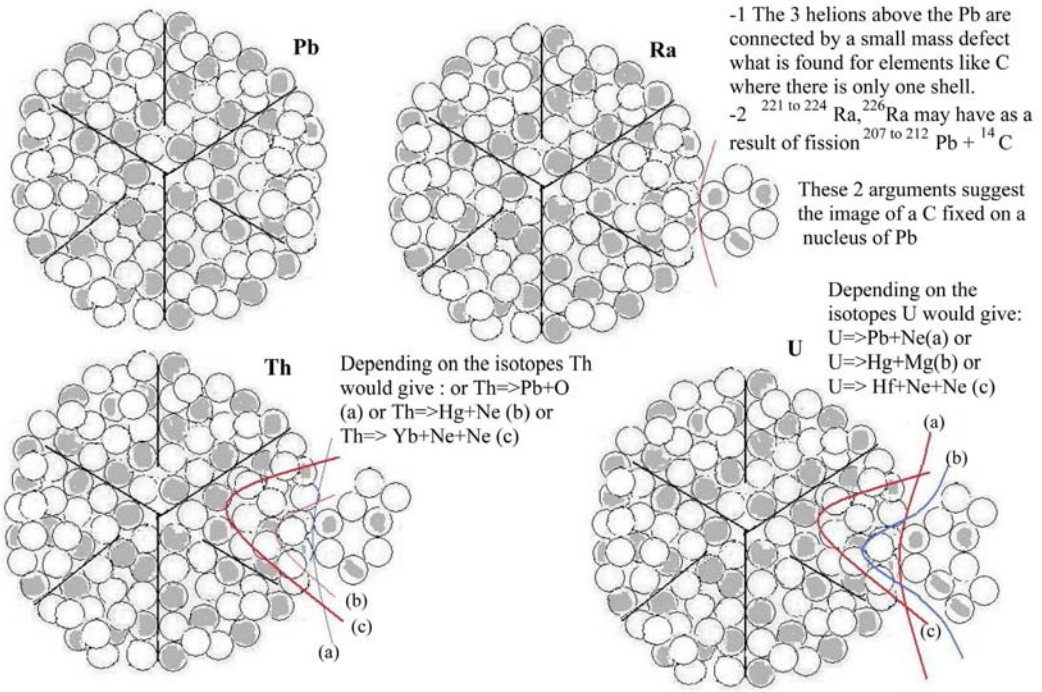

Figure 13. From Lead to Uranium.

(One could also imagine a sixth shell consisting of 14 helions which would be placed in front of the 14 helions of the shell 5 of the Pb. But it is difficult to see why there would appear an additional defect of $12\Delta m$ per helion necessary to constitute this shell when there is only $3.2\Delta m$ by helion from Po to U). It should be noted that knowing the mass defect of these stable elements, it is easy to verify that the immediately superior radioactive isotopes have a small number of bonds to retain their additional neutrons. The number of bonds can give us an idea of their position within the nucleus and will allow us to choose the formula to use to determine their ½ life. This geometric position would induce by what wave interferences they are bound and thus their radioactive ½ life.

3.3.3. Consequences of This Model on Stable Monoisotopic Nuclei (Odd *Z*)

The fact that they are monoisotopic is logical for our model since helion formation is a priority as soon as a neutron is added. We can predict which monoisotopic element will be stable: we take the stable isotope X of the element with the lowest mass A with Z even, or ${}^{A}_{Z}\mathrm{X}$, and we add a ${}^{3}\mathrm{H}$ group with 0 or 1 or 2 pairs of neutrons depending on the shell reached by the previous element with even Z.

- Thus, for even elements ${}^{A}_{Z}\mathrm{X}$ from ${}^{16}_{8}\mathrm{O}$ to ${}^{40}_{20}\mathrm{Ca}$ stable without neutron in addition to helions, elements Y with a stable number of odd protons will all be of the form:

$$\mathrm{Y} = {}^{A+3}_{Z+1}\mathrm{X} \quad (Z \text{ even},\ 6 < Z < 20) \tag{21}$$

- Between ${}^{40}_{20}\mathrm{Ca}$ and ${}^{90}_{40}\mathrm{Zr}$, the stable element Y, with number of odd protons will have a mass number of: $A + 3 + 2$.

$$\mathrm{Y} = {}^{A+3+2}_{Z+1}\mathrm{X} \quad (Z \text{ even},\ 18 < Z < 40) \tag{22}$$

- Between ${}^{90}_{40}\mathrm{Zr}$ and ${}^{142}_{60}\mathrm{Nd}$, the stable odd element is obtained by adding to group ${}^{3}\mathrm{H}$ either a pair of neutrons (Ag, Pr),or 2 pairs (Rh, In, I), or 3 pairs (Sb, Cs, La), or no pair (Nb). For our model it can be interpreted by the progressive filling of shells 4 to 2.
- Between ${}^{144}_{62}\mathrm{Sm}$ and ${}^{204}_{82}\mathrm{Pb}$, the stable element Y with number of odd protons will have a mass number of: $A + 3 + 4$ (except ${}^{165}_{67}\mathrm{Ho}$ which has 6n more instead of 4).

$$\mathrm{Y} = {}^{A+3+4}_{Z+1}\mathrm{X} \quad (Z \text{ even},\ 60 < Z < 82) \tag{23}$$

For our model, this stability in the addition rule could be explained by filling only of shell 5.

In the few cases where there are two stable isotopes, (Cu, Ga, Br, Ag, Sb, Ir, Tl), the second stable isotope is obtained by adding a pair of neutrons.

As soon as an additional neutron is added to this group in addition to the pairs of neutrons needed to stabilize the nucleus, a neutron will most often be transformed into a proton (β-decay) to form a new helion. This is the possible explanation for the low number of stable isotopes for elements with odd Z.

3.4. Results on ½ Lives

It is the number of δ'' and therefore the geometry that will make us choose one of the formulas below to use to determine the ½ lives.

3.4.1. ½ Life When There Is a Nucleon for Several Bonds ($\delta'' > 3$)

The ½ life will be calculated from the formula $T = P^k$ (17).

In Table A3 in the Appendix 2, we reproduce all isotopes of masses greater than stable elements (Radioactivity α and β) of ½ long lives (>10 years) from the classification (64 isotopes) and find a very good correlation between the observed½ lives and what our calculation provides (only 4 heavy isotopes come out of our calculation). The deviation that often exists from the mean value could be explained by the variation in the distance of the nucleon or helion bonds concerned by the radioactivity. The ½ life is then a way to calculate the distance d of the bonds. ((12) (17) $\Rightarrow$ $d = P_{pn} \times c/2 \times T^{1/k}$) (24)

It is also interesting to note that for all these elements at ½ long life, from the lightest to the heaviest, δ'' is always greater than 3 and between 5 and 8.

3.4.2. ½ Life When There Is One or More Nucleons for a Bond ($0 < \delta'' \leq 3$)

- The first thing is to note that there is a total correlation for isotopes between their ½ lives between 10^{-4} s and 10^{7} s and their δ'' between 0 and 3.
- The formula $T = \left(P_{pn} \times c/2\right) \times \left|d_1 - d_2\right| / d_1 d_2$ (16) allows to find the exact durations of ½ lives. This is done from distances d_1 and d_2 below the maximum that we have set to remain within the framework of standing waves. The knowledge of the 1/2 life allowing to predict the distances, the validation of this formula could come from such measures.
- For some periods, for example around 10^{-9} s halfway between ultra short and short periods, the existence of a peak might suggest a different type of interaction than described for short periods. The combination of 2 waves T_1 and T_2 from the formula (16) with periods around 10^{-4} s would allow to find the periods T of the peak at 10^{-9} s according to a formula $T = T_1 \times T_2$, but in the absence of any observation, this is only a conjecture.

3.4.3. Ultra Short ½ Lives (<10^{-20} s)

Similarly, for these ½ lives, we can verify that all radioactive elements have a $\delta'' \leq 0$.

4. Discussions and Conclusion

The model we propose remains valid from the H to the heaviest elements.

4.1. On Characteristics of the Bond

The initial postulate is that the bonds between the nucleons start from the two-body interaction between a proton and a neutron; the energy of the bond then corresponds to the difference in mass between this neutron and this proton. Since the neutron has lost 0.00139u, neutron and proton then vibrate at the same frequency; it is then postulated the existence of standing waves whose periods

will interfere with that of the energy corresponding to the difference in mass between a neutron and a proton. The period will be $P = P_{pn}/P_p$ (2).

- This model based on standing waves makes it possible to set a precise distance of 0.65 fm between the nucleons. The maximum length of the bond will be at the level of the antinode of the wave which will give a maximum length of dm = 0.975×10^{-15} m and a minimum length of 0.325×10^{-15} m. This variation in the distance d between 2 nodes induces a variation in the period P, $P = P_{pn} \times c/2d$ (12) which will give a period between 363 s and 1088 s with an average of 726 s. This principle of a standing wave where the nucleons stabilize at the vibration nodes would allow us to understand that the strong interaction is repulsive below 0.65 fm, attractive between 0.65 fm and 0.975 fm and weaker or absent beyond.

Considering superpositions for standing waves is not theoretically impossible. When, for a geometric reason, the distance cannot be identical for 2 bonds involving a nucleon, the difference in the periods of the 2 standing waves will cause instability responsible for the radioactivity. This hypothesis makes the fission mechanisms understandable but is less satisfactory for radioactivity β.

- The energy of the bond allows to calculate the precise distance of 1.11 fm (greater than the maximum distance of 0.975 fm) where the energy of the electrostatic force of Coulomb equals the force of the bond. This allows us to understand how a neutron allows 2 protons to remain neighbours.

4.2. The Helions Are Constituted in Priority

The increase of the mass defect as the masses increase is used to verify that the nucleons are first grouped to form helions since each time 2 protons and 2 neutrons appear, either by addition or following a decay β, an additional mass defect of about $21\Delta m$ is immediately observed corresponding to the number of bonds constituting a helion. Similarly, each time a neutron and two protons or a proton and two neutrons are added, there is a mass defect supplement of 5 or 6 Δm corresponding to the bonds contained in the groups ^{3}He or ^{3}H. The 3 added free nucleons form these 2 triplets in priority. When in addition to helions, a neutron proton pair is added, the additional loss of $1\Delta m$ suggests that this proton and neutron bind. This observation that helions are formed in priority explains why stable nuclei with even Z are more numerous than those with odd Z.

4.3. Model of the Nucleus in Concentric Shells or Corona

Starting from the idea that helion is the basic element for constructing the nuclei, it is possible to represent the geometry of the nuclei from 3 criteria:

1) The neutrons inserted between the helions have the role of allowing protons to remain nearby but up to the Ca, to be stable the nuclei do not need additional neutrons which indicates that the protons are not neighboring.

2) For stable elements, the additional mass defect for each new helion and new neutrons necessary to keep protons close together, makes it possible to make the hypothesis of a positioning of the helions in shells, The additional mass defect

makes it possible to specify what this shell is. (a) It is a minimum of $2\Delta m \times n$ (n = shell number) for each additional helion. b) The shell n is determined from the empirical formulae $n = \delta_s/6$ with $\delta_s < 25$ (18) or $n = \delta_s/7$ when $25 < \delta_s < 35$ (19) or $n = \delta_s/8$ when $\delta_s > 35$ (20), δ_s = additional mass defect of the last 3 helions compared to the previous element multiple of 3 helions).

3) When helions begin to bind, starting from 3, so from ^{12}C (consisting of 3 helions bound by 6 simple bonds making necessary a ring shape), the standing waves will have nodes of vibration in the plane of the corona. The waves will be "destructive" above or below this plane, hence the choice of a corona or snowflake model and not a ball model.

These 3 criteria lead to the hypothesis of a nucleus where helions are arranged in concentric shells.

In order for the nucleus to remain stable without additional neutrons until Ca, we have tried to show that the nucleus, from ^{12}C, begins to be built into a 3-pointed star. Up to Ca, helions can be added without the protons being in "contact" since the nuclei are stable without the addition of neutrons. This mechanism continues until Fe and Ni after the addition of 2 neutrons with Ti. The installation of helions or ^{3}H groups between these 3 branches then requires the presence of neutrons from ${}^{45}_{21}\mathrm{Sc}$ and ${}^{46}_{22}\mathrm{Ti}$. Indeed, when a helion is placed between existing helions its 2 protons will necessarily be close to 2 protons. Neutrons, in addition to helions or ^{3}H groups, are therefore in even numbers and this hypothesis explains why between C and Pb when Z even, the first 2 stable isotopes have $2n$ then $2n + 2$ neutrons.

Similarly, when the number of protons is odd, we can verify that the stable nucleus has, in addition to helions and the ^{3}H group, a number of null or even neutrons depending on the shell, according to a formula: $\mathrm{Y} = {}^{A+3}_{Z+1}\mathrm{X}$ (even Z, $6 < Z < 20$) (21) or $\mathrm{Y} = {}^{A+3+2}_{Z+1}\mathrm{X}$ (even Z, $18 < Z < 40$) (22) or $\mathrm{Y} = {}^{A+3+4}_{Z+1}\mathrm{X}$ (even Z, $60 < Z < 82$) (23) (${}^{A}_{Z}\mathrm{X}$ = stable element of lower mass immediately below Y)

The 5th shell finishes filling with Pb. Above, the small increase in mass defect and the type of fission decay suggest that the nucleus grows by fixing an element between C and Mg on a nucleus of Pb.

This corona model has a large diameter (6.45 fm when 5 shells) but its thickness remains relatively constant (1.2 fm).

Nucleon periods and distances within the nucleus are correlated according to equation $P = P_{pn} \times c/2d$ (12) for the short ½ lives or $d = P_{pn} \times c/2 \times T^{1/k}$ (24) for some isotope bonds with long ½ lives. This means that, starting from ½ life, it should be possible to specify some of the dimensions of a nucleus and the distances between the nucleons within it. The ½ life is so a way of calculating distances. In addition, if an ultra-short ½ life of the order of 10^{-20} s corresponds to a time of passage of a wave through all or part of the nucleus, then the time of the ½ life allows to determine a dimension of the nucleus.

Therefore, one way to confirm or invalidate our model would be to make very accurate measurements of the dimensions in the nucleus.

Of course, it is not said that there cannot be other possible configurations

meeting these 3 criteria. This corona model is identical to shells models where we start from interactions with 2 bodies; the geometry allows to define locations that could explain the "boxes" defined by the quantum numbers. (with the difference that we finish filling the 5th and last shell with the Pb). The shells that we define are different from those from previous shells models and we do not find all the magic numbers.

4.4. The ½ Lives

The fact that this model is based on standing waves and their superpositions could explain that the radioactive periods are not randomly distributed but have preferential zones around 10^{-22} s, around 10^{-7} s, between 10^{-4} and 10^{7} s, then in 4 waves between 10^{10} and 10^{30} s.

The number of bonds concerned by radioactivity and the number of nucleons are deduced from the mass defect resulting from the experimental observation. The number of additional bonds in relation to the immediately below isotope, almost without exception, makes it possible to deduce for all the elements if the radioactive ½ life is short or long and induces the use of the corresponding formula. These formulas, $T = P^k$ (17) for the long ½ lives,
$T = \left(P_{pn} \times c/2\right) \times \left|d_1 - d_2\right| / d_1 d_2$ (16) for the short ½ lives and to match a passage time of a wave for the ultra short ½ lives, allow to find the radioactive ½ lives. However, these formulas have limits: the ultra short ½ lives are found starting from a distance travelled but this distance is not a fact of observation. For the short ½ lives, it is necessary to set a precise distance between nucleons; this distance is likely and possible, but has not been measured. (For some periods, for example around 10^{-9} s halfway between ultra-short and short periods, the existence of a peak could conjecture another type of interaction than that described for short periods; the combination of 2 waves from the formula. (16) with periods around 10^{-4} s would allow to find the periods of the peak at 10^{-9} s). For long ½ lives the number k of bonds involved in radioactivity is not calculated from the number of new bonds δ''. k could only be deduced from a geometry that we do not know.

However, the fact that we can find the radioactive ½ lives of all the elements by a theoretical calculation that requires experimental verifications could be a step forward. This raises a question since the only postulate we have put is to associate a wave to a nucleon and then study the interferences between the nucleons.

4.5. Limits to This Theory

Our theory does not call into question the standard model but we must ask ourselves if, for the nucleus in the part we studied, it would not be better to use what was first put forward at the beginning of quantum mechanics by Bohr, namely wave mechanics rather than the probabilistic mechanics introduced by Bohm. Indeed, the model is in agreement with only part of the fundamental hypotheses of quantum mechanics: the nucleons interact according to a 2-body interaction,

the nucleus is an N-body system, it is not relativistic. But nucleons are not pointed objects and there is no correspondence for our shell with quantum numbers that assume a number of shells and sub-shells.

Radioactivity is explained by superpositions of waves that we imagine being in phase at an interval of time, but even if there are arguments, other solutions could be imagined. To say that the link is due to interference is an assumption. The element of verification of our theory is a more accurate measurement of distances and mass defects which could make it possible to precise our model especially for elements of significant mass where the uncertainty does not allow to place with precision the pairs of neutrons ensuring the stability of the nucleus.

Acknowledgements

I thank all those who have given me the idea of this article by discussing this subject and, in particular, those who, by rereading the document, have provided advice and criticism that helped to improve the text. They have contributed to this article.

Conflicts of Interest

The author declares no conflicts of interest regarding the publication of this paper.

References

[1] Xiong, W., Gasparian, A., Gao, H., *et al.* (2019) *Nature*, **575**, 147-150. https://doi.org/10.1038/s41586-019-1721-2

[2] Sazdjian, H. (2013) Ondes: Cordes Vibrantes, Ondes Sonores, Ondes Optiques. Thèse, Université Paris-Sud, Orsay.

[3] Audi, G., Wapstra, A.H., Thibault, C., Blachot, J. and Bersillon, O. (2003) *Nuclear Physics A*, **729**, 3-128. https://doi.org/10.1016/j.nuclphysa.2003.11.001

[4] de Laeter, J.R., Böhlke, J.K., De Bièvre, P. (2003) *Pure and Applied Chemistry*, **75**, 683-800. https://doi.org/10.1351/pac200375060683

[5] Wieser, M.E. (2006) *Pure and Applied Chemistry*, **78**, 2051-2066. https://doi.org/10.1351/pac200678112051

[6] Holden, N.E. and Lide, D.R. (dir.) (2004) CRC Handbook of Chemistry and Physics. 85e éd., CRC Press, Boca Raton, 2712 p.

[7] Krauth, J.J. *et al.* (2021) *Nature*, **589**, 527-531. https://doi.org/10.1038/s41586-021-03183-1

[8] Ebran, J.P., Khan, E., Nikšić, T. and Vretenar, D. (2014) *Physical Review C*, **90**, Article ID: 054329. https://doi.org/10.1103/PhysRevC.90.054329

[9] Mutschler, A., Lemasson, A., Sorlin, O., *et al.* (2017) *Nature Physics,* **13**, 152-156. https://doi.org/10.1038/nphys3916

[10] Duguet, T., Somà, V., Lecluse, S., Barbieri, C. and Navrátil, P. (2017) *Physical Review C*, **95**, Article ID: 034319. https://doi.org/10.1103/PhysRevC.95.034319

Appendix 1

Calculation of the vibration periods of the standing wave forming the bond as a function of the distance d and of the period of the wave coming from 2 standing waves.

- The distance d between the centres of 2 nucleons will correspond to the ½ wavelength λ of the standing wave that is established between the 2 nucleons. When the standing wave has the period of vibration of the proton P_p (P_p = 4.33×10^{-24} s), the frequency P of the bond will be $P = P_{pn}/P_p$ (2) = 725.18 s and $d = \lambda/2 = P_p \times c/2$ (11) $d = 0.645 \times 10^{-15}$ m (c = speed of light, $P_{pn} = 3.19 \times 10^{-21}$ s).

(when the mass loss is more important, for example $6\Delta m$ for the neutron in a helion, the period P may decrease to 720.18 s and the distance d will be 0.6455 fm, a decrease of only about 0.05 fm)

(2) and (11) make it possible to express the period P according to the distance.

(2), (11) $\Rightarrow$ $P = P_{pn} \times c/2d$ (12).

- This distance d is the distance between 2 nodes of vibration and we will consider that this bond does not break if the centre of a nucleon does not vibrate beyond an anti-node. The maximum distance dm between the 2 nucleon centres will therefore be $d_m = \lambda/2 + \lambda/4$ or $d_m = (3/2)d$ (13). Or $d_m = 0.9675 \times 10^{-15}$m. The minimum distance d_{mi} will be $d_{mi} = (1/2)d$ (14).
- When the geometry of the nucleus imposes a distance dm between 2 nucleons the minimum period P' of the bond will become: (12) (13) $\Rightarrow$ $P' = P_{pn} \times c/3d$ or $P' = P \times (2/3)$ or $P' = 483.45$ s.
- In the case of periods in the order of the second up to several minutes it is assumed that the ½ life T is explained by the difference between two neighboring periods P_1 and P_2 of two bonds (there is only one Δm for two bonds), $T = P_1 - P_2$ (15); (12) (15) $\Rightarrow$ $T = P_{pn} \times c/2d_1 - P_{pn} \times c/2d_2$ or $T = \left(P_{pn} \times c/2\right) \times \left|d_1 - d_2\right| / d_1 d_2$ (16).

Theoretically, a very small difference in distance between d_1 and d_2 makes it possible to find T between 0 and 1 s. Ex: for ^{8}Li, T = 840 ms, (16) $\Rightarrow$ $d_1 - d_2 = 0.73 \times 10^{-3}$ fm or (1) $\Rightarrow$ $\Delta m = 1.56 \times 10^{-6}$ u.

If one of the two bonds has the maximum distance, the ½ life can reach (16) $\Rightarrow$ T = 159.5 s with $d_1 = 1.5d$ and $d_2 = d = 0.65$ fm.

If one of the two bonds has the maximum distance and the other the minimum length ($d_1 = 1.5 \times 0.65$ fm and $d_2 = 0.5 \times 0.65$ fm), then (16) $\Rightarrow$ T = 981.5 s which is the maximum ½ life in the assumption of a ½ life explained by a difference between two neighboring periods.

Appendix 2

Table A1. Number of bonds of some isotopes from NUBASE (3, 4, 5, 6), as examples.

Symbol	Z	N	atomic mass (u)	½ life	Decay	daughter-isotope (s)	δ	δ'	δ"	Comment
^{1}H	1	0	1.00782503207		Stable					
^{2}H	1	1	2.0141017778		Stable		1		1	
^{3}H	1	2	3.0160492777	12.32 (2) an	β^-	^{3}He	6.41		5	The group ^{3}H was formed
^{4}H	1	3	4.02781 (11)	$1.39\ (10) \times 10^{-22}$ s	n	^{3}H				
^{5}H	1	4	5.03531 (11)	$>9.1 \times 10^{-22}$ s?	n	^{4}H				
^{6}H	1	5	6.04494 (28)	$2.90\ (70) \times 10^{-22}$ s	3n, 4n	^{3}H,^{2}H				
^{7}H	1	6	7.05275 (108)	$2.3\ (6) \times 10^{-27}$ s	4n	^{3}H				
^{3}He	2	1	3.0160293191		Stable		5.17		/	^{3}He was formed
^{4}He	2	2	4.00260325415		Stable		21.07	0	/	^{4}He (a) was formed
^{5}He	2	3	5.01222 (5)	$700\ (30) \times 10^{-24}$ s	n	**^{4}He**	20.37	0	0	
^{6}He	2	4	6.0188891 (8)	806.7 (15) ms	β^- (99.99%)	**^{6}Li**	21.82	1	1	
^{7}He	2	5	7.028021 (18)	$2.9\ (5) \times 10^{-21}$ s	n	^{6}He	21.48	1	0	
^{8}He	2	6	8.033922 (7)	119.0 (15) ms	β^- 83.1%; β^- n 16%; β^- fis 0.09%	^{8}Li, **^{7}Li,** ^{5}He ^{3}H	23.47	2	1	
^{9}He	2	7	9.04395 (3)	$7\ (4) \times 10^{-21}$ s	n	^{8}He	22.49	1	−1	
^{10}He	2	8	10.05240 (8)	$2.7\ (18) \times 10^{-21}$ s	2n	^{8}He	22.64	1-2	0	
^{4}Li	3	1	4.027 19 (23)	$91\ (9) \times 10^{-24}$ s	p	**^{3}He**	2.37			No group formed except ^{2}H
^{5}Li	3	2	5.012 54 (5)	$370\ (30) \times 10^{-24}$ s	p	**^{4}He**	19.15	0	/	
^{6}Li	3	3	6.015122795 (16)	**Stable**			23.53	2	4	$\Delta m > 21$. the nucleus a was formed
^{7}Li	3	4	7.016 00455 (8)	**Stable**			29.12	2	6	One group ^{3}H was formed

Continued

^{8}Li	3	5	8.022 48736 (10)	840.3 (9) ms	β^--fission	2 **^{4}He**	30.69	3	2	
^{9}Li	3	6	9.026 789 5 (21)	178.3 (4) ms	β^- n (50.8%)	^{8}Be	33.83	6	3	
					β^- (49.2%)	**^{9}Be**				
^{10}Li	3	7	10.035 481 (16)	2.0 (5) × 10^{-21} s	n	^{9}Li	33.81	6	0	
^{10m1}Li			200 (40) keV	3.7 (15) × 10^{-21} s						
^{10m2}Li			480 (40) keV	1.35 (24) × 10^{-21} s						
^{11}Li	3	8	11.043 798 (21)	8.75 (14) ms	β^- n 84.9%, β^- 8.07%	^{10}Be, ^{11}Be	34.06	7	1	
					β^- 2n 4.1%, β^- 3n 1.9%	^{9}Be, ^{8}Be				
					β^- fiss. (1.0%)	^{7}He + **^{4}He**				
					β^-, fi (0.014%)	^{8}Li + ^{3}H				
^{12}Li	3	9	12.053 78 (107)	<10 ns	n	^{11}Li	33.12	12	−1	
^{5}Be	4	1	5.04079 (429)		p	^{4}Li	-2.17			
^{6}Be	4	2	6.019726 (6)	5.0 (3) × 10^{-21} s	2p	**^{4}He**	19.21	0	/	The difference with 5Be is 21.38. One nucleus of He4 was formed
^{7}Be	4	3	7.01692983 (11)	53.22 (6)j = 4.6 × 10^{6} s	CE	**^{7}Li**	27.46	6	/	α (21) + ^{3}He (5) = 26. One 3He was formed
^{8}Be	4	4	8.00530510 (4)	6.7 (17) × 10^{-17} s	fission	2 **^{4}He**	42.05	0	/	A second α was formed
^{9}Be	4	5	9.0121822 (4)	**Stable**			43.34	1	1	Stable despite a single bond. It is necessary to imagine that the neutron 5 is at the same distance of the 2 α
^{10}Be	4	6	10.0135338 (4)	1.39 Ma = 8.16 × 10^{13} s	β^-	**^{10}B**	48.60	7	5	The n has 5 bonds (13) => T = 726^{5} = 4.76 × 10^{13} s
^{11}Be	4	7	11.021658 (7)	13.81 (8) s	B^- 97.1 β^-, α 2.9%	**^{11}B, ^{7}Li**	48.99	7	1/2	
^{12}Be	4	8	12.026921 (16)	21.49 (3) ms	β^- (99.48%)	^{12}B	51.44	9	2	
					β^-, n (0.52%)	**^{11}B**				
^{13}Be	4	9	13.03569 (8)	0.5 (1) ns	n	^{12}Be	51.37	9	0	

Continued

^{14}Be	4	10	14.04289 (14)	4.84 (10) ms	β^-, n (81.0%)	^{13}B	52.42	10	1
					B^- 14.0%, β^- 2n 5.0%	^{14}B, ^{12}B			
^{15}Be	4	11	15.05346 (54)#	<200 ns			51.04	9	−1
^{16}Be	4	12	16.06192 (54)#	<200 ns			51.20	9	0
^{7}B	5	2	7.02992 (8)	350 (50) × 10^{-24} s	p	^{6}Be	17.12		<21, The nucleus of ’He4 is not formed
^{8}B	5	3	8.0246072 (11)	770 (3) ms	β^+ fission	2 (**^{4}He**)	27.17	1	/ Formed with 1He (21) + ^{3}He (5); stay 1bond
^{9}B	5	4	9.0133288 (11)	800 (300) × 10^{-21} s	p	^{8}Be	41.52	0	0
^{10}B	5	5	10.0129370 (4)	**Stable**			48.03	6	6
^{11}B	5	6	11.0093054 (4)	**Stable**			56.88	9	9 One 3H was formed
^{12}B	5	7	12.0143521 (15)	20.20 (2) ms	β^- 98.4%, β^-, α 1.6%	**^{12}C,** ^{6}Be	59.48	12	3
^{13}B	5	8	13.0177802 (12)	17.33 (17) ms	β^- 99.72%, β^- n 0.28%	**^{13}C, ^{12}C**	63.25	15	3
^{14}B	5	9	14.025404 (23)	12.5 (5) ms	β^- (93.96%)	^{14}C	64.00	16	1
					β^-, n (6.04%)	**^{13}C**			
^{15}B	5	10	15.031103 (24)	9.87 (7) ms	β^-, n (93.6%)	^{14}C	66.13	18	2
					β^- (6.0%)	^{15}C			
					β^-, 2n (0.40%)	**^{13}C**			
^{16}B	5	11	16.03981 (6)	<190 × 10^{-12} s	n	^{14}B	66.10	18	0
^{17}B	5	12	17.04699 (18)	5.08 (5) ms	β^-, n (63.0%)	^{16}C	67.17	19	1
					β^- (22.1%)	^{17}C			
					β^-, 2n (11.0%)	^{15}C			
					β^-, 3n (3.5%)	^{14}C			
					β^-, 4n (0.40%)	**^{13}C**			
^{18}B	5	13	18.05617 (86)	<26 ns	n	^{17}B	66.80	19	0

Continued

^{19}B	5	14	19.06373 (43)	2.92 (13) ms	β^-	^{19}C	67.60	20	1
^{8}C	6	2	8.037675 (25)	2.0 (4) × 10^{-21} s	2p	^{6}Be	16.77		<21 so helion no formed
^{9}C	6	3	9.0310367 (23)	126.5 (9) ms	β^+ 60%	^{9}B	27.78	2	/ 1 hélion + ^{3}He = 26; stay 2
					β^+, p (23%)	^{8}Be			
					β^+, α (17%)	^{5}Li			
^{10}C	6	4	10.0168532 (4)	19.290 (12) s	β^+	**^{10}B**	44.21	2	/ 2 α formed
^{11}C	6	5	11.0114336 (10)	20.334 (24) min	β^+ (99.79%)	**^{11}B**	54.35	7	/ two α + one ^{3}He = 47
					K^- CE (0.21%)	**^{11}B**			
^{12}C	6	6	12 exactement	**Stable**			68.81	6	/ 3 helions (63) + 6 internal bonds
^{13}C	6	7	13.0033548378 (10)	**Stable**			72.63	10	4
^{14}C	6	8	14.003241989 (4)	5.73 × 10^{3} ans	β^-	**^{14}N**	78.94	16	6
^{15}C	6	9	15.0105993 (9)	2.449 (5) s	β^-	**^{15}N**	79.89	17	1
^{16}C	6	10	16.014701 (4)	0.747 (8) s	β^-, n (97.9%)	**^{15}N**	83.17	20	3
					β^- (2.1%)	^{16}N			
^{17}C	6	11	17.022586 (19)	193 (5) ms	β^- (71.59%)	^{17}N	83.73	21	1
					β^-, n (28.41%)	^{16}N			
^{18}C	6	12	18.02676 (3)	92 (2) ms	β^- (68.5%)	^{18}N	86.96	24	3
					β^-, n (31.5%)	^{17}N			
^{19}C	6	13	19.03481 (11)	46.2 (23) ms	β^-, n (47.0%)	^{18}N	87.40	24	0
					β^- (46.0%)	^{19}N			
					β^-, 2n (7%)	^{17}N			
^{20}C	6	14	20.04032 (26)	16 (3) ms	β^-, n (72.0%)	^{19}N	89.67	27	3
					β^- (28.0%)	^{20}N			
^{21}C	6	15	21.04934 (54)	<30 ns	n	^{20}C	89.42	26	−1

Continued

^{22}C	6	16	22.05720 (97)	6.2 (13) ms	β^-	^{22}N	90.00	28	2	
^{10}N	7	3	10.04165 (43)	200 (140) × 10^{-24} s	p	^{9}C	25.38			
^{11}N	7	4	11.02609 (5)	590 (210) × 10^{-24} s	p	^{10}C	42.81	1	/	2 α formed
^{12}N	7	5	12.0186132 (11)	11.000 (16) ms	β^+ 96.5%	^{12}C	54.42	7	/	+ one ^{3}He formed
					β^+, α (3.5%)	^{8}Be				
^{13}N	7	6	13.00573861 (29)	9.965 (4) min	β^+	^{13}C	69.92	7 (1)	/	3α (63) + 6 = ^{12}C, stay 1
^{14}N	7	7	14.0030740048 (6)	**Stable**			78.11	14 (8)	8	^{12}C (69) + ^{2}H (1) = 70, stay 8
^{15}N	7	8	15.0001088982 (7)	**Stable**			86.43	17 (11)	8	^{12}C (69) + ^{3}H (6) = 75, stay 11
^{16}N	7	9	16.0061017 (28)	7.13 (2) s	β^- (99.99%	^{16}O	88.36	19	1	Reminder: above stable nuclei after C, the additional groups or neutrons will be on a second shell
					β^-. α (0.001%)	**^{12}C**				bonds are double. δ'' is calculated by dividing the difference of the δ' by 2
^{17}N	7	10	17.008450 (16)	4.173 (4) s	β^-. n (95.0%)	**^{16}O**	92.90	24	2.5	
					β^- (4.99%)	**^{17}O**				
					β^-. α 0.0025%	**^{13}C**				
^{18}N	7	11	18.014079 (20)	622 (9) ms	β^- (76.9%)	**^{18}O**	95.08	26	1	
					β^-, α 12.2%	^{14}C				
					β^-, n (10.9%)	**^{17}O**				
^{19}N	7	12	19.017029 (18)	271 (8) ms	β^-, n 54.6%	**^{18}O**	99.20	30	2	
					β^- (45.4%)	^{19}O				
^{20}N	7	13	20.02337 (6)	130 (7) ms	β^- n 56.99%	^{19}O	100.87	32	1	
					β^- (43.00%)	^{20}O				
^{21}N	7	14	21.02711 (10)	87 (6) ms	B^-, n 80%	^{20}O	104.41	35	1.5	
					β^- 20.0%	^{21}O				

Continued

^{22}N	7	15	22.03439 (21)	13.9 (14) ms	β^- 65%, β^-, n (35%)	^{22}O ^{21}O	105.41	36	1/2	
^{23}N	7	16	23.04122 (32)	14.5 (24) ms	β^- 20.0%	^{21}O	106.72	38	1	
^{24}N	7	17	24.05104 (43)	<52 ns	n	^{23}N	105.90	37	−1/2	
^{25}N	7	18	25.06066 (54)	<260 ns			105.21	36	−1/2	
^{12}O	8	4	12.034405 (20)	580 (30) × 10^{-24} s	2p (60%)	^{10}C	42.06			
					p (40.0%)	^{11}N				
^{13}O	8	5	13.024812 (10)	8.58 (5) ms	β^+ (89.1%)	^{13}N	55.20			
					β^+, p (10.9%)	**^{12}C**				
^{14}O	8	6	14.00859625 (12)	70.598 (18) s	β^+	**^{14}N**	73.10			
^{15}O	8	7	15.0030656 (5)	122.24 (16) s	β^+	**^{15}N**				
^{16}O	8	8	15.99491461956	**Stable**			95.41	11	/	4 *α* formed
^{17}O	8	9	16.99913170 (12)	**Stable**			98.61	15	4	
^{18}O	8	10	17.9991610 (7)	**Stable**			104.82	21	6	
^{19}O	8	11	19.003580 (3)	26.464 (9) s	β^-	**^{19}F**	107.87	24	1.5	
^{20}O	8	12	20.0040767 (12)	13.51 (5) s	β^-	^{20}F	113.75	30	3	
^{21}O	8	13	21.008656 (13)	3.42 (10) s	β^-	^{21}F	116.69	33	1.5	
^{22}O	8	14	22.00997 (6)	2.25 (15) s	β^- (78.0%)	^{22}F	121.98	38	2.5	
					β^-, n (22.0%)	^{21}F				
^{23}O	8	15	23.01569 (13)	82 (37) ms	β^-, n (57.99%)	^{22}F	124.10	40	1	
					β^- (42.0%)	^{21}F				
^{24}O	8	16	24.02047 (25)	65 (5) ms	β^-, n (57.99%)	^{23}F	126.89	43	1.5	
					β^- (42.01%)	^{24}F				
^{25}O	8	17	25.02946 (28)	5.2 × 10^{-8} s	n	^{24}O	126.66	43	0	

Continued

^{26}O	8	18	26.03834 (28)	4.0×10^{-8} s	β^-	^{26}F	126.50	43	0
					n	^{25}O			
^{27}O	8	19	27.04826 (54)	<260 ns	n	^{26}O	125.60	42	−1/2
^{28}O	8	20	28.05781 (64)	<260 ns	n	^{27}O	124.96	42	−1/2

1) There is a sharp increase of δ to $21\Delta m$ from ^{3}He to ^{4}He (δ''= 16 is the highest value for all the classification, δ''usually does not exceed 6, exceptionally 9 (^{11}B)). 2) Every time, when Z even, the number N of neutron reaches Z, then there is an increase of δ allowing the formation of a new helion (ex: passage from ^{7}Be to ^{8}Be,^{11}C to ^{12}C, ^{15}O to^{16}O,^{19}Ne to ^{20}Ne). 3) When, in addition to helions, there are 1p and 2n, they will form a ^{3}H (δ'increases at least 6 between ^{6}Li and ^{7}Li, ^{10}B and ^{11}B). Similarly, when 2p and 1n are available, δ'increases by at least 5 to form a ^{3}He (between ^{8}C and ^{9}C, ^{11}N and ^{12}N, ^{12}O and ^{13}O). 4) Stable elements can be detected; $\delta''$is highest for the elements stable or with a very long ½ life (δ''> 3). Taking into account the shell, 0 < δ''≤ 3 for short ½ lives, δ''≤ 0 for ultra-short ½ lives. δ= total number of bonds. δ'= number of bonds reduced to the unit, above helions and groups ^{3}H, ^{3}He or pair p-n (according to Equation (9) δ''= additional bonds, whether single or multiple, relative to the immediately below isotope ($\delta''$is not noted when it corresponds to the creation of a ^{4}He (α), ^{3}H or ^{3}He). For elements having several shells, $\delta''$is obtained according to Equation (10) $\delta'' = (\delta_y - \delta_x)/n$ with n = 2 since it is assumed that the additional neutrons are fixed by double bonds. We made the same table for F, Ne, Ar, Kr, Fe and Pb. δ' always follows the same rule: when δ''> 3, the elements are stable or with a long ½ life, when δ''≤ 3 ½ lives are short. For, F, Ne, Ar, Kr and Fe, as for N and O, $\delta''$is found assuming that neutrons have double bonds (n = 2 in Equation (10)). For Pb, $\delta''$is obtained without dividing by 2, suggesting simple bonds for additional neutrons.

Table A2. Number N of stable nuclei for each element.

Z	1	2	3	4	5	6	7	8	9	10	11	12	13	14	15	16	17	18	19	20	21	22	23	24	25	26	27	28	29	30
N	**2**	**2**	**2**	**1***	**2**	**2***	**2**	**3**	**1**	**3**	**1**	**3**	**1**	**3**	**1**	**4**	**2**	**3**	**2***	**5***	**1**	**5**	**1***	**4**	**1**	**4**	**1**	**5**	**2**	**5**
Z	31	32	33	34	35	36	37	38	39	40	41	42	43	44	45	46	47	48	49	50	51	52	53	54	55	56	57	58	59	60
N	**2**	**4***	**1**	**5***	**2**	**5**	**1***	**4**	**1**	**4***	**1**	**6***	**0***	**7**	**1**	**6***	**2**	**6***	**1**	**10**	**2**	**6***	**1**	**7***	**1**	**6***	**1***	**4**	**1**	**5***
Z	61	62	63	64	65	66	67	68	69	70	71	72	73	74	75	76	77	78	79	80	81	82								
N	**0**	**5***	**1**	**6***	**1**	**7***	**1**	**6**	**1**	**7**	**1**	**5**	**1**	**4***	**1**	**6***	**2**	**5***	**1**	**7**	**2**	**3***								

The * indicates one or two additional isotopes with a very long ½ life. From Z > 6, without any exception, when Z odd, $N \leq 2$, when Z even, $N \geq 3$. Beyond Z = 82 (Pb), all elements are unstable. Elements where Z is odd are more unstable because an additional neutron added to the stable isotope will be converted by radioactivity β^- into a proton to form a new helion.

Table A3. Radioactive isotopes with a δ''> 3.

k	Calculated ½ life (17)	isotope	nber bonds δ" cal. For isot.	Observed ½ life	decay	% dev. from mean value (0% = mean value; 100% = possible limite value)
1	(726 s)					
2	(5.27×10^5 s)					
3	0.48 to 12.88×10^8 s (3.83×10^8 s)	$^{228}_{90}$Th	5.49	0.60×10^8 s	α	−92.2%
		^{85}Kr	6	3.4×10^8 s	β^-	−4.75%
		^{3}H	5.49	3.88×10^8 s	β^-	0.5%

Continued

		^{154}Eu	5.49	5.04×10^{8} s	β^-	13.4%
		$^{227}_{89}$Ac	5.04	6.8×10^{8} s	β^- (98.6%)	32.8%
		^{210}Pb	4	7.03×10^{8} s	β^-	35.4%
		$^{}_{90}$Sr	6	9.07×10^{8} s	β^-	58%
		$^{232}_{92}$U	5.61	22×10^{8} s	α	201%
		$^{209}_{84}$Po	5.38	32.5×10^{8} s	α (99.5%)	317%
4	0.17 to 14.01 $\times 10^{11}$ s (2.78×10^{11} s)	$^{226}_{88}$Ra	4.94	0.51×10^{11} s	α or $\beta^-\beta^-$	−69%
		^{14}C	6	1.8×10^{11} s	β^-	−37.5%
		$^{229}_{90}$Th	4.06	2.32×10^{11} s	α	−8.80%
		$^{231}_{91}$Pa	5.27	10.34×10^{11} s	α	67%
		$^{230}_{90}$Th	5.25	23.8×10^{11} s	α	187%
5	0.63 to 152 $\times 10^{13}$ s (20.17×10^{13} s)	$^{233}_{92}$U	4.45	0.5×10^{13} s	α	−1.04
		^{99}Tc	7	0.66×10^{13} s	β^-	−99%
		$^{126}_{50}$Sn	6.32	0.73×10^{13} s	β^-	−97%
		$^{234}_{92}$U	5.29	0.77×10^{13} s	α	−96%
		^{36}Cl	7	0.95×10^{13} s	β^-	−91%
		^{79}Se	5.38	1.03×10^{13} s	β^-	−89.7%
		$^{208}_{83}$Bi	5.32	1.16×10^{13} s	β^+	−87%
		^{10}Be	5	4.76×10^{13} s	β^-	−50%
		^{93}Zr	5.20	4.82×10^{13} s	β^-	−49.7%
		$^{150}_{64}$Gd	6.72	5.64×10^{13} s	α ($\beta^-\beta^-$ rare)	−45%
		^{135}Cs	6.77	7.25×10^{13} s	β^-	−37%
		$^{154}_{66}$Dy	7.20	9.45×10^{13} s	α ($\beta^-\beta^-$ rare)	−28%
		^{98}Tc	5.6	14.7×10^{13} s	β^-	−12.3%
		$^{107}_{46}$Pd	5.05	20.48×10^{13} s	β^-	0.24%
		$^{182}_{72}$Hf	5.19	28×10^{13} s	β^-	5.9%
		$^{129}_{43}$I	6.82	49.4×10^{13} s	β^-	22.2%
		$^{236}_{92}$U	5.06	73.9×10^{13} s	α	40.7%
		$^{92}_{41}$Nb	6.09	109.3×10^{13} s	β^+ (99%)	67.6%
6	0.23 to 166 $\times 10^{16}$ s (14.64×10^{16} s)	^{146}Sm	6.50	0.32×10^{16} s	α	−94%
		$^{235}_{92}$U	4.09	2.22×10^{16} s	α	−54%
		^{40}K	6	4.02×10^{16} s	β^-	−38.7%
		$^{238}_{92}$U	4.75	20.41×10^{16} s	α	3.8%
		$^{232}_{90}$Th	4.97	44.2×10^{16} s	α	19.5%
		$^{176}_{71}$Lu	4.86	121×10^{16} s	β^-	70% overlap
		$^{187}_{75}$Re	5.68	130×10^{16} s	β^- (99%)	76% overlap

Continued

7	83×10^{16} to 180×10^{19} s (10.6×10^{19} s)	$^{87}_{37}$Rb	7.6	151×10^{16} s	β^- overlap	−91% if k = 7 or +90%if k = 8
		$^{138}_{57}$La	5.79	3.2×10^{18} s	$\beta^+\beta^-$	−78%
		^{147}Sm	4.90	0.5×10^{19} s	α	−71%
		^{190}Pt	6.88	20.48×10^{18} s	α	−42%
8	30×10^{19} to 196×10^{22} s (7.71×10^{22} s)	$^{152}_{64}$Gd	6.63	0.34×10^{22} s	α	−64.6%
		^{115}In	7	1.39×10^{22} s	β^-	−38.6%
		^{59}Co	8	1.61×10^{22} s	stable	−35.6%
		$^{186}_{76}$Os	6.38	6.30×10^{22} s	α	−5%
		$^{174}_{72}$Hf	6.57	6.3×10^{22} s	α	−5%
		$^{44}_{60}$Nd	6.04	7.21×10^{22} s	α	−1.7%
		$^{113}_{48}$Cd	5.05	24.26×10^{22} s	β^-	8.8%: overl. with k = 9
		^{148}Sm	6.29	25.2×10^{22} s	α	9.3%: overl. With k = 9
9	11×10^{22} to 214×10^{25} s (5.60×10^{25} s)	^{50}V	7.2	0.44×10^{25} s	β^+ (83%) β^- (17%)	−7.8%
		$^{180}_{74}$W	6.50	5.65×10^{25} s	α	0.02% overlap
		^{151}Eu	6.13	15.2×10^{25} s	α	3.8% for these 7
		$^{150}_{60}$Nd	5.7	21.1×10^{25} s	$\beta^-\beta^-$	6.2% elements
		$^{100}_{42}$Mo	6.4	26.78×10^{25} s	$\beta^-\beta^-$	8.5% with k = 10
		$^{209}_{83}$Bi	5.76	60.0×10^{25} s	α	21.7%
		^{96}Zr	6.06	63×10^{25} s	$\beta^-\beta^-$	23%
		$^{116}_{48}$Cd	6.72	97.7×10^{25} s	$\beta^-\beta^-$	36%
10	4×10^{25} to 232×10^{28} s (4.06×10^{28} s)	^{48}Ca	7.68	0.13×10^{28} s	$\beta^-\beta^-$	−58%
		^{82}Se	7.16	0.306×10^{28} s	$\beta^-\beta^-$	−45.6%
		^{130}Te	6.50	2.48×10^{28} s	$\beta^-\beta^-$	−0.7% overlap
		^{136}Xe	6.24	6.62×10^{28} s	$\beta^-\beta^-$	1.1% with k = 11
11	1.4×10^{28} to 253×10^{31} s (2.95×10^{31} s)	^{128}Te	6.78	6.93×10^{31} s	$\beta^-\beta^-$	1.6%

We took back all isotopes with a long ½ life (>10 years) from NUBASE (3, 4, 5, 6) with a radioactivity β or α, or 64 isotopes. The number of bonds δ'' refers to the last neutron added and is usually indicative of the number of bonds k concerning the decay. (e.g.: ^{3}H has 5 bonds more than ^{2}H which has one bond, so each neutron has 3 bonds). The ½ life is $T = P^k$ (17) and P varies between 363 s and 1088 s with an average value of 726 s according to Equation (12) depending on the distance d which is between 0.325 and 0.967 fm. ("ideal" average distance: 0.65 fm). It is found that for all isotopes except 4 heavy elements, the observed ½ life is included in the area provided by the calculation. Note that, from $k = 7$, the areas provided by the calculation overlap. It is only for the ^{87}Rb that it is not possible to know whether $k = 6$ or 7 (90% deviation from the mean values for $k = 6$ or 7), the 25 elements with $k > 6$ have a ½ life that can deviate by more than 90% from the mean value; the 11 elements with $k > 7$ where there is overlap are close to a maximum of less than 36% of the mean value. It can therefore also be considered that for all the elements with $k \geq 7$, the observed ½ life is most probably included in the area provided by the calculation. The deviation that often exists from the mean value can be explained by the variation in the distance of the bonds of the nucleon or helion concerned by the radioactivity. The ½ life is then a way to calculate distances. ((12) (17) $\Rightarrow$ $d = P_{pn} \times c/2 \times T^{1/k}$) (24). Another hypothesis to find the exact value would be to imagine a different number of bonds. For example, for the ^{209}Po, to find the value of 32.5×10^8 s, we would have 88.33% of atoms with 3 bonds and 11.67% with 4 bonds). It is an "ad hoc" explanation that allows to find precisely the observed value but which may have the disadvantage of implying that the geometry is different from one nucleus to another for the same isotope (ratio isotopes in state of lower energy/excited states?). It is also interesting to note that for all these elements at long ½ life from the lightest to the heaviest, δ'' is always greater than 3 and between 5 and 8.

Table A4. Stable nuclei with a Z multiple of 6, determination of the shell.

Element	Mass defect in number of $\Delta m = \delta$	Nber δs of Δm remaining after subtraction of δ from previous even précédent & of the new helions	neutrons in addition to helions	probable role of δs	N° of the last helion shell given by the type of bond	N° shell formula (18) (19) (20)	comments
$^{12}_{6}$C	**68.81**				1		
$^{24}_{12}$Mg	**148.38**	**148 − 69 − 63 = 16**		2 double bonds (L2) per helion (or 12Δm)	**2**	2.66	
$^{36}_{18}$Ar	**229.77**	**230 − 148 − 63 = 19**		2 L3/helion (or18Δm)	**3**	3.17	
$^{50}_{24}$Cr	**326.53**	**327 − 230 − 63 = 34**	**2**	2 L4/helion (24Δm) 10 left either 1L4 per n or at least 2L2 per n	4	4.86	The 2 n stable would be more at the 2nd shell level
$^{64}_{30}$Zn	419.96	420 − 327 − 63 = 30	4	2 L4/helion or 24Δm, 6 left for 2n (2L3)	4	4.28	shell 5 requires 30Δm and there is 2n more. So rather shell 4 (24). les 2 n are on a lower shell
$^{80}_{36}$Kr	522.89	523 − 420 − 63 = 40	8	2L5/helion or 30Δm, 10 left for 4n	5	5.00	The last 4 n are on a lower shell with several bonds
$^{92}_{42}$Mo	598.58	599 − 523 − 63 = 13	8	6L2 for 3 helions	2	2.17	Shell 2 fills up
$^{106}_{48}$Cd	680.11	680 − 599 − 63 = 18	10	6L3 for 3 helions	3	3.00	Shell 3 fills up. The 2 n take bonds to the other n
$^{124}_{54}$Xe	786.73	787 − 680 − 63 = 44	16	*2L5/helion or 30Δm, 14 left for 6n*	5	5.50	Shell 5 fills
$^{142}_{60}$Nd	891.63	892 − 787 − 63 = 42	22	*2L5/helion or 30Δm, 8 left for 6n*	5	5.25	Shell 5 fills
$^{154}_{66}$Dy*	948.43	948 − 892 − 63 = −7	22				The next 3 elements are unstable
$^{174}_{72}$Hf*	1055.87	1056 − 948 − 63 = 45	30				
$^{190}_{78}$Pt*	1135.31	1135 − 1056 − 63 =	34				

For the 1st shell, in ^{12}C, the 3 helions are linked by 6 simple bonds (6Δm) between each time a proton and a neutron. To determine on which shell n are the helions, we take the element having 3 more helions. The excess of mass defect δ_s corresponds to 6 additional bonds (2 per helion) which can be double, triple and to bonds for additional neutrons. The shell n is given by an empirical formula to account for neutron bonds. $n = \delta_s/6$ ($\delta_s < 25$) (18), $n = \delta_s/7$ ($35 > \delta_s > 25$) (19), $n = \delta_s/8$ ($\delta_s > 35$) (20).

Table A5. Stable nuclei with even Z from O to U.

Element	Mass defect in number of $\Delta m = \delta$	δs	N° shell given by Table A4	Probable role of this remaining Δm	Neutrons in add. to hélions	Comments
$^{16}_{8}$O	95.41	5 95.41 − 68.81 − 21.07 = 5.53	2	2 double bonds for the last hellion (2 × 2.76d)		

Continued

$^{20}_{10}$Ne	120.12	4 120.12 − 95.41 − 21.07 = 3.64	2	Idem ($2 \times 1.82d$)		
$^{24}_{12}$Mg	**148.38**	**7** 148.4 − 120.12 − 21.07 = 7.19	2	**idem**		**Calculation/C (shell 1) gives: 148 − 69 − 63 = 16 or 16/6 = 2.66Δm per bond thus shell 2**
$^{28}_{14}$Si	177	8	3	2 triple bonds		
$^{32}_{16}$S	204	6	3	2 triple bonds		
$^{36}_{18}$Ar	**229.77**	**230 − 204 − 21 = 5**	**3**	**2 triple bonds**		**230 − 148 − 63 = 19 or 19/6 = 3.17 (shell 3)**
$^{40}_{20}$Ca	256.28	256 − 230 − 21 = 5	4			
$^{46}_{22}$Ti	298.85	299 − 256 − 21 = 22	4		2	.δs increases strongly when 2 add. n are needed.
$^{50}_{24}$Cr	**326.53**	**327 − 299 − 21 = 7**	**4**		2	
$^{54}_{26}$Fe	354.09	354 − 327 − 21 = 6	4		2	
$^{58}_{28}$Ni	380.10	380 − 354 − 21 = 5	4		2	
$^{64}_{30}$Zn	**419.96**	**420 − 380 − 21 = 19**	**4**		**4**	
$^{70}_{32}$Ge	458.88	459 − 420 − 21 = 18	5		6	
$^{74}_{34}$Se	483	483 − 459 − 21 = 3	5		6	
$^{80}_{36}$Kr	**522.89**	**523 − 483 − 21 = 19**	**5**		**8**	
$^{84}_{38}$Sr	548	548 − 523 − 21 = 4	2		8	
$^{90}_{40}$Zr	589.63	590 − 548 − 21 = 21	2		10	
$^{92}_{42}$Mo	**598.58**	**599 − 548 − 42 = 9****	**2**		**8**	
$^{96}_{44}$Ru	620.95	621 − 599 − 21 = 1	3		8	
$^{102}_{46}$Pd	657.79	658 − 621 − 21 = 16	3		10	
$^{106}_{48}$Cd	**680.11**	**680 − 599 − 63 = 18**	**3**		**10**	
$^{112}_{50}$Sn	716.70	717 − 680 − 21 = 16	5		12	
$^{120}_{52}$Te	765.14	765 − 717 − 21 = 27	5		16	
$^{124}_{54}$Xe	**786.73**	**787 − 680 − 63 = 44**	**5**		**16**	
$^{130}_{56}$Ba*	821.83	822 − 787 − 21 = 14	5	The new He go to shell 5 with 2n	18	
$^{136}_{58}$Ce	856.62	857 − 822 − 21 = 14	5	The new He go to shell 5 with 2n	20	
$^{142}_{60}$Nd	**891.63**	**892 − 857 − 21 = 14**	**5**	**The new He go to shell 5 with 2n**	**22**	

Continued

$^{144}_{62}$Sm	899.02	899 − 892 − 21 = −14		20	From Sm to Er, we see 2 decreases of −14 followed by 2 strong increases of 21 and 24
$^{152}_{64}$Gd	941.29	941 − 899 − 21 = 21		24	It is interpreted as saying that the last helion of the Sm is placed at a nivel 4 and drives at least one other helion previously arrived in 5 at a level 4
$^{154}_{66}$Dy*	**948.43**	**948 − 941 − 21 = −14**		**22**	2 n are no longer necessary The helion brought by Gd is then placed at level 5 and requires 4n. The same goes for Dy and Er
$^{162}_{68}$Er	993.17	993 − 948 − 21 = 24		26	
$^{168}_{70}$Yb	1024.89	1025 − 993 − 21 = 11	The new He go to shell 5 with 2n	28	Yb, Hf, W. The 3 He occupy first 3 places in level 5 (filling sequence idem Kr Cd)
$^{174}_{72}$Hf*	**1055.87**	**1056 − 1025 − 21 = 10**	**The new He go to shell 5 with 2n**	**30**	
$^{180}_{74}$W	1086.48	1087 − 1056 − 21 = 10	The new He go to shell 5 with 2n	32	Os sees the end of the filling of level 4 with another He going
$^{184}_{76}$Os	1105.26	1105 − 1087 − 21 = −3		32	in 4. No new n. n decrease in level
$^{190}_{78}$Pt	1135.31	1135 − 1105 − 21 = 5		34	
$^{196}_{80}$Hg	1166.47	1167 − 1135 − 21 = 11		36	Pt to Pb end of filling shell 5
$^{204}_{82}$Pb	1209.15	1209 − 1167 − 21 = 21		40	
$^{209}_{84}$Po*	1231.57	1232 − 1209 − 21 = 1		41	
$^{222}_{86}$Rn*	1285.32	1285 − 1232 − 21 = 32		50	
$^{226}_{88}$Ra*	1302.62	1303 − 1285 − 21 = −3		50	
$^{232}_{90}$Th*	1328.93	1329 − 1303 − 21 = 5		52	
$^{234}_{92}$U*	1337.32	1337 − 1329 − 21 = −13		50	

When taking the intermediate elements (with even Z pairs), the mass defect makes it possible to verify that each new helion (its 2 neutrons) will bind by 2 multiple bonds corresponding to the shell (*The method of fixing in corona makes that the 3rd helion terminating a corona can be fixed with a longer length* (*e.g., for 2nd shell length of 2.73d close to 3 instead of 2.18d close to 2*) *and this would explain the variations to 1 or 2 near the number of Δm remaining at each new helion. Hence the importance of determining the shell on the average of each new corona of 3 helions*). δ'_s = number of remaining Δm for an element X with $\delta = \delta_x$ after subtraction of the Δm (δ_y) of the previous even element Y and of the new helion (21.07 = mass defect in Δm of helion). $\delta'_s = \delta_x - \delta_y - 21.07$.

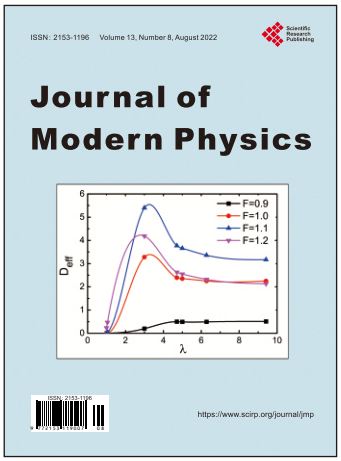

Call for Papers

Journal of Modern Physics

ISSN: 2153-1196 (Print) ISSN: 2153-120X (Online)
https://www.scirp.org/journal/jmp

Journal of Modern Physics **(JMP)** is an international journal dedicated to the latest advancement of modern physics. The goal of this journal is to provide a platform for scientists and academicians all over the world to promote, share, and discuss various new issues and developments in different areas of modern physics.

Editor-in-Chief

Subject Coverage

Journal of Modern Physics publishes original papers including but not limited to the following fields:

Biophysics and Medical Physics
Complex Systems Physics
Computational Physics
Condensed Matter Physics
Cosmology and Early Universe
Earth and Planetary Sciences
General Relativity
High Energy Astrophysics
High Energy/Accelerator Physics
Instrumentation and Measurement
Interdisciplinary Physics
Materials Sciences and Technology
Mathematical Physics
Mechanical Response of Solids and Structures
New Materials: Micro and Nano-Mechanics and Homogeneization
Non-Equilibrium Thermodynamics and Statistical Mechanics
Nuclear Science and Engineering
Optics
Physics of Nanostructures
Plasma Physics
Quantum Mechanical Developments
Quantum Theory
Relativistic Astrophysics
String Theory
Superconducting Physics
Theoretical High Energy Physics
Thermology

We are also interested in: 1) Short Reports—2-5 page papers where an author can either present an idea with theoretical background but has not yet completed the research needed for a complete paper or preliminary data; 2) Book Reviews—Comments and critiques.

Notes for Intending Authors

Submitted papers should not have been previously published nor be currently under consideration for publication elsewhere. Paper submission will be handled electronically through the website. All papers are refereed through a peer review process. For more details about the submissions, please access the website.

Website and E-Mail

https://www.scirp.org/journal/jmp **E-mail: jmp@scirp.org**

What is SCIRP?

Scientific Research Publishing (SCIRP) is one of the largest Open Access journal publishers. It is currently publishing more than 200 open access, online, peer-reviewed journals covering a wide range of academic disciplines. SCIRP serves the worldwide academic communities and contributes to the progress and application of science with its publication.

What is Open Access?

All original research papers published by SCIRP are made freely and permanently accessible online immediately upon publication. To be able to provide open access journals, SCIRP defrays operation costs from authors and subscription charges only for its printed version. Open access publishing allows an immediate, worldwide, barrier-free, open access to the full text of research papers, which is in the best interests of the scientific community.

- High visibility for maximum global exposure with open access publishing model
- Rigorous peer review of research papers
- Prompt faster publication with less cost
- Guaranteed targeted, multidisciplinary audience

Scientific Research Publishing

Website: https://www.scirp.org
Subscription: sub@scirp.org
Advertisement: service@scirp.org